Author(s)	Hatcher, Ervin B.
Title	Investigating the effects of higher spatial resolution on benthic classification accuracy at Midway Atoll
Publisher	Monterey, California. Naval Postgraduate School
Issue Date	2008-09
URL	http://hdl.handle.net/10945/3884

NAVAL POSTGRADUATE SCHOOL

MONTEREY, CALIFORNIA

THESIS

INVESTIGATING THE EFFECTS OF HIGHER SPATIAL
RESOLUTION ON BENTHIC CLASSIFICATION
ACCURACY AT MIDWAY ATOLL

by

Richard K. Arledge
Ervin B. Hatcher

September 2008

Thesis Advisor: Daria Siciliano
Co-Advisor: Richard C. Olsen
Second Reader: Glenn Cook

Approved for public release; distribution is unlimited

THIS PAGE INTENTIONALLY LEFT BLANK

REPORT DOCUMENTATION PAGE		*Form Approved OMB No. 0704-0188*
Public reporting burden for this collection of information is estimated to average 1 hour per response, including the time for reviewing instruction, searching existing data sources, gathering and maintaining the data needed, and completing and reviewing the collection of information. Send comments regarding this burden estimate or any other aspect of this collection of information, including suggestions for reducing this burden, to Washington headquarters Services, Directorate for Information Operations and Reports, 1215 Jefferson Davis Highway, Suite 1204, Arlington, VA 22202-4302, and to the Office of Management and Budget, Paperwork Reduction Project (0704-0188) Washington DC 20503.		
1. AGENCY USE ONLY *(Leave blank)*	**2. REPORT DATE** September 2008	**3. REPORT TYPE AND DATES COVERED** Master's Thesis
4. TITLE AND SUBTITLE Investigating the Effects of Higher Spatial Resolution on Benthic Classification Accuracy at Midway Atoll		**5. FUNDING NUMBERS**
6. AUTHOR(S) Arledge, Richard K., Hatcher, Ervin B.		
7. PERFORMING ORGANIZATION NAME(S) AND ADDRESS(ES) Naval Postgraduate School Monterey, CA 93943-5000		**8. PERFORMING ORGANIZATION REPORT NUMBER**
9. SPONSORING /MONITORING AGENCY NAME(S) AND ADDRESS(ES) N/A		**10. SPONSORING/MONITORING AGENCY REPORT NUMBER**
11. SUPPLEMENTARY NOTES The views expressed in this thesis are those of the author and do not reflect the official policy or position of the Department of Defense or the U.S. Government.		
12a. DISTRIBUTION / AVAILABILITY STATEMENT Approved for public release; distribution is unlimited.		**12b. DISTRIBUTION CODE** A

13. ABSTRACT (maximum 200 words)

Effective monitoring of coral reefs is important for ecological and economic reasons, and satellite remote sensing has been shown to be useful for mapping and monitoring these ecosystems. This thesis will compare 2 multispectral systems and investigate the effects of increased spatial resolution on benthic classifications in the highly heterogeneous coral reef environment of Midway Atoll. It will evaluate the utility of QuickBird's increased spatial resolution compared to IKONOS imagery in the same study area at multiple scales. Previous studies (e.g., Mumby and Edwards, 2002; Capolsini et al., 2003; Wang et al., 2004; Benefeild et al., 2007) comparing various satellite sensors suggest that greater spatial resolution should lead to more accurate classifications, but a direct comparison of QuickBird and IKONOS sensors has not been carried out in marine environments. Light interactions in marine environments are complex and add difficulty to spectral discrimination, producing more variable results in classification accuracy than in terrestrial environments. This research does not find any significant improvements in thematic mapping accuracy of benthic environment from QuickBird's higher spatial resolution satellite imagery. Additionally, a cost benefit analysis did not show a decisive advantage in choosing either imagery type for the application of monitoring the extent, biodiversity, and health of coral reef habitats.

14. SUBJECT TERMS: Benthic classification, spatial resolution, QuickBird, IKONOS, cross-scale, remote sensing, multispectral, ENVI, ACORN, satellite, Midway Atoll, coral reef, cost benefit analysis			**15. NUMBER OF PAGES** 141
			16. PRICE CODE
17. SECURITY CLASSIFICATION OF REPORT Unclassified	**18. SECURITY CLASSIFICATION OF THIS PAGE** Unclassified	**19. SECURITY CLASSIFICATION OF ABSTRACT** Unclassified	**20. LIMITATION OF ABSTRACT** UU

NSN 7540-01-280-5500

Standard Form 298 (Rev. 2-89)
Prescribed by ANSI Std. 239-18

THIS PAGE INTENTIONALLY LEFT BLANK

**INVESTIGATING THE EFFECTS OF HIGHER SPATIAL RESOLUTION ON
BENTHIC CLASSIFICATION ACCURACY AT MIDWAY ATOLL**

Richard K. Arledge
Lieutenant, United States Navy
B.A., Jacksonville State University, 2001

Submitted in partial fulfillment of the
requirements for the degree of

MASTER OF SCIENCE IN SPACE SYSTEMS OPERATIONS

Ervin B. Hatcher
Lieutenant, United States Navy
B.S., North Carolina State University, 2002

Submitted in partial fulfillment of the
requirements for the degrees of

MASTER OF SCIENCE IN SPACE SYSTEMS OPERATIONS
and
MASTER OF SCIENCE IN INFORMATION TECHNOLOGY MANAGEMENT

from the

NAVAL POSTGRADUATE SCHOOL
September 2008

Authors: Richard K. Arledge

                         Ervin B. Hatcher

Approved by: Dr. Daria Siciliano
                         Thesis Advisor

                         Dr. Richard C. Olsen
                         Thesis Co-Advisor

                         Mr. Glenn Cook
                         Second Reader

                         Dr. Rudolf Panholzer
                         Chairman, Space Systems Academic Group

                         Dr. Dan C. Boger
                         Chairman, Department of Information Sciences

THIS PAGE INTENTIONALLY LEFT BLANK

ABSTRACT

Effective monitoring of coral reefs is important for ecological and economic reasons, and satellite remote sensing has been shown to be useful for mapping and monitoring these ecosystems. This thesis will compare 2 multispectral systems and investigate the effects of increased spatial resolution on benthic classifications in the highly heterogeneous coral reef environment of Midway Atoll. It will evaluate the utility of QuickBird's increased spatial resolution compared to IKONOS imagery in the same study area at multiple scales. Previous studies (e.g., Mumby and Edwards, 2002; Capolsini et al., 2003; Wang et al., 2004; Benefeild et al., 2007) comparing various satellite sensors suggest that greater spatial resolution should lead to more accurate classifications, but a direct comparison of QuickBird and IKONOS sensors has not been carried out in marine environments. Light interactions in marine environments are complex and add difficulty to spectral discrimination, producing more variable results in classification accuracy than in terrestrial environments. This research does not find any significant improvements in thematic mapping accuracy of benthic environment from QuickBird's higher spatial resolution satellite imagery. Additionally, a cost benefit analysis did not show a decisive advantage in choosing either imagery type for the application of monitoring the extent, biodiversity, and health of coral reef habitats.

THIS PAGE INTENTIONALLY LEFT BLANK

TABLE OF CONTENTS

THIS PAGE INTENTIONALLY LEFT BLANK

LIST OF FIGURES

LIST OF TABLES

THIS PAGE INTENTIONALLY LEFT BLANK

I. INTRODUCTION

Reef habitats face numerous, increasing threats from local interests, such as coastal development, over-fishing, and global warming (Pandolfi et al., 2003; Bellwood et al., 2004; Carpenter et al., 2008). Effective monitoring of coral reefs is important for ecological and economic reasons, because of the critical role reefs play in biodiversity, tourism, and fisheries (Berg et al., 1998; Harborne et al., 2006; Brander et al., 2007). Coral reef ecosystems lend themselves to being mapped by passive satellite sensors because of their location in shallow, clear waters, and satellite sensing has been shown to be useful for mapping and monitoring their global distribution and health (Lubin et al., 2001). Many of the world's coral reefs are under the governance of developing countries, which may not have the resources to employ traditional mapping or monitoring techniques and, therefore, rely heavily on satellite technology for natural resource monitoring (Benefield et al., 2007). Also, the use of satellite remote sensing has been shown to be more cost effective than traditional fieldwork (Mumby et al., 1999). Additionally, satellite sensors provide a means for access to denied territories and can allow for routine monitoring of selected areas, including target detection applications.

High resolution, multispectral or hyperspectral, satellite sensors currently available give users the ability to detect and spectrally analyze light reflected from the bottom of shallow water bodies, and to discriminate bottom types based on their reflectance signatures (Louchard et al., 2003). IKONOS, launched in 1999 (GeoEye), and QuickBird, launched in 2001 (DigitalGlobe), are commercially available multispectral satellites that provide the highest spatial resolution currently available (4 m and 2.8 m respectively) and have comparable spectral resolution. In the near term, 2 new satellite sensors will begin providing even higher resolution data. Worldview, scheduled for launch in mid-2009, will provide multispectral imagery with 1.84 m resolution (at nadir), imaging in 4 additional bands allowing numerous new applications (DigitalGlobe, 2008). TacSat-3, scheduled for launch in October 2008, will carry ARTEMIS, a hyperspectral sensor capable of 3.84 m resolution in 5 nm bands ranging from 0.38-2.5 μm (AFRL, 2008; Cooley, 2008).

In an effort to develop coral reef maps for monitoring purposes, Holden and Ledrew (1999) found that there are robust differences between the spectra of corals and related noncoral objects independently of geographic sampling, and that these spectral contrasts could be used to construct a scene identification algorithm. The output of such an algorithm is the grouping of related spectral patterns into classes or themes, called a thematic map, which provides a representation of land cover types in a scene (Lillesand et al., 2004). When this technique is applied to describing the features of the sea bottom, it is called a benthic classification.

Unfortunately, some of the spectral features identified by Holden and Ledrew (1999) and others after them (e.g., Lubin et al., 2001; Hochberg et al., 2003; Louchard et al., 2003) used to distinguish coral species are obscured in data collected from space, because of the complex interactions with the atmosphere and water column (Lubin et al., 2001). This phenomenon can lead to low classification accuracy in marine environments. A number of coral reef scientists (e.g., Mumby and Edwards, 2002; Capolsini et al., 2003; Wang et al., 2004; Benefield et al., 2007) have proposed that increased spatial resolution could aid in spectrally separating classes. Mumby and Edwards (2002) demonstrated that the use of the IKONOS satellite sensor improved benthic classification accuracy over conventional airborne and previously available satellite sensors due to its enhanced spatial resolution.

The question of how much, if any, improvement in thematic accuracy gained from increased spatial resolution has been explored in previous studies (e.g., Mumby and Edwards, 2002; Capolsini et al., 2003; Wang et al., 2004; Benefeild et al., 2007) but without consistent results. Additionally, no assessments have been made in coral reef environments, which are highly spatially heterogenous and would be expected to benefit from increased spatial resolution. This thesis will investigate the effects of increased spatial resolution on benthic classifications in a coral reef environment, specifically at Midway Atoll in the Northwest Hawaiian Islands. In particular, it will evaluate the utility of QuickBird's increased spatial resolution on benthic classifications, directly comparing IKONOS and QuickBird data in the same study area.

Both satellites will be used to generate thematic maps of the central portion of Midway Atoll to evaluate performance at a landscape scale of the entire area. A smaller patch reef selection will be classified and surveyed in fine detail to evaluate performance at benthic classification boundaries on this smaller spatial scale. The benthic classifications produced by each sensor will be evaluated using standard accuracy assessment techniques for the central atoll and a more qualitative analysis for the classification boundaries of the patch reef selection. Their accuracies will be compared to determine what advantage, if any, is gained by using the higher spatial resolution QuickBird data. Finally, this thesis will consider a cost benefit analysis related to the use of higher spatial resolution imagery for this application.

THIS PAGE INTENTIONALLY LEFT BLANK

II. RADIATIVE TRANSFER THEORY FOR MARINE REMOTE SENSING

Optical remote sensing using satellite imagery has become an effective tool to use in observing and monitoring the characteristics of the world's land and oceans (Lillesand et al., 2004). Today most satellite monitoring systems employ passive remote sensing techniques, collecting the radiation received from the reflection of solar energy off the surface of the Earth (Jensen, 2000). This energy is referred to as radiance. Passive sensing methods are used for marine classification studies because they can penetrate the surface of the ocean up to several meters and observe the ocean bottom (Robinson, 2004). It is important to understand the effects of both atmospheric interactions as well as the water column on energy that is detected by satellite sensors. This section will discuss the basic principles of multispectral satellite imagery and radiative transfer theory that affect data collection and analysis.

A. MULTISP   ECTRAL SATELLITE IMAGERY

1. Fundamentals of Remote Sensing Satellites

Satellites are useful platforms for remotely monitoring the Earth and its oceans. Various wavelength ranges of the electromagnetic spectrum are detected using a variety of collection techniques in these satellites. It is important to note that operating in space brings many additional considerations such as the unique operating environment, orbital limitations, revisit times, and communications challenges (Lillesand et al., 2004). Multispectral imagery has a variety of applications in marine remote sensing (Robinson, 2004). This section will discuss the sensors and the applications of multispectral imagery, as well as, the analysis, resolution parameters, and challenges inherent to using such imagery in marine environments.

a. Sensor Types

Satellite sensors can be broadly classified into 2 basic categories: passive and active. Passive sensors operate across the visible, infrared, and microwave portions of the electromagnetic spectrum, while active sensors operate, primarily, in the visible

and microwave bands (Green et al., 2000). Sensors can further be categorized into classes defined by the region of the electromagnetic spectrum exploited. Active sensors typically use radar instruments to generate their own radiation. Each sensor class is characterized by a specific sensor type, such as radiometers, spectrometers, or radar (Robinson, 2004). Each of these sensor types provide data that can be used directly or, with analysis, generate derived parameters for specific applications. Figure 1 illustrates the relationships among these sensor classes and application types. Note that multispectral scanners are linked to ocean color observation which can be used, among other things, to derive bathymetric information (Robinson, 2004). Multispectral imagery is used to create benthic classification maps, and it will be used in this thesis.
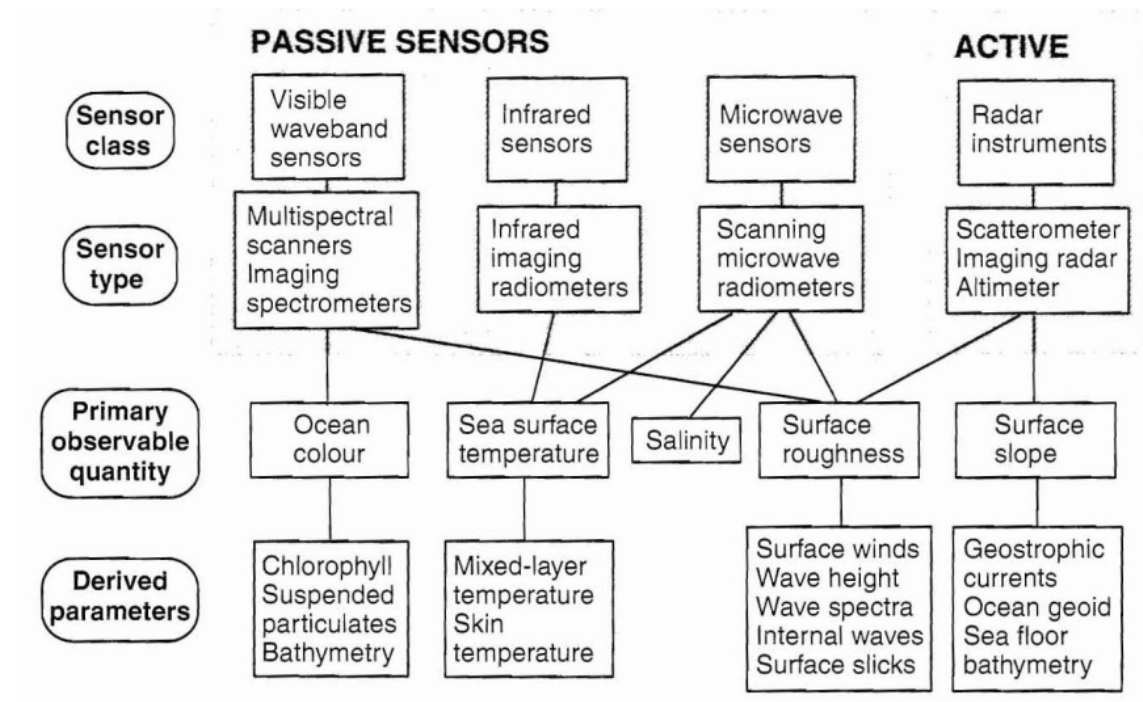
Figure 1.   Applications for remote sensing methods and classes (From Robinson, 2004)

b. *Multispectral Imagery*

Multispectral remote sensing is the collection, from an area of interest, of reflected, emitted, or scattered energy in multiple bands of the electromagnetic spectrum (Jensen, 2000). For many applications, such as marine remote sensing, acquiring information in multiple spectral bands is necessary to obtain information on different seafloor bottom types (Louchard et al., 2003). Ocean color, a "primary observable quantity" in multispectral imagery, is a characteristic seawater property that refers to the magnitude and spectral composition of the light leaving the water's surface. This color may not be the same as what is seen by the human eye but is a discrete measure of the radiation received by the sensor that describes a unique spectral composition (Robinson, 2004). Information about the factors influencing the spectral composition recorded can be derived from these spectra. These include: chlorophyll concentration; dissolved material; and, under the right conditions in clear shallow water, bottom type or depth.

The collection of this information can be accomplished in several ways. Various collector configurations are presented in Figure 2. Each of the arrangements depicted in Figure 2 captures the desired information in a different way.
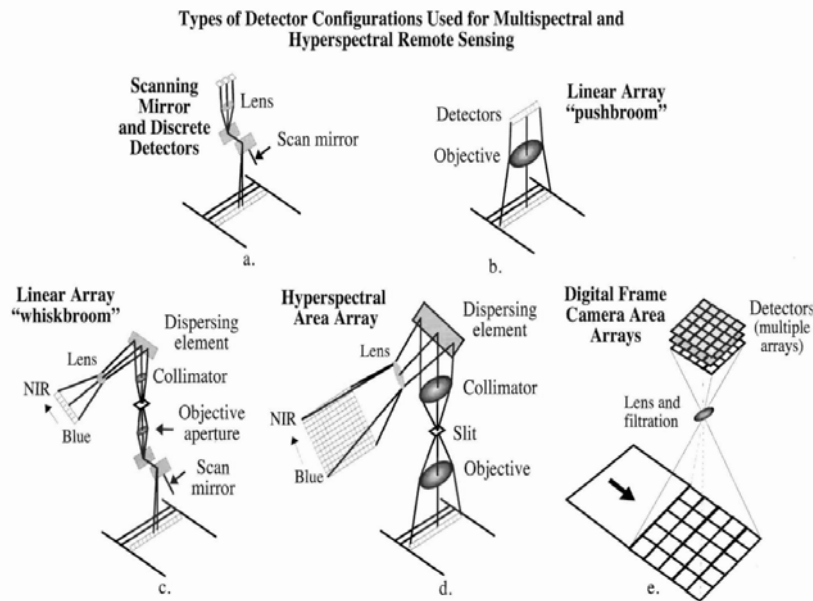
Figure 2.   Detector configurations used in remote sensing (From Jensen, 2000)

The linear array, "pushbroom" sensors are chosen for use in most of today's higher resolution satellite sensors, including IKONOS, QuickBird, and SPOT (Olsen, 2007). Pushbroom sensors use a line of detectors, positioned end to end, that record energy from a single column. This motion is depicted in Figure 3.
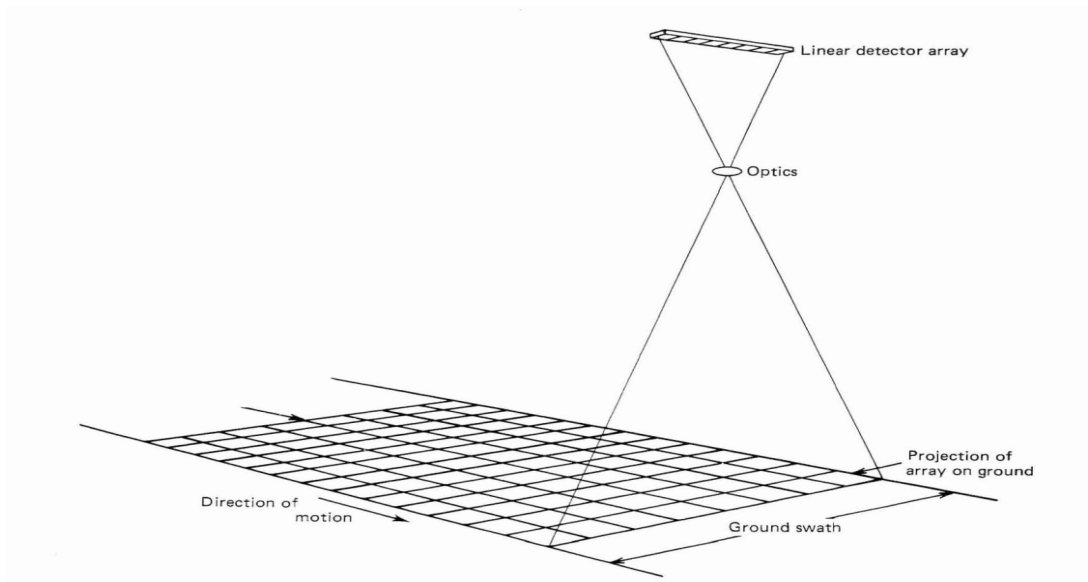
Figure 3.   Pushbroom scanner operation (From Lillesand et al., 2004)

This type of array has several advantages. First, it gives each detector a longer dwell time over the area of interest, allowing stronger signal levels to be detected and recorded (Jensen, 2000). Second, because the sensor depends mainly on vehicle motion, there is a fixed relationship among the detector elements, leading to less geometric error from the scanning process. Finally, because this technology uses solid state microelectronics, it is smaller, requires less power, is more reliable, and has longer life expectancy (Lillesand et al., 2004).

2. Resolution

Resolution is defined as the ability a system has to distinguish between signals that are spectrally similar or spatially close together (Jensen, 2000). Four major categories of satellite resolution are commonly used to describe image data obtained from

digital sensors: spatial, spectral, temporal, and radiometric. Each of these will have a different impact on the data received by the end user and should be understood. Temporal resolution describes the revisit time for imaging a specific point. Radiometric resolution describes the light sensitivity of a sensor (Green et al., 2000). This thesis focuses on spatial resolution. Both spectral and spatial resolution will be discussed in more detail in the following sections.

a. Spectral Resolution

Sensors are designed to detect certain regions of the electromagnetic spectrum. Spectral resolution refers to the range of the electromagnetic spectrum and the number of intervals to which an instrument is sensitive (Jensen, 2000). Sensors can be classified as panchromatic, multispectral, or hyperspectral based on the number of bands that can be detected. Panchromatic sensors record data in one continuous band that covers the visible and infrared portions of the electromagnetic spectrum; multispectral uses several bands; and hyperspectral, hundreds of bands (Green et al., 2000). Both IKONOS and QuickBird satellite sensors collect multispectral data and have comparable spectral resolutions. The multispectral bands are presented in Table 1 and their spectral response curves are presented in Figure 4.

Spectral Band	IKONOS	QuickBird
Blue	445–516 nm	450 – 520 nm
Green	506–595 nm	520 – 600 nm
Red	632–698 nm	630 – 690 nm
NIR	757–853 nm	760 – 900 nm

Table 1.   Spectral bands of IKONOS and QuickBird (GeoEye, 2006; DigitalGlobe, 2004)
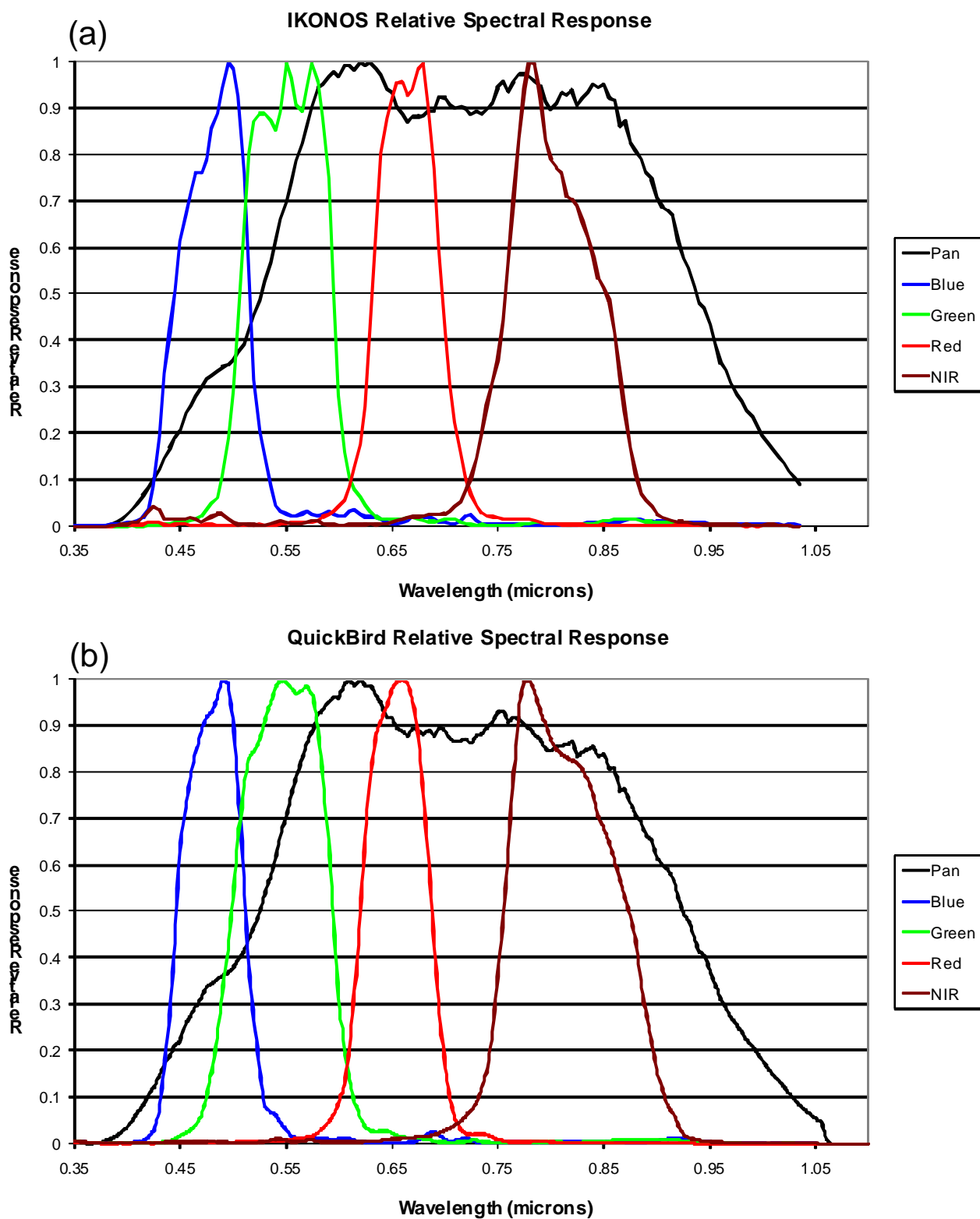
Figure 4.   Spectral response curves for (a) IKONOS and (b) QuickBird

b. *Spatial Resolution*

Spatial resolution is defined as a measure of the smallest separation, angular or linear, between two objects that can be determined by a sensor (Jensen, 2000). This quantity is dependent on altitude and sensor design. Spatial resolution can be thought of as pixel size and is commonly measured in meters or kilometers (Green et al., 2000). This term is also known as Instantaneous Field Of View (IFOV). In general, a sensor's spatial resolution should be one-half the size of the smallest dimension of a feature that needs to be detected (Jensen, 2000). IKONOS and QuickBird both belong to a class of satellites referred to as very high resolution, or VHR (Wang et al., 2004). Satellites have different levels of spatial resolution in different operating modes based on the detectors used. IKONOS can achieve resolutions of 1 m or better for panchromatic and 4 m or better for multispectral imagery (GeoEye, 2006). QuickBird can achieve spatial resolutions of 0.7 m or better for panchromatic and 2.8 m or better for multispectral imagery (Digital Globe, 2007). Mumby and Edwards (2002) found that enhanced spatial resolution can improve benthic classification accuracy, and this study will investigate the utility of the increased spatial resolution available from QuickBird on benthic classifications.

B. RADI   ATIVE TRANSFER

Radiative transfer is the theoretical basis for modeling the interactions of solar energy with various mediums, such as the Earth's surface, atmosphere, and the ocean, prior to collection by a sensor (Thomas and Stamnes, 1999). The effects of atmospheric attenuation and scattering, the air-sea interface, and elements in the water column must all be considered when using remotely sensed optical data (Morel and Prieur, 1977). The exploited electromagnetic bands and the attenuation effects are discussed below.

1. Electromagnetic Spectrum

The electromagnetic spectrum is a representation of the wavelengths of radiant energy and defines the data used in remote sensing. Figure 5 illustrates the most common range of energy exploited by satellite sensors for characterization, surveillance, and monitoring of the Earth's surface.
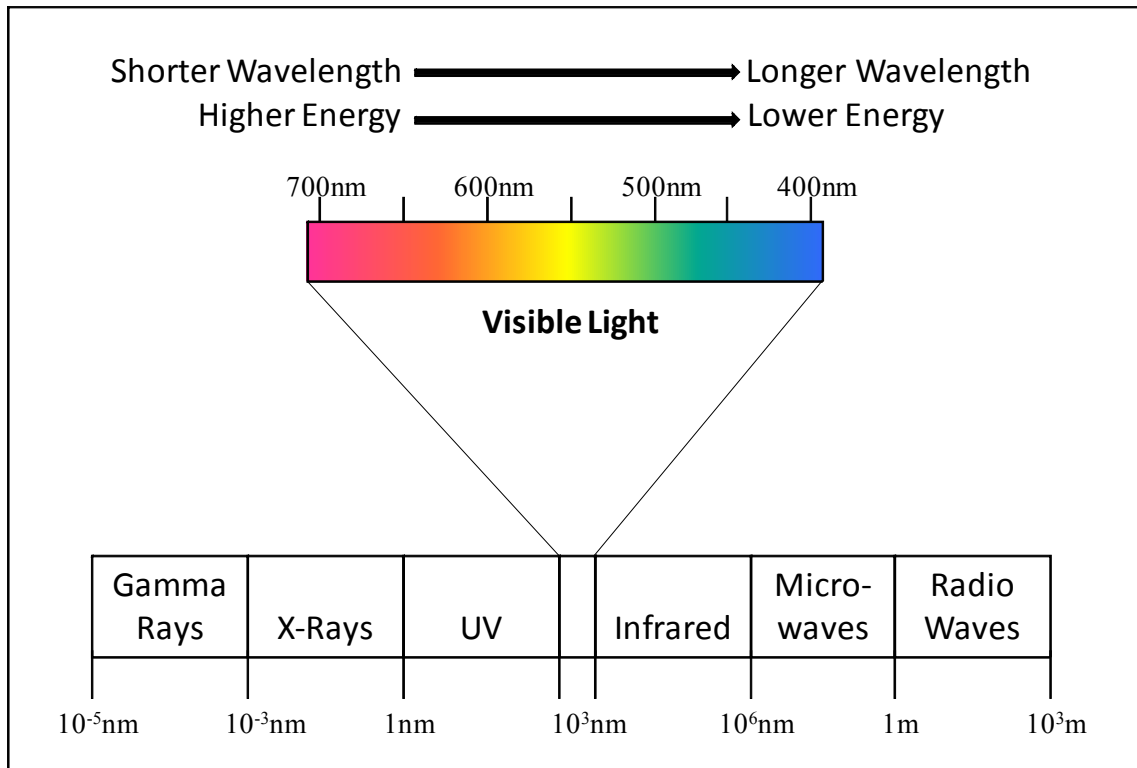
Figure 5.   The visible portion of the electromagnetic spectrum

The visible portion of the spectrum, which consists of blue, green, and red wavelengths, extends from 400 nm to 700 nm. This range of solar radiation is best suited for marine remote sensing, particularly benthic classifications, because it can penetrate the water column to about 20-30 meters (Robinson, 2004; Green et al., 2000). The near infrared portion of the spectrum (i.e., wavelengths from 700 nm to 1000 nm; Jensen, 2000), provides few returns in marine applications due to absorption by the water; however, it can still be used in image processing (e.g., sun glint removal; Hochberg et al., 2003). Passive, multispectral satellite systems commonly detect electromagnetic radiation in the 400 – 1000 nm wavelength range.

2. Interaction   with Matter

Electromagnetic energy that is incident on a surface will undergo one or all of the following fundamental interactions: reflection, absorption, transmittance, and scattering (Jensen, 2000). Figure 6 demonstrates these interactions.

12
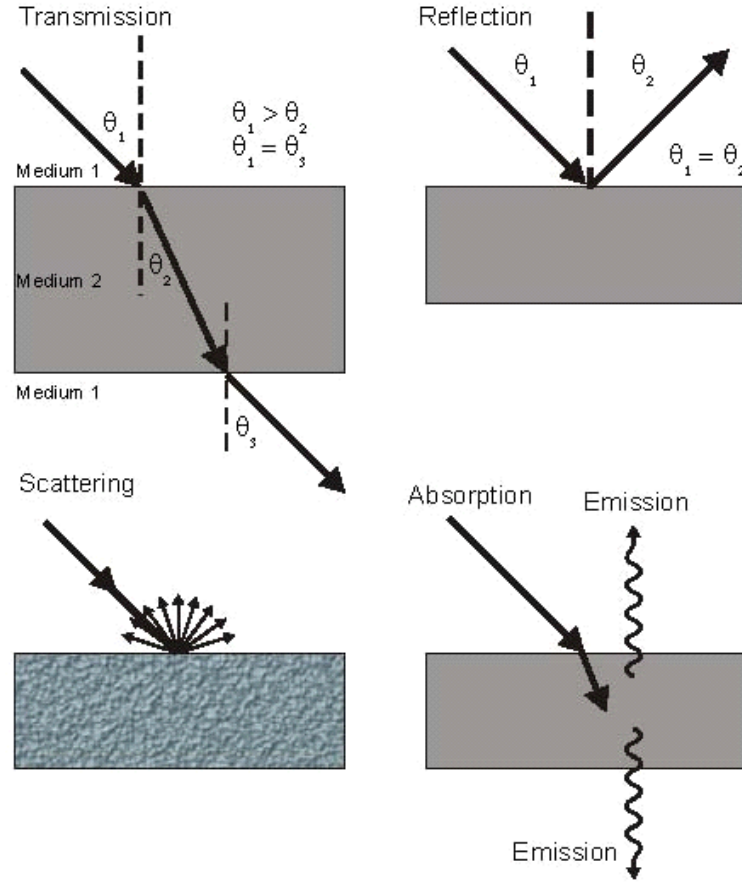
Figure 6.   Light interactions with matter (From Olsen, 2007)

Equation (1) mathematically represents the energy balance among the 3 main interactions of electromagnetic radiation and matter.

$$E_I(\lambda) = E_R(\lambda) + E_A(\lambda) + E_T(\lambda) \tag{1}$$

Where E_I is the incident energy, E_R is the reflected energy, E_A is the absorbed energy, and E_T is the transmitted energy. All of these are a function of wavelength (λ). The incident energy is a function of all 3 interactions and is dependent on the wavelength, material type, and material condition (Lillesand et al., 2004). Scattering occurs after energy is absorbed and reemitted in an unpredictable direction and will be discussed in further detail in Section C of this chapter.

It is also necessary to consider the way a surface reflects energy. There are 2 major types of reflectors: specular reflectors have mirrorlike interactions where the angle

of reflection is equal to the angle of incidence; and diffuse, or Lambertian, reflectors reflect uniformly in all directions. Most surfaces on earth are some combination of the 2 types (Lillesand et al., 2004). Figure 7 illustrates the various types and combinations of reflectors.
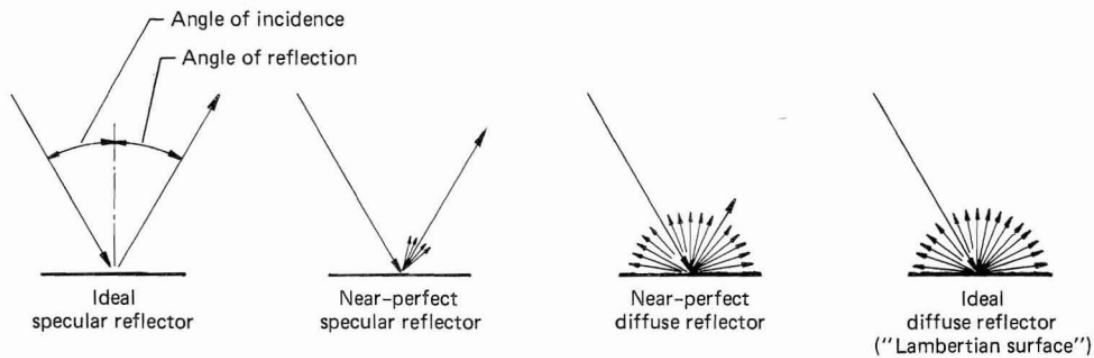
Figure 7.   Specular versus diffuse reflectance (From Lillesand et al., 2004)

The radiation field will also be affected by gaseous matter, aqueous matter, particles, solids, and ocean surfaces (Thomas and Stamnes, 1999). Analysis of satellite imagery must account for these interactions. The energy collected by the sensor on a satellite has traversed the atmosphere twice and has interacted with the water column before reaching the sensor in space. These interactions must be considered when using remotely sensed data for marine applications, such as benthic classification studies. These mechanisms will be accounted for in image processing which is discussed in Chapter IV.

C. ATMOSPHERIC   INTERACTIONS

As electromagnetic radiation passes through the atmosphere, all the interactions discussed above take place. Absorption and scattering are a primary concern for marine remote sensing (Green et al., 2000). These optical processes will change the signal received at the satellite sensor and must be understood and accounted for when using this type of data for studies of the Earth's surface.

1. Atmospheric Optical Processes

The optical pathways between the sea surface and a satellite sensor are complex. Robinson (2004) provides an illustration of the many pathways and interactions that occur before the energy reaches a satellite sensor. This is reproduced in Figure 8 below.
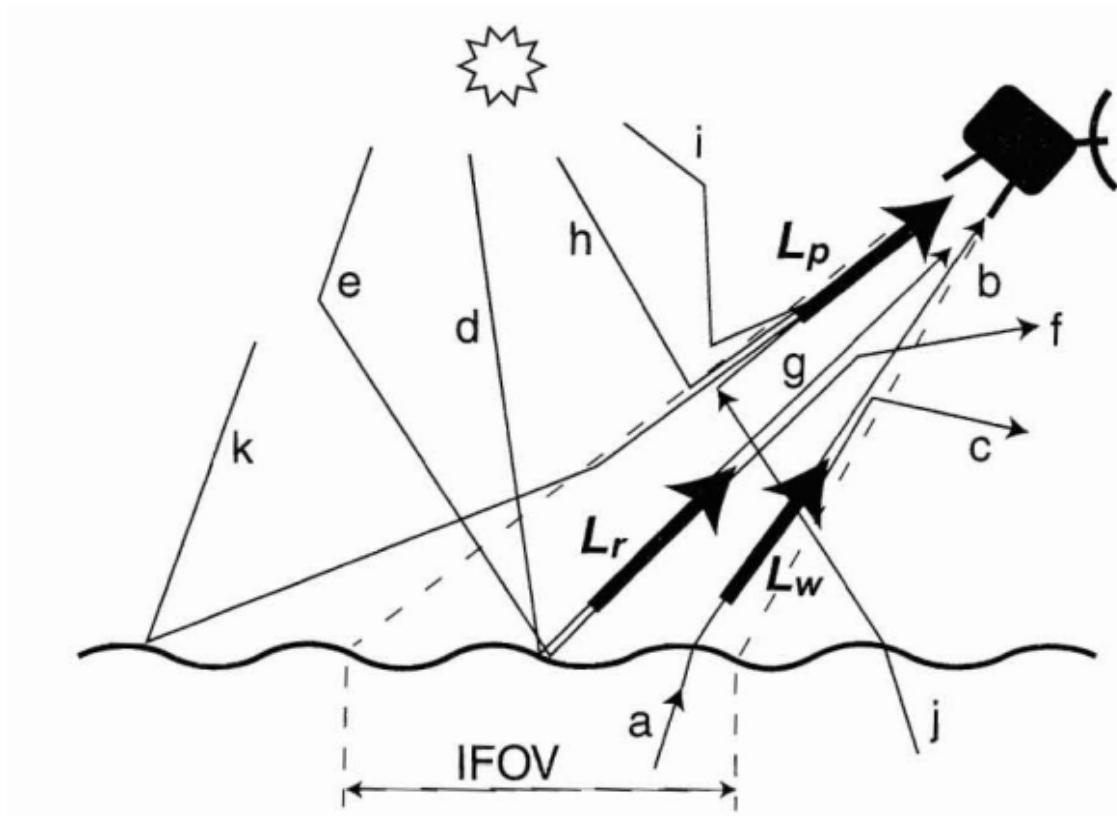
Figure 8.   Optical pathways to the sensor (From Robinson, 2004)

The terms used in Figure 8 are defined as follows: a depicts the light rays after refraction that are pointed in the direction of the sensor and contribute to L_w, the water leaving radiance. Term a is split into 2 parts: b is the portion of L_w which reaches the sensor, and c are the rays that are absorbed or scattered and lost before reaching the sensor. Term d represents sun glitter. This is the solar radiation that is reflected directly from the sea surface. Term e illustrates sky glitter. This is the portion of the sun's rays

that are scattered in the atmosphere and directed at the sensor. Terms d and e contribute to the radiance due to all surface reflection, L_r. Term f shows the radiation from L_r that is scattered out of the sensors field of view, and g shows the portion of L_r that is received by the sensor. The final radiance depicted is L_p, atmospheric path radiance, made up of h, i, j, and k. The portion of rays scattered towards the sensor by the atmosphere that comes directly from the sun is shown by h. The solar radiation that is directed to the sensor after some other atmospheric scattering is illustrated by i. Term j shows the contribution from the rays that upwell from the sea outside the sensor's field of view and get scattered toward the sensor by the atmosphere. Finally, term k represents the portion of rays reflected off the surface of the ocean, initially outside the sensor's field of view, which are scattered into the sensor by the atmosphere (Robinson, 2004).

L_s, radiance received by the sensor, is made up of contributions from L_p, L_w, and L_r. The relationship is shown in Equation (2).

$$L_s = L_p + TL_w + TL_r \qquad (2)$$

Where T is the beam transmittance of the atmosphere (Robinson, 2004). This demonstrates that the two largest effects of the atmosphere can be attributed to scattering and absorption.

2. Absorption

The atmosphere will have a varying effect on the electromagnetic energy based on wavelength. At wavelengths less than 0.3 μm or greater than 10 μm, atmospheric constituents absorb most of the incident energy making those parts of the spectrum opaque to solar radiation. The primary contributors to this phenomenon are ozone, carbon dioxide, and water vapor (Lillesand et al., 2004). Remote sensing technology exploits atmospheric areas of transparency called spectral windows (Thomas and Stamnes, 1999). Spectral windows occur throughout the electromagnetic spectrum as shown in Figure 9.
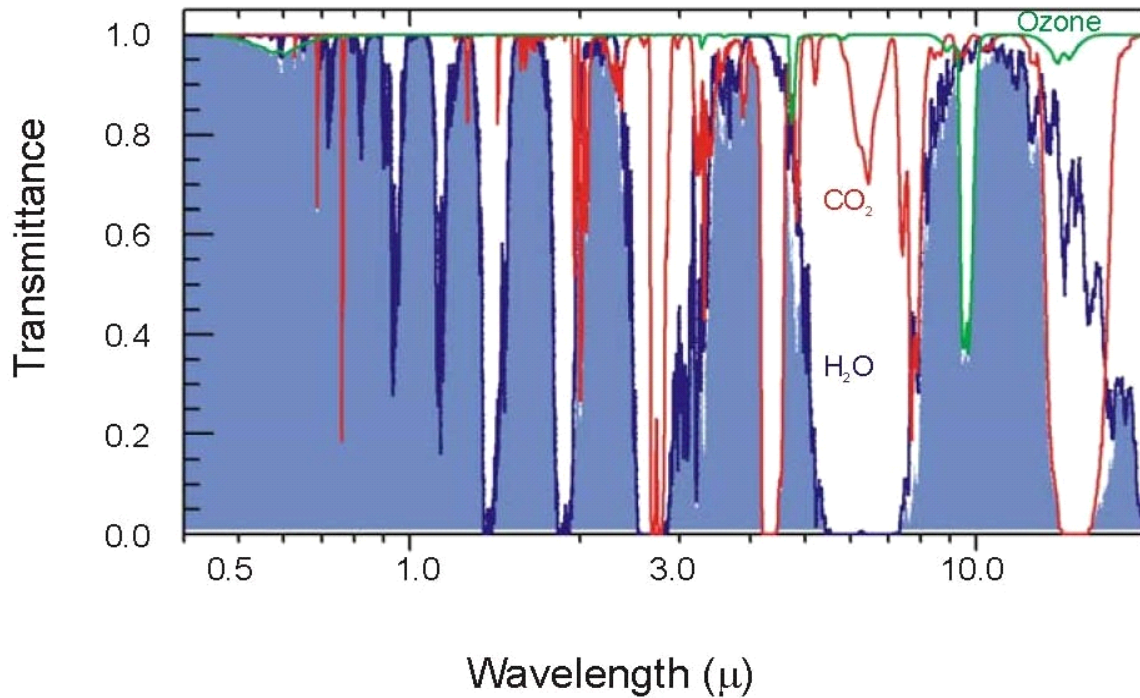
Figure 9.   Atmospheric spectral windows (shown in blue) (From Olsen, 2007)

3. Scattering

Scattering is the effect of atmospheric particles on electromagnetic radiation which causes the unpredictable redirection of energy (Jensen, 2000). The major consequences of atmospheric scattering on remote sensing are the reduction of radiant energy and the presence of unwanted gain at the sensor (Martin, 2004). Only 8 – 10% of the signal received at the satellite is due to ocean reflectance, while atmospheric scattering dominates the rest of the signal (Mishra et al., 2005). Three types of scattering occur in the atmosphere: Rayleigh, Mie, and Non-selective scattering.
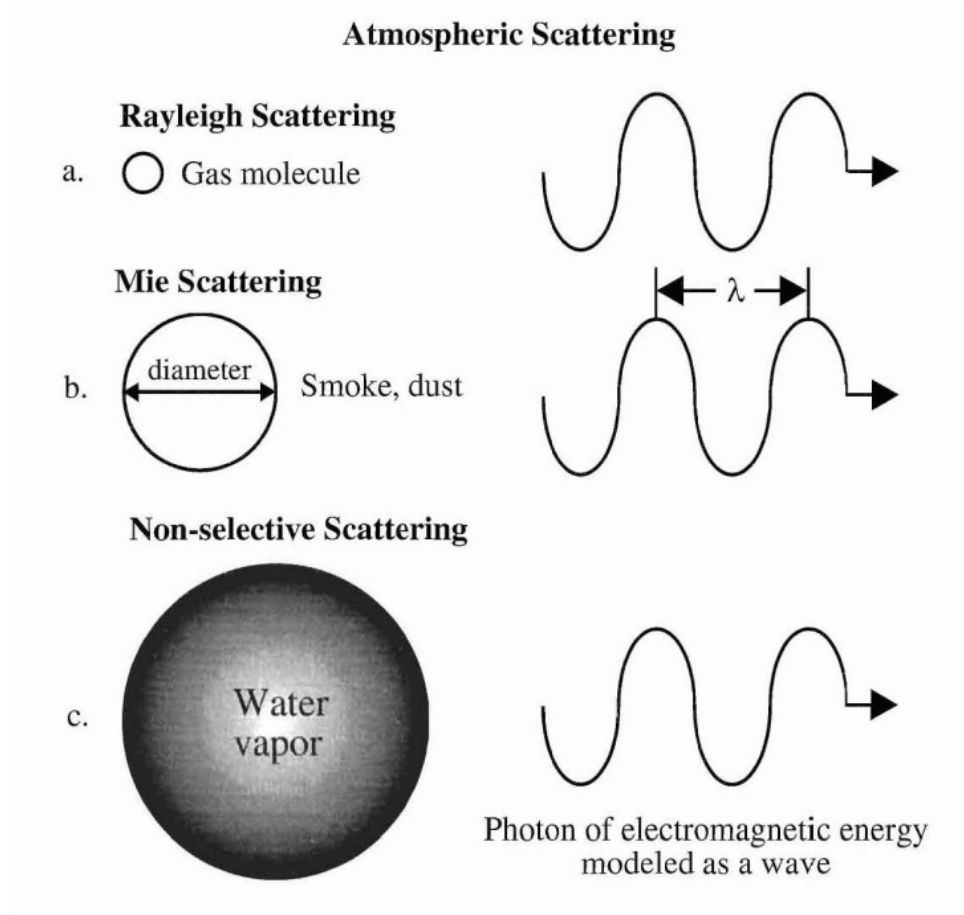
Figure 10.   Types of atmospheric scattering (From Jensen, 2000)

Figure 10 illustrates how the type of scattering that occurs is related to the wavelength of the incident energy and the size of the water droplet, gas molecule, or dust particle encountered (Jensen, 2000).

Rayleigh scattering occurs with particles that are many times smaller than the wavelength of incident energy. The effects of this type of scattering have an inversely proportional relationship to the fourth power of wavelength (Jerlov, 1976). This relationship creates a tendency for short wavelengths to be scattered more than longer ones. These effects are apparent in the visible range of the electromagnetic spectrum and are responsible for the blue color of water and the sky (Lillesand et al., 2004).

Mie scattering, or nonmolecular scattering, occurs when the wavelength of the energy and the size of the particles is comparable. This type of scattering is caused by dust, smoke, and particulates and influences longer wavelengths (Jensen, 2000). The third type, nonselective scattering, affects all wavelengths and occurs with large particles (5 - 100 μm) like water vapor. This scatters equal portions of the visible spectrum causing clouds and fog to appear white (Lillesand et al., 2004). All 3 types of scattering contribute to the portion of light that reaches the sensor which does not come directly from the Earth's surface, called path radiance (Depicted as L_P in Figure 8; Mishra et al., 2005).

D.   LIGHT AND WATER

As described earlier, light interactions within the atmosphere are complicated but have been studied and described by atmospheric scientists for some time. In order to use remotely sensed data for benthic classification purposes, the optical processes that occur in the water column must also be considered, and their effects removed. These processes are generally more complex because of the varying optical properties of water, the number of interactions that take place in the water column (Robinson, 2004), and the non-linearity of these interactions (Green et al., 2000). These interactions are affected by the highly variable presence of dissolved and particulate matter present in the water column which causes the optical properties of natural waters to vary over time and space (Mobley, 1994).

1.   Light Interactions with Water

Electromagnetic energy undergoes a number of interactions with the water column before reaching the satellite sensor. Jensen (2000) provides an illustration of these energy-matter interactions that affect aquatic remote sensing investigation. These are reproduced in Figure 11.

19
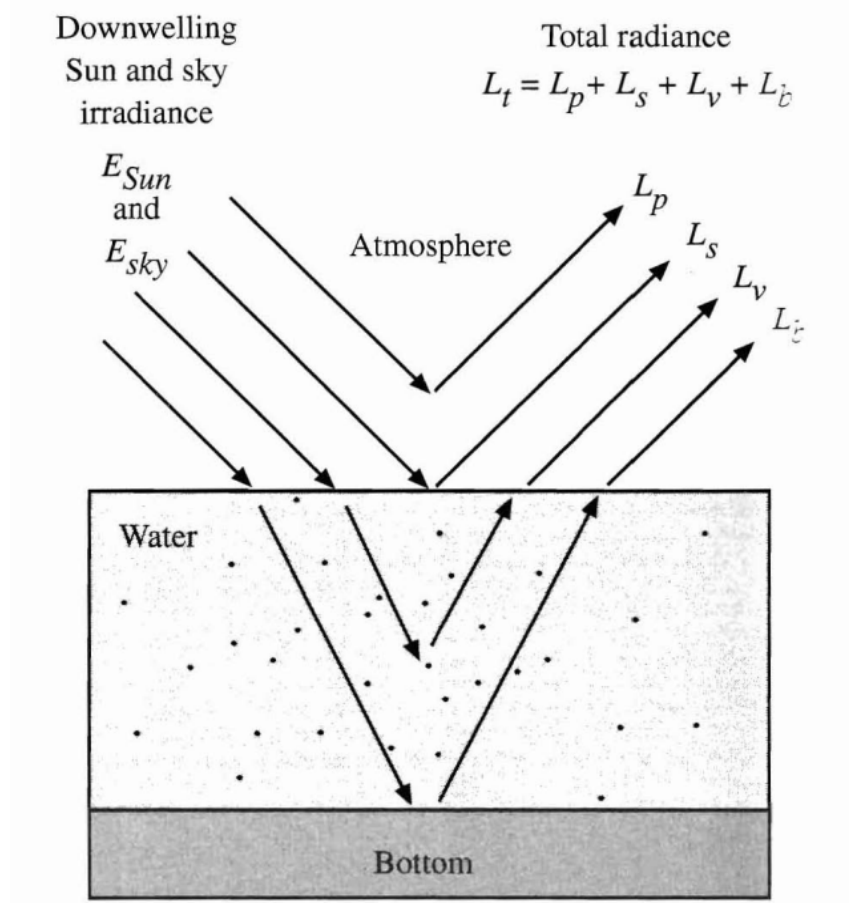
Figure 11.   Light interactions with water (From Jensen, 2000)

E_{Sun} represents the downwelling irradiance from the sun. E_{sky} Represents the sky irradiance. L_p is the path radiance referred to in Section C and in Figure 8. This is the portion of the downwelling radiation that is recorded by the sensor but has never reached the water. Water surface radiance, L_s, is the radiation that is reflected back to the sensor directly from the water's surface.   This term, also known as specular reflection (Robinson, 2004), is the cause of sunglint which provides little useful information and must be accounted for in image processing (Hedley et al., 2005). L_v is the subsurface volumetric reflection and illustrates the portion of radiation that interacts with the water column and then emerges without reaching the bottom.   This is the water column equivalent of L_p. L_b is the bottom radiance. This is the radiation that reaches the bottom

of the water body and is reflected back through the water column to the satellite sensor. This is the portion of the signal that is of greatest interest for benthic classification and mapping (Jensen, 2000).

2. Optical Properties and the Effects of Constituents

Water can be divided into 3 broad categories: pure water, pure seawater, and natural waters. Chemically pure water and seawater are free from traces of dissolved organic substances and are not found in nature (Morel and Prieur, 1977), but are useful as a baseline for the characteristics of natural waters (Robinson, 2004). Natural waters are those with varying concentrations of solutes and particulates that normally occur on Earth and are sensed by remote sensing systems. Water displays 2 types of optical properties: inherent optical properties (IOP's) and Apparent Optical Properties (AOP's). IOP's are those properties that depend only on the medium and are independent of the incident light (Smith and Baker, 1981). This type of property includes characteristics such as the absorption coefficient, index of refraction, and beam attenuation coefficient. AOP's are the properties that depend on both the medium and the ambient light field. These include the average cosines, irradiance reflectance, and diffuse attenuation coefficients (Mobley, 1994).

In addition to these basic optical properties of natural waters, the spectral response is affected by the presence of dissolved and particulate matter. These materials impact the absorption and scattering that occurs in the water column. Commonly encountered optically significant constituents of natural water include: suspended particulate matter, phytoplankton, and dissolved organic material (Robinson, 2004). These constituents come from biological and physical processes and vary widely in concentration and location over space and time. This problem has led to a development of water classification systems that account for the varying presence of these particles.

A basic system of classification was developed by Morel and Prieur (1977). In their system 2 large classes were developed, Case 1 and Case 2. Case 1 consists of water dominated by phytoplankton, while Case 2 water is dominated by inorganic particles. A more popular and detailed system was developed by Jerlov (1976) based on the water

clarity. This system divides open ocean waters into 5 classes: I, IA, IB, II, and III based on their transmittance curves. Type I represents the clearest oceanic waters and type III waters are the most turbid, generally found in coastal areas. Most coral reef waters are classified as Type I or II, allowing light to penetrate sufficiently for bottom cover classifications (Green et al., 2000).

E. SPECTRAL   CLASSIFICATION

The information gathered remotely can be used to identify the habitats or other features present in a particular location. Classification is the process of identifying, organizing into groups, and labeling pixels with similar properties, which can also be referred to as thematic mapping (Green et al., 2000; Lillesand et al., 2004). Many objects have well known and documented energy return characteristics, called spectral signatures, which can be used for terrain classification.

The information received at the sensor, and then used for classification, is affected by the previously discussed atmospheric and seawater interactions which must be accounted for to accurately map the area of interest. Following image processing aimed at correcting these effects, the data will be input into a statistical algorithm that will organize the individual pixels into distinctive groups (Green et al., 2000). This process can be supervised or unsupervised. Once the image is classified, the accuracy of the classification must be assessed using a descriptive or analytical method.

1.   Spectral Signatures

Spectral signatures, also referred to as response patterns or reflectance curves, are representations of the distinctive, characteristic energy reflected and absorbed by materials at specific wavelengths (Jensen, 2000). These energy patterns can be used to differentiate and classify substrates. In addition to the absorbing and reflective characteristics of these materials, these signatures are influenced by time, space, and the atmosphere. Spectral signatures are dependent on the wavelength and the effects of reflection, absorption, and transmission on the energy being measured (Lillesand et al., 2004). Terrain classification maps can be developed by exploiting the different spectral signatures collected from different locations in the imagery. These classifications take

advantage of the differences in material response patterns to separate various substrates into classes. Figure 12 illustrates the varying response between several types of manmade and natural materials.
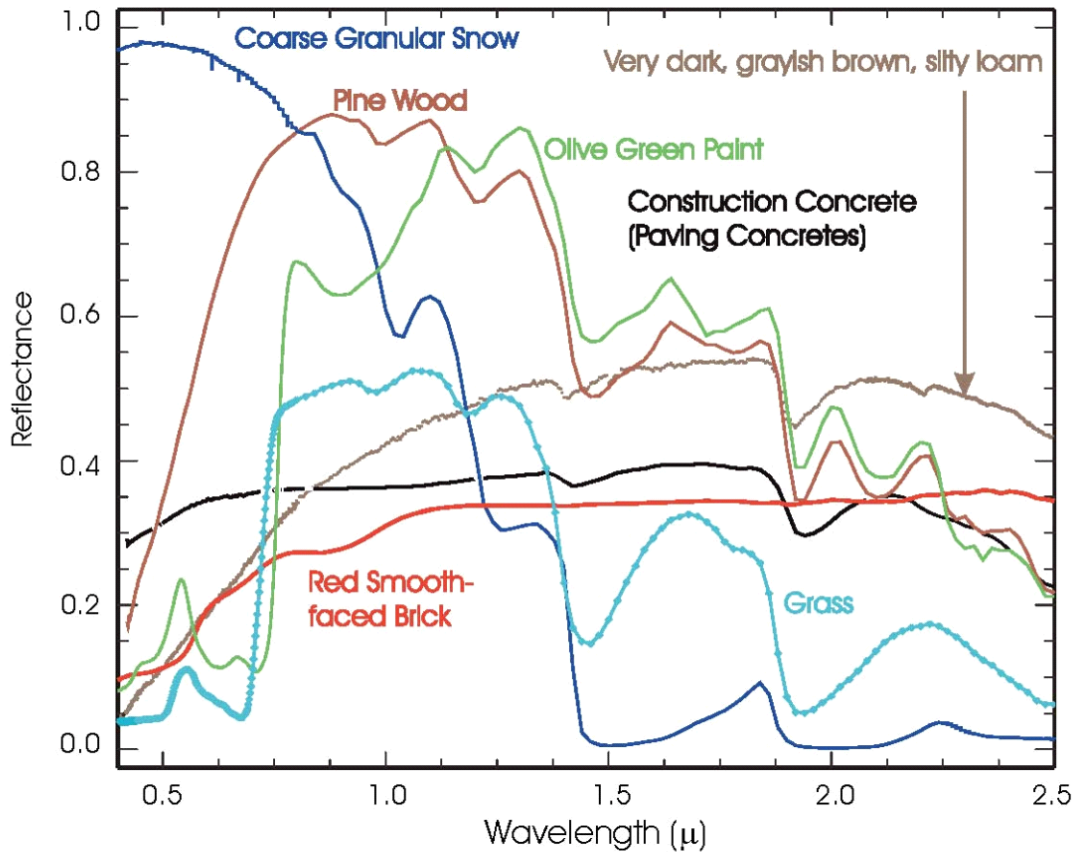
Figure 12.   High resolution spectral response curves of several materials (From Olsen, 2007)

Spectral signatures from marine and coastal environments can be used to guide coastal and benthic classifications, such as identifying mangrove populations (Wang et al., 2004), or mapping coral reefs and sublittoral habitats (Benfield et al., 2007). Figure 13 shows the distinct spectral response curves from a coral reef habitat, including non-coral substrates (Part A) and four types of coral (Part B). All of these substrates commonly occur in sublittoral environments.
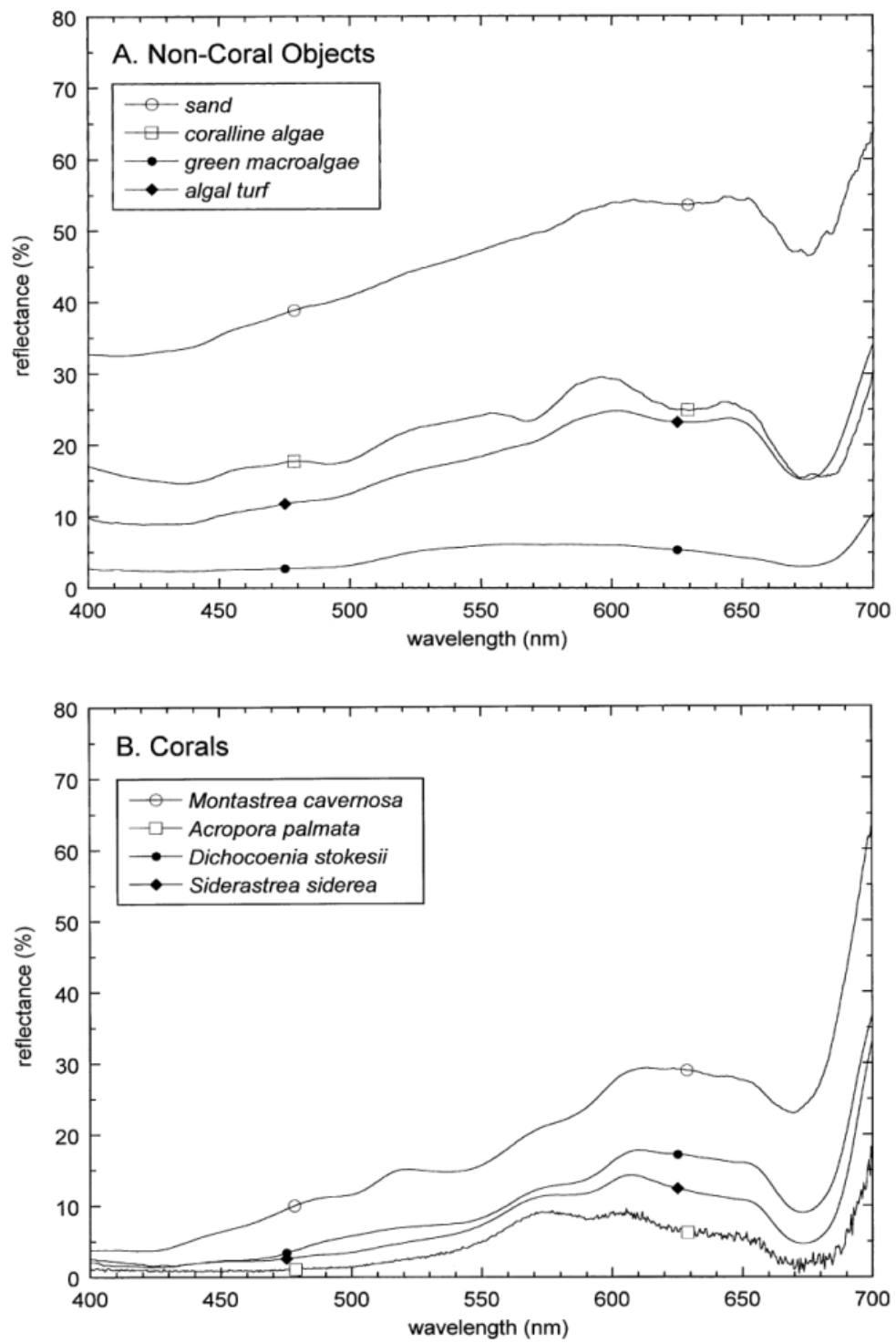
Figure 13.   Spectral responses of coral and non-coral substrates (From Lubin et al., 2001)

2. Image   Processing

The data collected at the sensor includes a significant amount of information that is not reflectance from the area of interest: because of the complex pathways in the atmosphere and water column, only about 10% of the data received comes from the ocean bottom (Mishra et al., 2005). In fact, atmospheric scattering accounts for the majority of the signal received by the sensor (Robinson, 2004). Several techniques designed to reduce these contributions are used to process the data prior to classification. These techniques include geometric correction, radiometric correction, sunglint removal, and water column correction.

a.   Geometric Correction

The raw data collected by a satellite sensor contains some inherent geometric distortions and requires some initial processing to be useful in mapping. These errors come from known sources such as panoramic distortion, Earth's rotation, orientation, instrument error, and variations in satellite orbits (Green et al., 2000). The correction process for these errors takes place in 2 steps: removing predicted errors and then accounting for unpredictable elements (Lillesand et al., 2004). These steps are usually performed by the image suppliers. The image received from the supplier should conform to a map projection and have a coordinate system so that it can be used for measurements, comparisons, and field studies (Green et al., 2000). The images used in this study were geometrically corrected by the suppliers (GeoEye and DigitalGlobe) prior to receipt by Naval Postgraduate School.

b.   Radiometric Correction

Radiometric correction is a sequence of steps that converts the data from relative brightness units to physical units useful for comparison with other physical quantities. This process occurs in 3 steps: 1) conversion of digital numbers (DN) to spectral radiance values, 2) conversion of spectral radiance to apparent reflectance, and 3) removal of atmospheric effects from absorption and scattering (Green et al., 2000). Steps

1 and 2 are performed to account for the way each sensor operates and records data. Conversion of data to spectral radiance follows a linear relationship as illustrated in Figure 14.
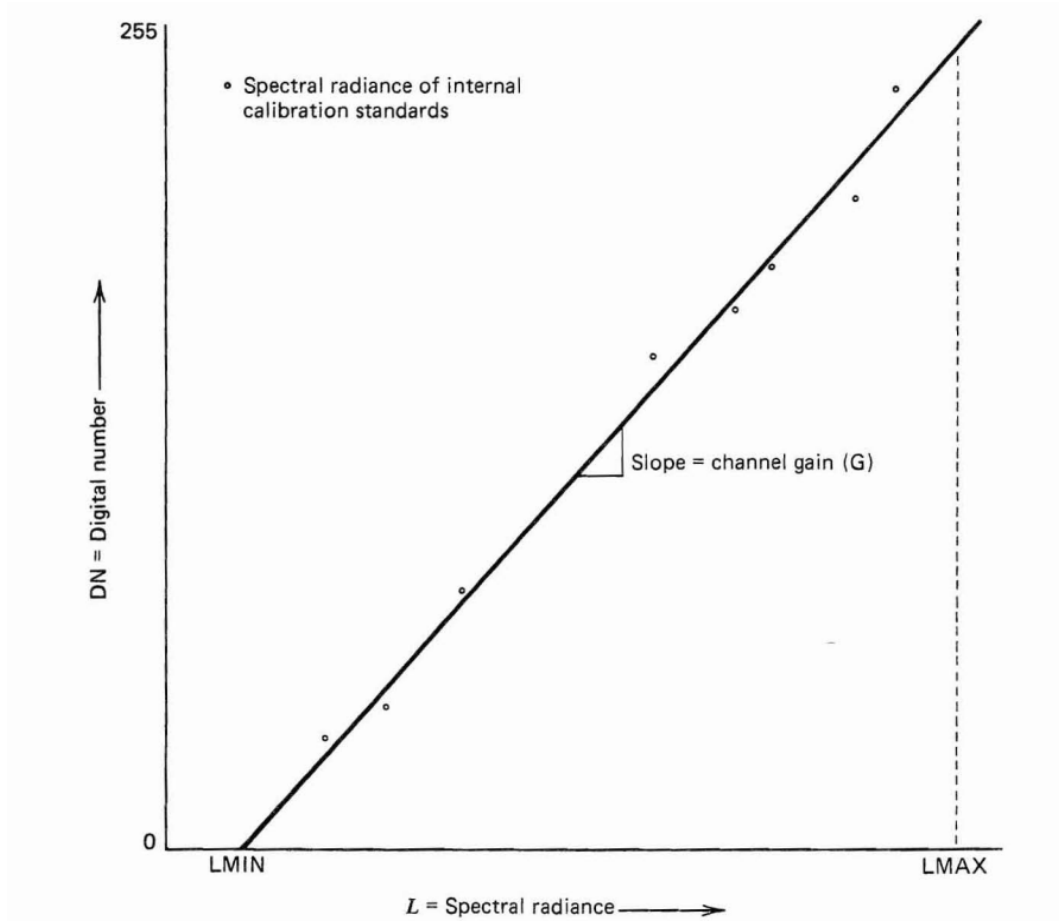
Figure 14.   Radiometric response function for a sensor channel (From Lillesand et al., 2004)

The spectral radiance can be found by solving the following linear equation (3):

$$DN = GL + B \qquad (3)$$

DN is the digital number recorded by the sensor. *G* is the slope of the response function, or gain. *L* is the spectral radiance. *B* represents the intercept of the response function or channel offset (Lillesand et al., 2004).

Conversion of this data to spectral radiance removes the effects of the sun elevation angle and the earth-sun distance at the time the image was aquired (Lillesand et al., 2004). This allows images taken at different times by different sensors to be compared directly. For example, Figure 15 illustrates the effects of seasonal changes on the solar elevation angle.
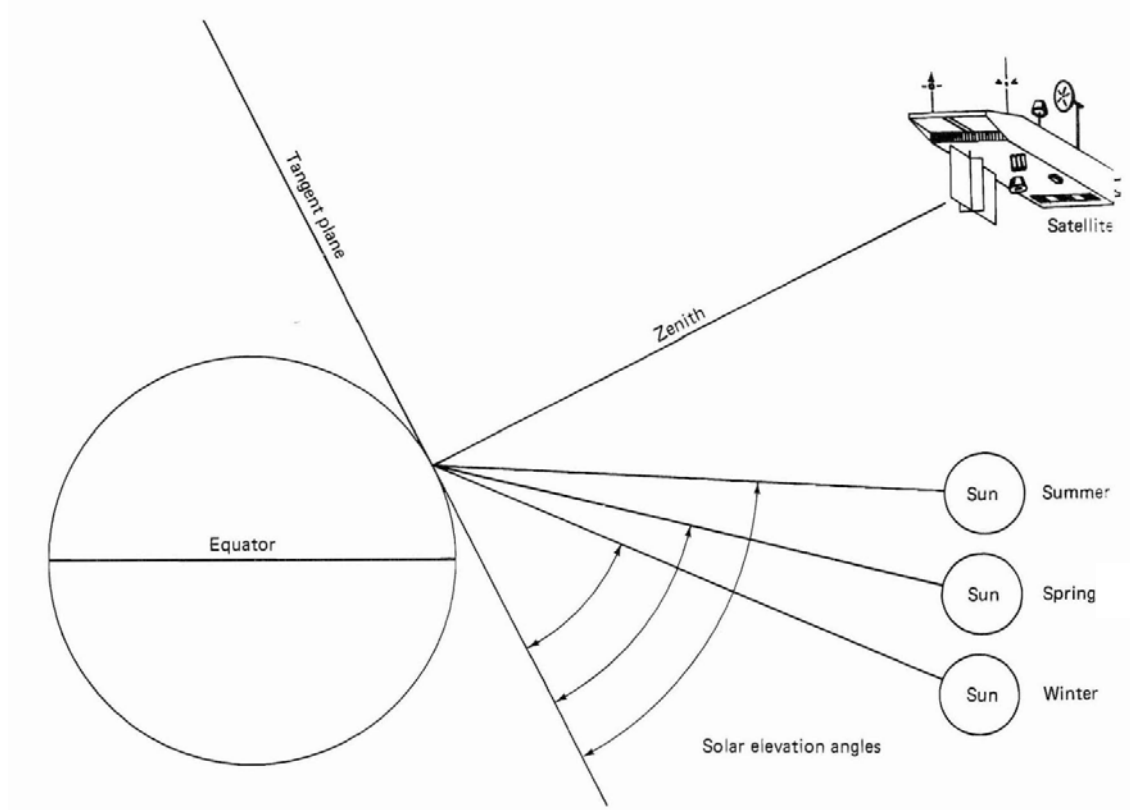
Figure 15.   Seasonal changes effect on solar elevation angle (After Lillesand et al., 2004)

Equation (4) represents the relationship between pixel values in radiance and apparent reflectance at the top of the atmosphere (Green et al., 2000).

$$\rho = \frac{\pi L d^2}{ESUN \cos(SZ)} \tag{4}$$

Here ρ is the unitless planetary reflectance at the satellite; L is the spectral radiance at the sensor calculated in the previous step; d^2 is the Earth-Sun distance in astronomical units, and is a function of the Julian Day of the image acquisition. *ESUN* is the mean solar

exoatmospheric spectral irradiance and is different for each sensor and band. *SZ* is the sun zenith angle in degrees when the data was collected, and is usually provided with the image (Green et al., 2000). The conversion from radiance to reflectance can be performed as a direct calculation by the user or can be accomplished using atmospheric correction software (e.g., ATCOR, a module for ERDAS IMAGINE).

In step 3 of the radiometric correction, the effects of atmospheric scattering and absorption can be removed. This is a crucial step because as much as 90% of the measured radiance can be due to the scattered light from the atmosphere (Robinson, 2004). Three atmospheric correction approaches are presented in Figure 16.
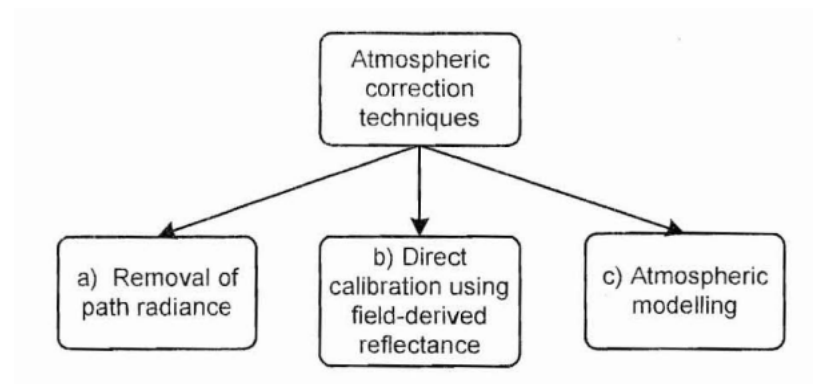
Figure 16.   Three approaches to atmospheric correction (From Green et al., 2000)

Methods that rely on the removal of path radiance, like the first approach, are generally simple and may require user input (Beisel and Woodhouse, 2004). These methods are not usually used for image to image comparisons and can range from simple to mathematically intensive calculations (Green et al., 2000). With sufficient field data, a direct calibration can be performed. In this second method, the reflectance of ground targets is measured *in situ* to generate a calibration curve that is then applied to the image (Green et al., 2000). The third approach relies on atmospheric modeling programs such as ACORN; ATCOR for ERDAS IMAGINE; and FLAASH for ENVI (Beisel and Woodhouse, 2004). This is perhaps the most sophisticated method and is suitable for image to image comparison (Green et al., 2000).

c. *Sunglint Removal*

Another unwanted contribution to the energy collected by the sensor is the light reflected from the sea surface, or sun glint (Robinson, 2004). In satellite remote sensing, the occurrence of sun glint is a common, usually unavoidable problem that can make images unusable for bottom feature mapping (Hedley et al., 2005). A technique using the characteristics of the near infrared band, developed by Hochberg et al. (2003), has shown increased accuracy in benthic habitat classifications. This technique uses the water absorption characteristics of the near infrared band to scale the glint intensities of the visible bands, effectively eliminating sun glint in the image and revealing previously obscured bottom features.

d. *Water Column Correction*

Light entering the water will experience exponential losses in intensity due to absorption and scattering in the water column (Robinson, 2004). Mapping underwater habitats is significantly affected by the depth of water because of the variable effects of attenuation on different regions of the electromagnetic spectrum (Green et al., 2000). Figure 17 shows variation in the spectral responses of the same substrate (i.e., seagrass) due to the non-uniform effects of attenuation on different electromagnetic bands at various depths.
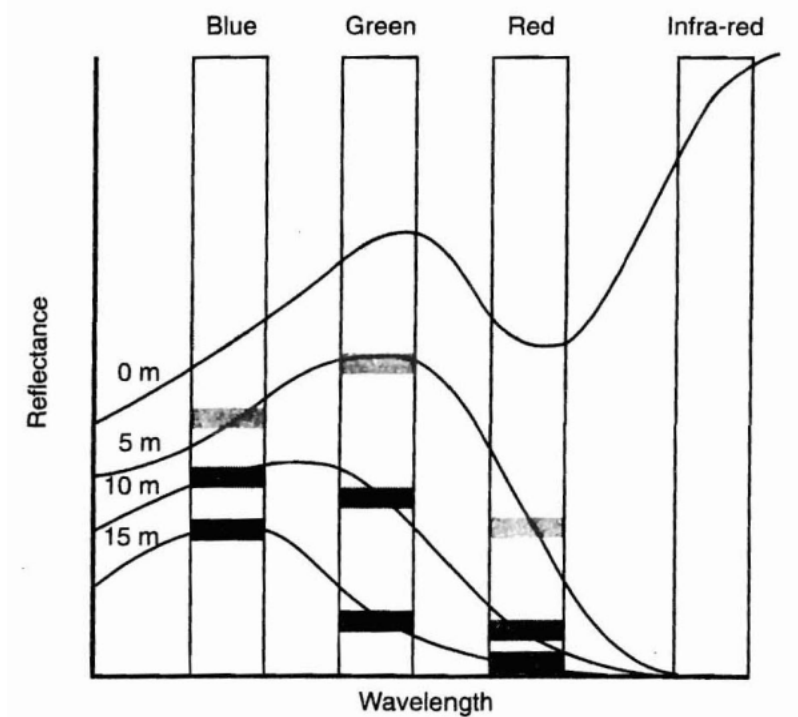
Figure 17.   Spectral response at varying depths (Green et al., 2000)

This effect is a commonly cited difficulty in marine remote sensing literature, and its removal has been shown to significantly improve classification accuracy in coral reef habitats (Mumby et al., 1998). In general, removal of these effects would require both measurement of depth for every pixel and knowledge of the characteristics of the water column (Green et al., 2000). Lyzenga (1978, 1981) proposed a simple image based method which compensates for these effects by producing a depth-invariant bottom index for pairs of spectral bands.

3. Supervised   Classification

Supervised classification techniques require the analyst to specify the types of ground cover in a scene through the use of training data (Lillesand et al., 2004). The generation of a classification has 2 distinct steps: training and classification. Training is the process of setting a spectral envelope for a class and, for supervised classification, requires *a priori* information about the image data and habitats to be mapped (Green et

al., 2000). The algorithm then compares the pixel data in the image to the user defined parameters and produces a classification output.

4. Unsupervised   Classification

Unsupervised classification does not use training data as the basis of classification. This method uses statistical clustering techniques to determine the dominant spectral signatures within an image (Green et al., 2000). Unsupervised classifications produce spectral classes based on natural groupings of image values and require no initial user knowledge of the area (Lillesand et al., 2004). This technique only requires the user to define the number of desired output classes and the statistical parameters for the algorithm to work within (Green et al., 2000). In the supervised approach useful information is defined and then spectral differentiation is examined, while the unsupervised method spectrally determines separable classes, and then the utility is defined (Lillesand et al., 2004).   The output classes should be evaluated, and possibly combined by the user to generate the final thematic map.

5.   Assessing Classification Accuracy

Accuracy assessment is a necessary step to determine the utility of remotely sensed data and its derived classification maps. One of the most common ways to present classification data for accuracy assessment is an error matrix (Congalton, 1991; Congalton and Green, 1999). Error matrices compare the results of an automated classification to known reference data on a category-by-category basis (Lillesand et al., 2004). The simplest form of assessing accuracy is the Overall accuracy. This method compares the number of pixels accurately classified to the total number of pixels (Congalton, 1991; Congalton and Green, 1999).

Additional information about each category identified can also be obtained through other measures of accuracy. Producer's accuracy is a measure of how well a certain area can be classified, and is obtained by dividing the total number of correctly identified pixels in a category by the total number of pixels in that category derived from reference data (Congalton, 1991; Congalton and Green, 1999). User's accuracy indicates the probability a pixel classified into a category actually represents that category on the

ground, and is calculated by dividing the number of correctly classified pixels in a category by the total number of pixels classified in that category (Lillesand et al., 2004). Each type of assessment provides a different measure and, in order to get a complete picture, all three should be considered.

III. PREVIOUS   WORK

Satellite remote sensing has become a valuable technique for benthic assessments and monitoring. By exploiting the reflected energy received by a satellite sensor, marine environments can be classified without requiring extensive field surveys (Lubin et al., 2001). As higher resolution data becomes available, new studies have been undertaken to determine what benefits can be derived from the additional information provided by more advanced systems. Recent studies have compared classifications of terrestrial and marine environments developed from airborne and space-based sensors, and have also investigated the potential advantages of increased spatial resolution. The studies of Mumby and Edwards (2002), Wang, et al. (2004), and Benefield, et al. (2007) are examples of this type of investigation.

Mumby and Edwards (2002) investigated the benefit of the increased spatial resolution available from IKONOS satellite imagery to mapping marine environments. This research compared the marine classification performances of LANDSAT, SPOT, IKONOS and CASI sensors in an area in the Turk and Caicos Islands. Image processing was used to develop benthic classification maps of a study area that had previously been extensively surveyed.   Mumby and Edwards hypothesized that the improved spatial resolution would lead to more accurate benthic classifications. This study concluded that classifications derived from IKONOS were 20% more accurate than previous satellite imagery (LANDSAT and SPOT), yet problems still existed in discriminating between coral, algae, and seagrass.

Wang, et al. (2004) performed a direct comparison of the classification accuracy obtained from IKONOS and QuickBird imagery for coastal habitats. This study tested the benefits of increased spatial resolution for mapping populations of mangroves on Panama's Caribbean coast. Images from both satellites were processed, subsets were chosen, and the spectral qualities of both satellites evaluated. Two sets of classification maps, based on 3 different types of mangrove canopies and 4 other land cover types, were produced using either multispectral data alone or including both multispectral and panchromatic data. The classification success of each method was evaluated using an

error matrix to compare statistical values. The authors found that IKONOS was slightly, yet significantly more accurate than QuickBird in the multispectral classification and that the addition of panchromatic data had little effect on either image (Wang, et al., 2004).

Benefield, et al. (2007) compared 2 sensors (LANDAT and QuickBird) and the accuracies of 3 mapping techniques for coral reef environments in Panama. This study was the first to assess QuickBird's accuracy in a coral reef habitat and surveyed an area containing previously unmapped substrates. The questions investigated included: determining what marine habitats could be discriminated; what benefit QuickBird's higher spatial resolution provides to classification accuracy; and what benefits were derived from contextual editing and object-oriented classification over traditional pixel based classification techniques. Accuracy was determined using error matrices and compared using Overall Accuracy, User's Accuracy, and Z-tests. This study determined that Overall and User's accuracies for QuickBird image classifications were significantly better than LANDSAT for all methods tested (Benefeild, et al., 2007). The benefits of QuickBird over LANDSAT in this study were found to be similar to those of IKONOS over LANDSAT from previous studies (e.g., Andréfouët et al., 2003; Capolsini et al., 2003).

IV. RESEARCH LOCATION

A. THE NORTHWEST HAWAIIAN ISLANDS

The Northwest Hawaiian Islands (NWHI) are a chain of largely uninhabited islands and atolls stretching about 1800 km across the North Pacific Ocean from Nihoa to Kure Atoll (Friedlander et al., 2008). Figure 18 illustrates the location of these islands, northwest of the main Hawaiian Islands.
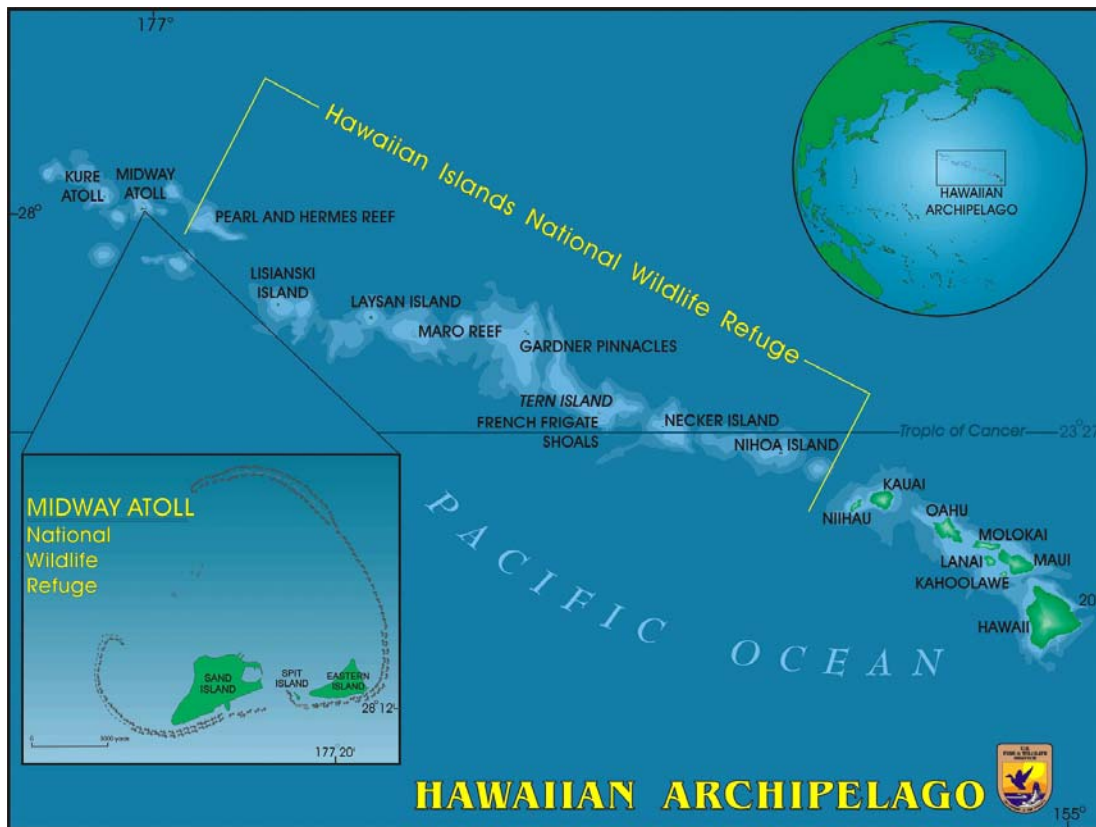
Figure 18.   Hawaiian Islands National Wildlife Refuge (From U.S. Fish & Wildlife Service)

Most of these islands are entirely built of coral and coralline algae carbonates. This area contains diverse wildlife, various habitat types, and the full range of marine life originally found in the main Hawaiian Islands (Rauzon, 2001). For these reasons, this area has a long history of protection by the U.S. Government, beginning in 1909 with the

35

creation of the Hawaiian Island Bird Reservation by President Roosevelt through Executive Order 1019 (Rooney et al., 2008). In 2006, Presidential Proclamation 8031 designated the NWHI as the Northwestern Hawaiian Islands Marine National Monument to preserve the unique ecosystems and cultural significance of the region. The area covers 13,000 square kilometers and is home to one of the most extensive and healthy coral reef systems in the world (Grigg et al., 2008). The combination of clear water, diverse substrates make this area an ideal test area for conducting this benthic terrain classification study.

B. MIDWAY ATOLL

Midway Atoll is located at 28.2 N latitude and 177.3 W longitude approximately 1850 km northwest of Honolulu, near the end of the NWHI chain. The site is both a National Wildlife Refuge and the Battle of Midway National Memorial managed by the U.S. Fish and Wildlife Service. The atoll contains 3 islands surrounded by a nearly circular fringing reef about 10 km in diameter (Rooney et al., 2008). See Figure 19 below.
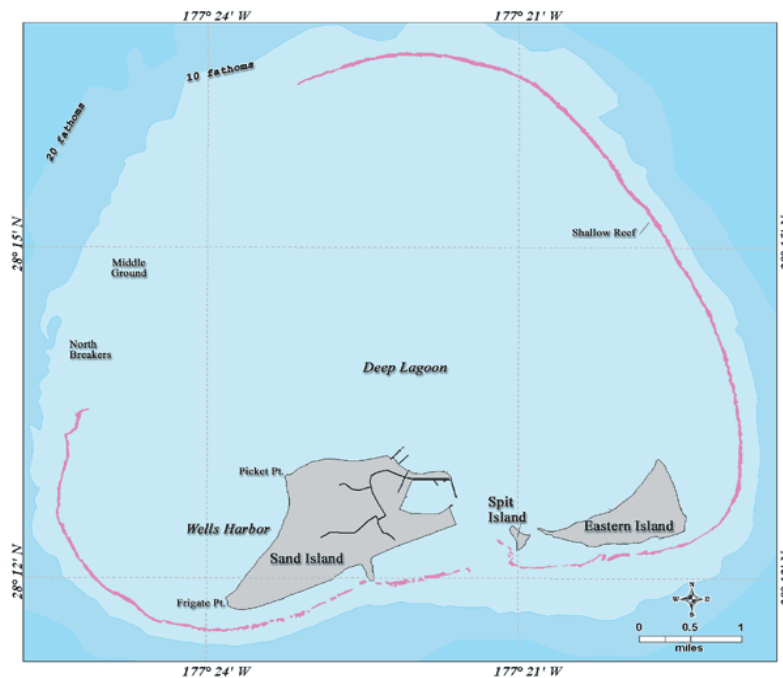
Figure 19.   Map of Midway Atoll (From http://www.nicholas.duke.edu/blog/hawaii/skin-photos/Midway.gif)

Sand Island is the largest (~1200 acres) and is the only continuously inhabited land in the NWHI archipelago. The 2 smaller land masses, Eastern Island and the ephemeral Spit Islet, are about 340 acres combined and are primarily bird habitats (Rooney et al., 2008). Midway Atoll was first inhabited and used as a communications station by the Pacific Cable company in the early 20th century. The atoll next served as a stop on the Pan American Airlines Clipper route and then became an important naval base during World War II (Rooney et al., 2008). The U.S. Navy maintained Midway as an active air facility and listening post throughout the Cold War and then, in July of 1997, turned over the entire atoll to the U.S. Fish and Wildlife Service (Burger and Gochfeld, 2000). Today, Midway Atoll is a nesting and resting place for many seabird species and home to critically endangered Hawaiian monk seals, endangered Laysan teals, and threatened green sea turtles.

A nearly circular fringing reef encloses and protects the lagoon of Midway Atoll. Its depths range from approximately 25 m to exposed reef crests, allowing the whole area to be mapped using satellite remote sensing (Camacho, 2006). The lagoon contains a wide range of wildlife and a variety of bottom types including: coral reefs, algae, sand, and rubble (Rauzon, 2001). Because of previous and ongoing Naval Postgraduate School research conducted at Midway Atoll, a library of multispectral imagery was available for this location, making this an ideal location for comparison of satellite classification accuracies.

THIS PAGE INTENTIONALLY LEFT BLANK

V. MATERIALS AND METHODS

A. MATERIALS

1. QuickBird

On 18 October 2001, Digital Globe Inc. launched the QuickBird remote sensing satellite. The onboard multispectral sensor delivers panchromatic images with 0.61 to 0.72 m resolution and multispectral images in blue, green, red, and near infrared with 2.44 to 2.88 m resolution from a 450 km orbit. When launched, QuickBird achieved the highest resolution imagery available commercially, surpassing the resolution collected by IKONOS. QuickBird can image targets up to 30º off nadir and has an orbital period of 93.5 minutes (Digital Globe, 2007). Table 2 provides an overview of QuickBird's characteristics.

Launch Date	18 October 2001
Launch Location	Vandenberg Air Force Base, CA
Orbit Altitude	450 km
Orbit Inclination	97.2º, sun-synchronous
Speed	7.1 km/second
Equator Crossing Time	10:30 a.m. (descending node)
Orbit Time	93.5 minutes
Revisit Time	1-3.5 days depending on lat (30º off-nadir)
Swath Width	16.5 km at nadir
Digitization	11 bits

Resolution	Pan: 61 cm (nadir)
	          72 cm (25º off-nadir)
	MS: 2.44 m (nadir)
	          2.88 m (25º off-nadir)

Image Bands	Pan: 725 nm Blue: 479.5 nm Green: 546.5 nm Red: 654 nm Near IR: 814.5 nm

Table 2.   QuickBird characteristics (Digital Globe, 2007)

A high resolution multispectral QuickBird image of Midway Atoll was acquired on 18 October 2007 at 23:02:34 GMT (12:02:34 local). The image is shown in Figure 20.
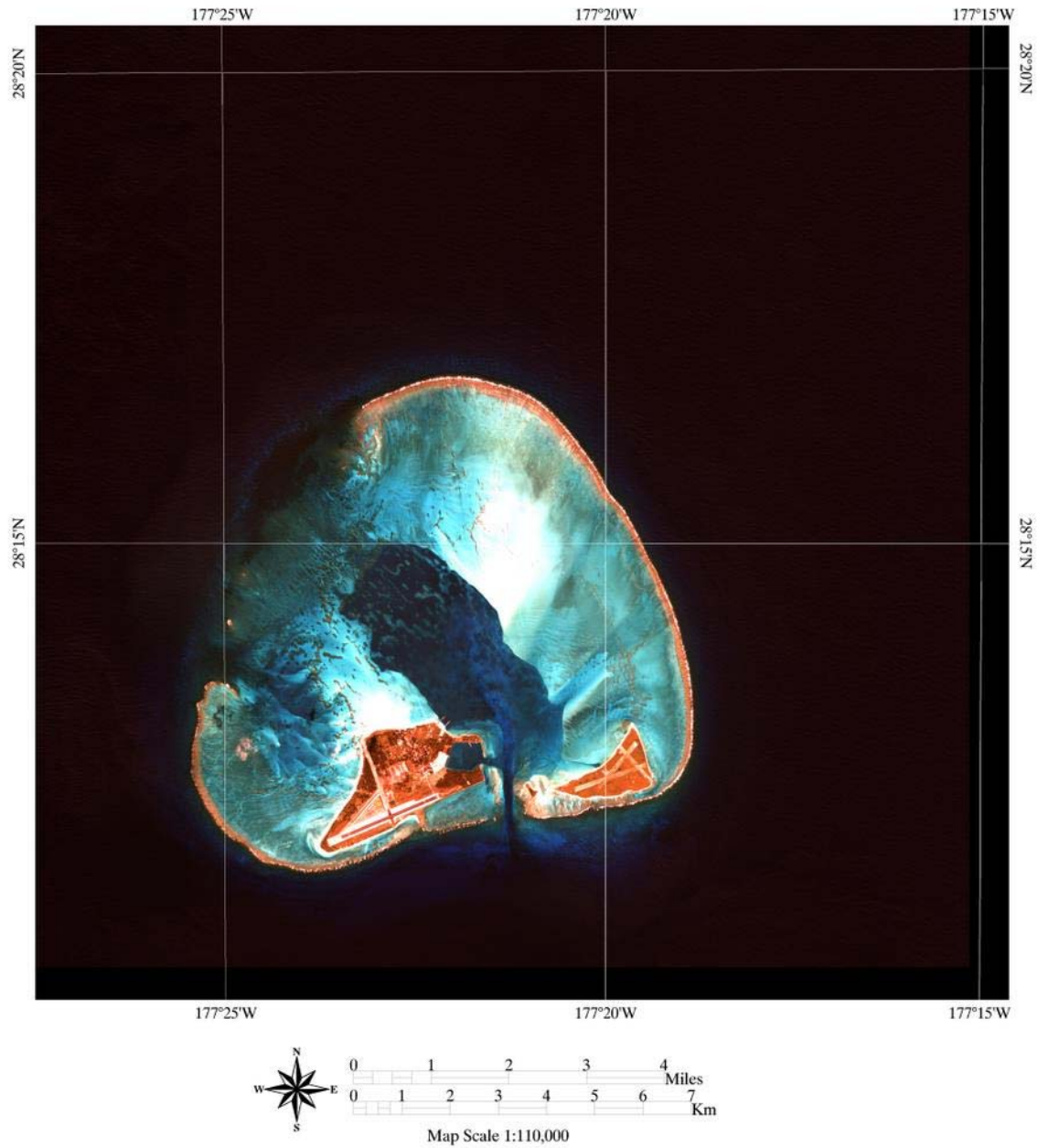
Figure 20.   18 October 2007 QuickBird image of Midway Atoll

2. IKONOS

The IKONOS multispectral imaging satellite was launched by Space Imagaing (now GeoEye) on 24 September 1999. Orbiting the Earth at 681 km, IKONOS produces panchromatic imagery with resolution ranging from 0.82 to 1.0 m and multispectral imagery with resolution from 3.2 to 4.0 m. The IKONOS panchromatic sensor made history as the world's first 1 meter commercial remote sensing satellite. The satellite's multispectral sensor collects data in 4 spectral bands (blue, green, red, and near infrared) and 1 panchromatic band. IKONOS orbits the Earth every 98 minutes and is capable of imaging targets up to 26º off-nadir (GeoEye, 2006). A summary of IKONOS's characteristics is provided in Table 3.

Launch Date	24 September 1999
Launch Location	Vandenberg Air Force Base, CA
Orbit Altitude	681 km
Orbit Inclination	98.1º, sun synchronous
Speed	7.5 km/second
Equator Crossing Time	Nominally 10:30 a.m. solar time
Orbit Time	98 minutes
Revisit Time	Approximately 3 days at 1-meter resolution, 40º altitude
Swath Width	11.3 km at nadir
Digitization	11 bits
Resolution	Pan: 0.82 m (nadir) 　　　1.0 m (26º off-nadir) MS: 3.2 m (nadir) 　　　4.0 m (26º off-nadir)
Image Bands	Pan: 0.526 - 0.929 μm Blue: 0.445 - 0.516 μm Green: 0.506 - 0.595 μm Red: 0.632 - 0.698 μm Near IR: 0.757 - 0.853 μm

Table 3.　　　IKONOS characteristics (GeoEye, 2006)

A multispectral IKONOS image of Midway Atoll was acquired on 16 May 2008 at 22:38:39 GMT (10:38:39 local). This image is displayed in Figure 21.
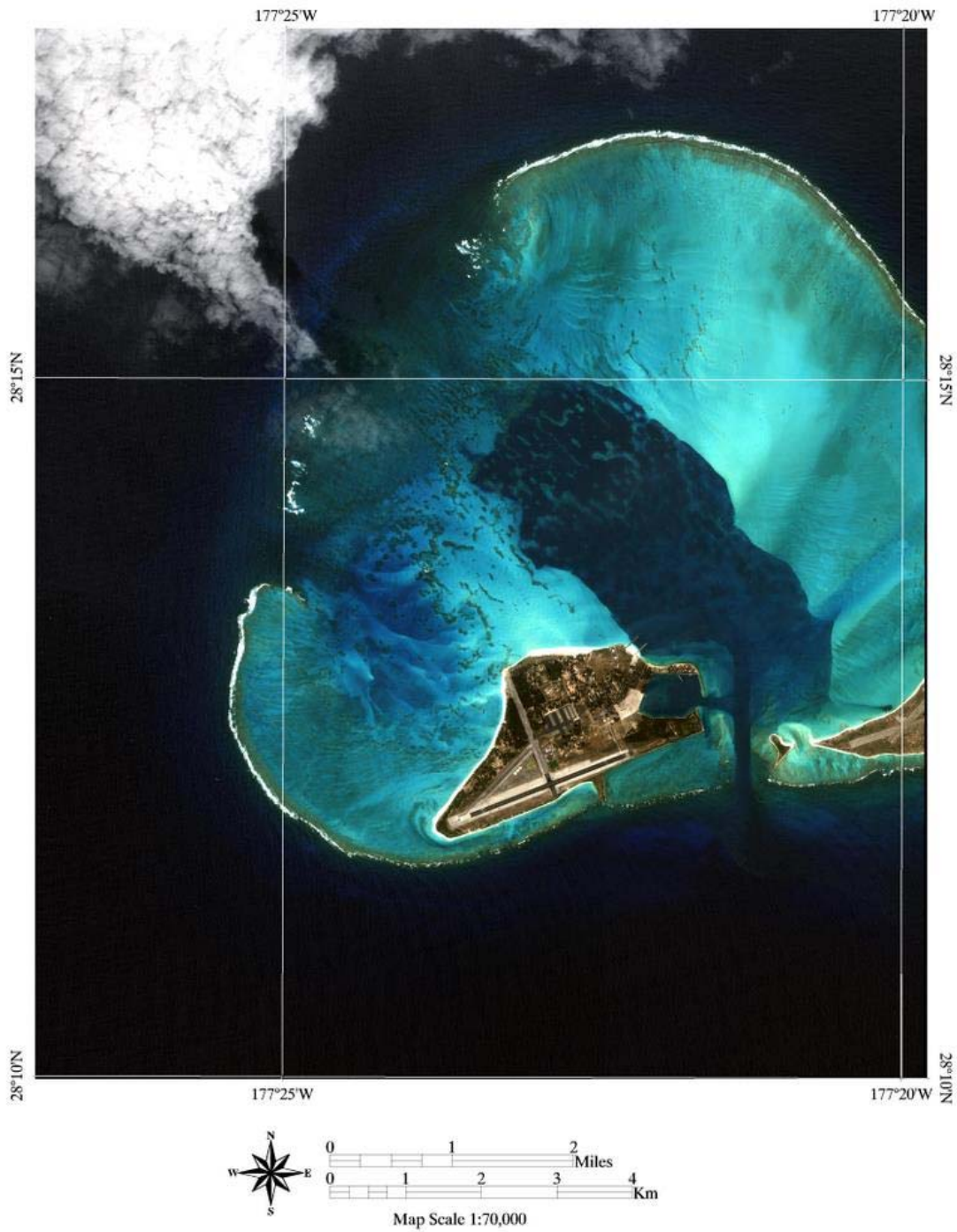
Figure 21.   16 May 2008 IKONOS image of Midway Atoll

3. Software

a.   ENVI 4.4

The Environment for Visualizing Images (ENVI), a product of the ITT Industries Corporation, is a software package for viewing, analyzing, and extracting information from numerous sources to include: panchromatic, multispectral, hyperspectral, radar, thermal, and lidar data (ITT, 2007). ENVI 4.4 was used to perform spatial subsetting, radiance conversion, atmospheric correction, glint removal, water column correction, and benthic classification on both the QuickBird and IKONOS imagery in this research. ENVI's band math function was used extensively throughout the image processing.

b.   ACORN 5.0

Atmospheric Correction Now (ACORN) is a software package by ImSpec LLC that provides atmospheric correction for multispectral and hyperspectral data in the range of 350 to 2500 nm. ACORN uses look-up-tables calculated with the MODTRAN-4 radiative transfer code to model atmospheric gas absorption and scattering effects (ImSpec, 2004). MODTRAN-4 is a version of the U.S. Air Force atmospheric transmission, radiance, and flux model developed jointly by Spectral Sciences, INC. and the Air Force Research Laboratory Space Vehicles Division (Berk et al., 1999). ACORN uses this model to convert calibrated sensor radiance measurements to apparent surface reflectance while accounting for the affects of the atmosphere (ImSpec, 2004). ACORN offers a range of atmospheric correction modes. All ACORN atmospheric corrections in this research were carried out using Mode 5: Radiative transfer atmospheric correction of calibrated multispectral data.

c.   ATCOR

Leica Geosystems Geospatial Imaging distributes the Atmospheric Correction (ATCOR) algorithm which operates as a module in their ERDAS IMAGINE 9.0 software imaging package. ATCOR performs de-hazing (terrestrial images only), atmospheric, and topographic corrections on multispectral and hyperspectral imagery. Its

atmospheric database contains a wide range of radiative transfer values for various weather conditions and sun angles calculated using the MODTRAN-4 code. ATCOR for IMAGINE 9.0 is comprised of 2 modules; ATCOR2 for relatively flat "two dimensional" terrain and ATCOR3 for rugged "three dimensional" terrain (Leica, 2006). All ATCOR atmospheric corrections in this research were performed using ATCOR2.

B. METHODS

1. Quic   kBird

a.   *Spatial Subsetting*

The 18 October 2007 QuickBird image was initially subset in order to remove unwanted portions of the image and to reduce processing time. A subset was chosen that comprises all habitats, including the entire lagoon, fore reef environments, and surrounding visible seaward benthic substrate, but leaving out deep ocean waters seaward of the crest. A mask was then applied to this subset to remove unwanted land and clouds. The mask was constructed by creating a band threshold Region Of Interest (ROI) using the image's NIR band to distinguish the land and clouds (high NIR returns) from the water (low NIR returns). Manual editing was used to fine tune ROI before converting it into an image mask. The masked subset is displayed in Figure 22.
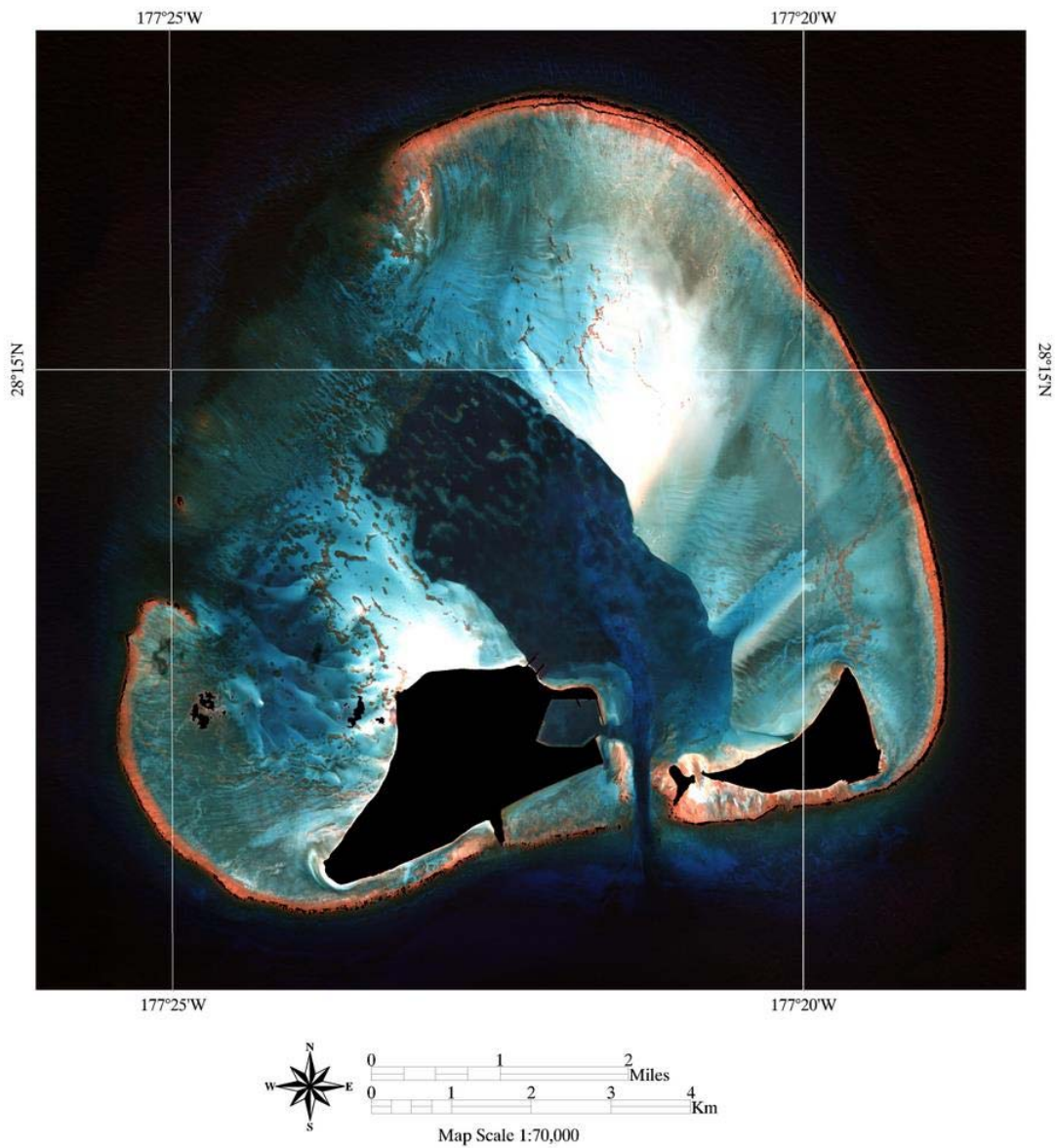
Figure 22.   Masked QuickBird image subset

b.   *Radiance Conversion*

QuickBird products are delivered to the user as radiometrically corrected image pixels. These pixels are represented as digital numbers (DN) whose values are a function of how much light (spectral radiance) enters the sensor's aperture at the time of acquisition. These DNs are unique to the sensor and the environmental conditions at the

time of acquisition and should not be directly compared to imagery from other sensors or to other QuickBird imagery captured under different conditions. Therefore the imagery must be converted to spectral radiance before analysis and comparison with other imagery can occur (Krause, 2003; 2005).

Conversion to top-of-atmosphere spectral radiance (L_λ) is a two step process that involves multiplying radiometrically corrected image pixels (q) by the appropriate absolute radiometric calibration factor (K) and dividing the product by the effective bandwidth ($\Delta\lambda$). This step is defined in Equation (5).

$$L_{\lambda Pixel, Band} = \frac{K_{Band} \bullet q_{Pixel, Band}}{\Delta\lambda_{Band}} \tag{5}$$

The absolute radiometric calibration factor was obtained from the metadata supplied with the QuickBird imagery, and the effective bandwidth was obtained from Krause (2005). This step was performed using the QuickBird Radiance Calibration Utility in ENVI's preprocessing software package.

c.   Atmospheric Correction

Removing the optical effects caused by light's interaction with the atmosphere before image analysis is imperative and yields significant improvements to subsequent results. As mentioned in Chapter II, Section E-2-*b*, Green et al. (2000) differentiate atmospheric correction techniques into three broad groups: removal of path radiance, direct calibration using field-derived reflectance, and atmospheric modeling. Two different atmospheric modeling techniques were applied to the QuickBird image along with a simple conversion to reflectance in order to assess which technique produced the best results, as detailed below. Corrected vegetation spectra were compared in order to choose the best correction technique.

(1) Conversion to Top-of-Atmosphere Reflectance (TOAR): The first technique used was a conversion to top-of-atmosphere reflectance. This method does not account for topographic or atmospheric distortions. The calculation for top-of-atmosphere band-averaged reflectance ($\rho\lambda$) is shown in Equation (6) (Krause, 2005).

$$\rho_{\lambda Pixel,Band} = \frac{L_{\lambda Pizel,Band} \bullet d_{ES}^2 \bullet \pi}{Esun_{\lambda_{Band}} \bullet \cos(\theta_s)} \tag{6}$$

L_λ is spectral radiance, d_{ES} is the Earth-Sun distance at the time of acquisition (calculated based on the guidance in Krause, 2005), Esunλ is the mean solar exoatmospheric spectral irradiance (obtained from Krause, 2005) and θS is the solar zenith angle (obtained from metadata). The band math utility in ENVI was used to perform this calculation. The results are shown in Figure 23, which illustrates spectral profiles of vegetation from the unprocessed DN image and the 3 atmospheric correction techniques (TOAR shown in red).
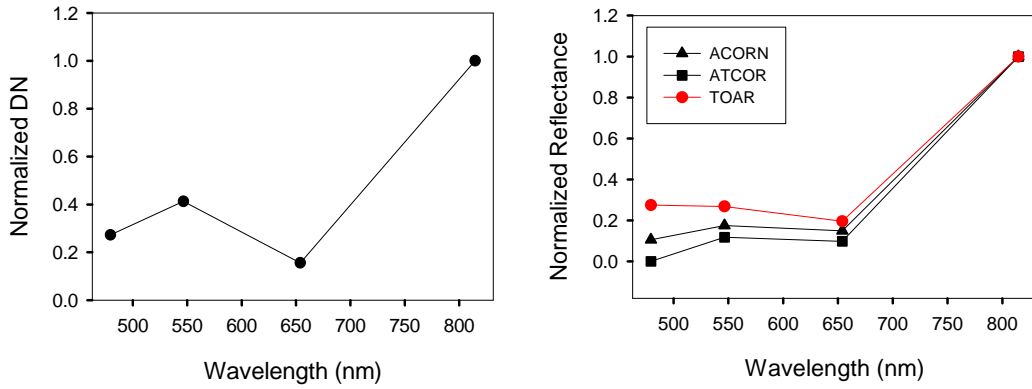
Figure 23. QuickBird vegetation spectral profiles: (left) unprocessed, (right) top-of-atmosphere reflectance (shown in red)

(2) ACORN 5.0: The image was also separately processed with ACORN's atmospheric correction algorithm. The input for this correction was the DN image subset (.bil format of signed integers as required by ACORN) since ACORN performs a radiance conversion as part of its algorithm. ACORN input files include a spectral response file, a gain file, and an offset file. The data for the multispectral response file was obtained directly from Digital Globe. Gain and offset files are used to convert the original data (varying units depending on the source) into radiance with units of W/m2·µm·sr (ImSpec, 2004). The mathematics outlined in Krause (2005) were used to calculate the coefficients for the gain file that convert unprocessed DNs to radiance values. Zero values were used for each of the 4 bands in the offset file since the

conversion to radiance does not require addition or subtraction. In addition to these 3 files Acorn required inputs for several variables in its model. Table 4 contains the input data used with ACORN that was not obtained from the image metadata along with the data source.

Variable	Value	Source
Atmospheric Model	"Tropical"	Experimentation
Atmospheric Visibility	100 km	ACORN User's Manual
Atmospheric Water Vapor	25 mm	ACORN User's Manual

Table 4.   QuickBird ACORN input values

The vegetation spectral profile from the ACORN atmospherically corrected image (shown in red) is displayed alongside a vegetation spectral profile from the unprocessed image (Figure 24).
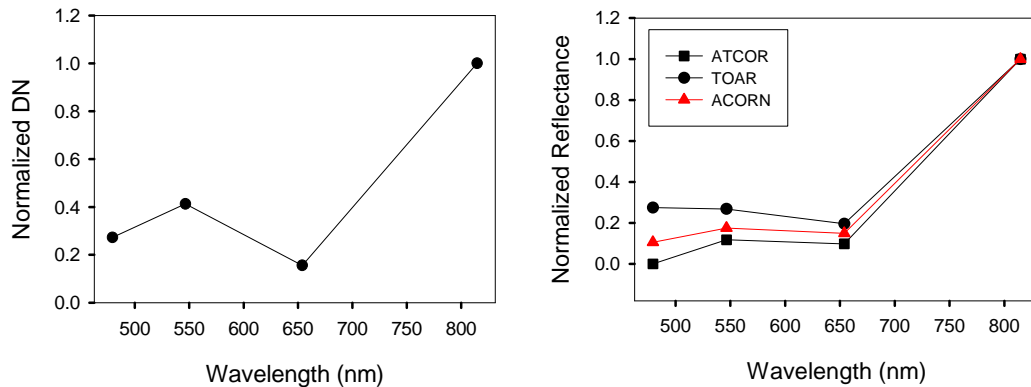
Figure 24.   QuickBird vegetation spectral profiles: (left) unprocessed, (right) ACORN atmospheric correction (shown in red)

(3) ATCOR: A third atmospheric correction algorithm was used on the original subset (ATCOR2 for ERDAS IMAGINE 9.0). This correction was applied to the subset of the unprocessed DN image file since ATCOR performs a radiance conversion as part of its correction algorithm. ATCOR2 requires a calibration file to convert the raw image DN to spectral radiance. Other required inputs include: sensor type, solar zenith angle, ground elevation, scene visibility, and a model for solar

region. This solar region model requires knowledge of the satellite and sun tilt angles, azimuth angle, and atmospheric model (Leica, 2006).

The ATCOR User Manual was used to derive the values in the calibration file. The manual also contains equations for calculating the solar zenith angle, tilt angle, and azimuth angle. The atmospheric model used was "US Standard Maritime." The value for scene visibility was then adjusted, and the quality of the output was reviewed. The visibility setting that produced the best result was the maximum allowed value of 120 km. The resulting vegetation spectral profile (shown in red) is displayed in Figure 25 and compared to a vegetation spectral profile from the unprocessed image.
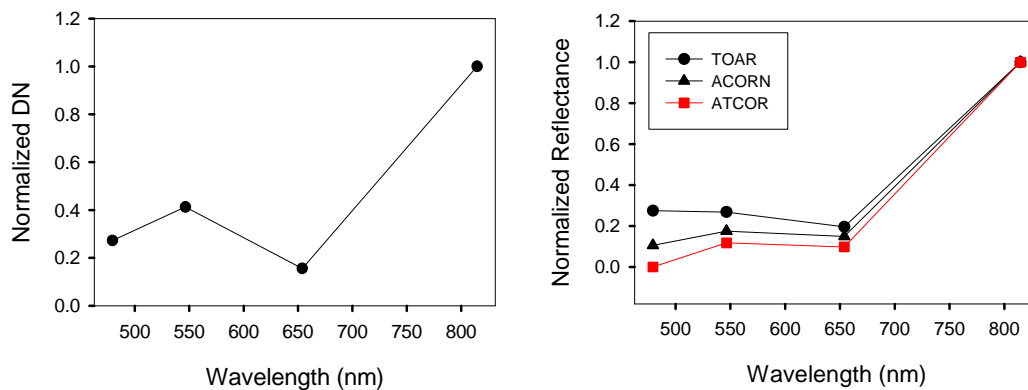
Figure 25.   QuickBird vegetation spectral profiles: (left) unprocessed, (right) ATCOR atmospheric correction (shown in red)

The displayed vegetation profiles were values averaged over a small area of grass pixels from the same location in each corrected image. Despite a reasonable vegetation spectrum, as shown in Figure 25, the results from the ATCOR atmospheric correction were flawed: they contained an unacceptable number of negative pixels, particularly in the red band of deep water pixels (i.e., the image was overcorrected). This result mirrors the findings obtained by Camacho (2006) during ATCOR processing of a different QuickBird image of Midway Atoll.

Following spectral comparisons for all 3 methods, ACORN was chosen as the best atmospheric correction algorithm and used for all subsequent

QuickBird image processing. This decision was based primarily on the quality of the spectral profiles for terrestrial vegetation in the corrected image.

d. Glint Removal

A large percentage of satellite imagery of shallow coastal environments contains sea surface effects that compromise the reconnaissance of benthic features. The imagery is often severely contaminated by reflected light (glint) on the crests and slopes of waves that are generated by surface winds. Hochberg et al. (2003) first addressed this issue and devised a method to filter out most of the glint effects by using data from the near-infrared (NIR) band to characterize the spatial distribution of relative glint intensity. Hedley et al. (2005) updated the Hochberg et al. method providing a more robust technique that was also simpler to implement. This technique establishes linear relationships between the NIR and the visible bands based on a sample of image pixels selected from multiple regions displaying a range of sun glint. The slope of the linear relationship (b_i) is then used to correct the image based on the expression shown in Equation (7).

$$R_i' = R_i - b_i(R_{NIR} - Min_{NIR})$$ (7)

Where R_i is the uncorrected pixel value for band i, b_i is the slope of the regressed line between band i and the NIR band, R_{NIR} is the pixel NIR value, and Min_{NIR} is the lowest NIR pixel value in the image. Hochberg et al. (2003) point out that the inclusion of the Min_{NIR} term constitutes a simple linear atmospheric correction in addition to the glint correction. This term was omitted since an ACORN atmospheric correction had already been performed.

This step was applied to the ACORN atmospherically corrected image subset with a mask applied to remove any land and cloud cover. A sample of image pixels was selected from multiple sites of optically deep water displaying a range of sun glint. Figure 26 illustrates the sample sites.
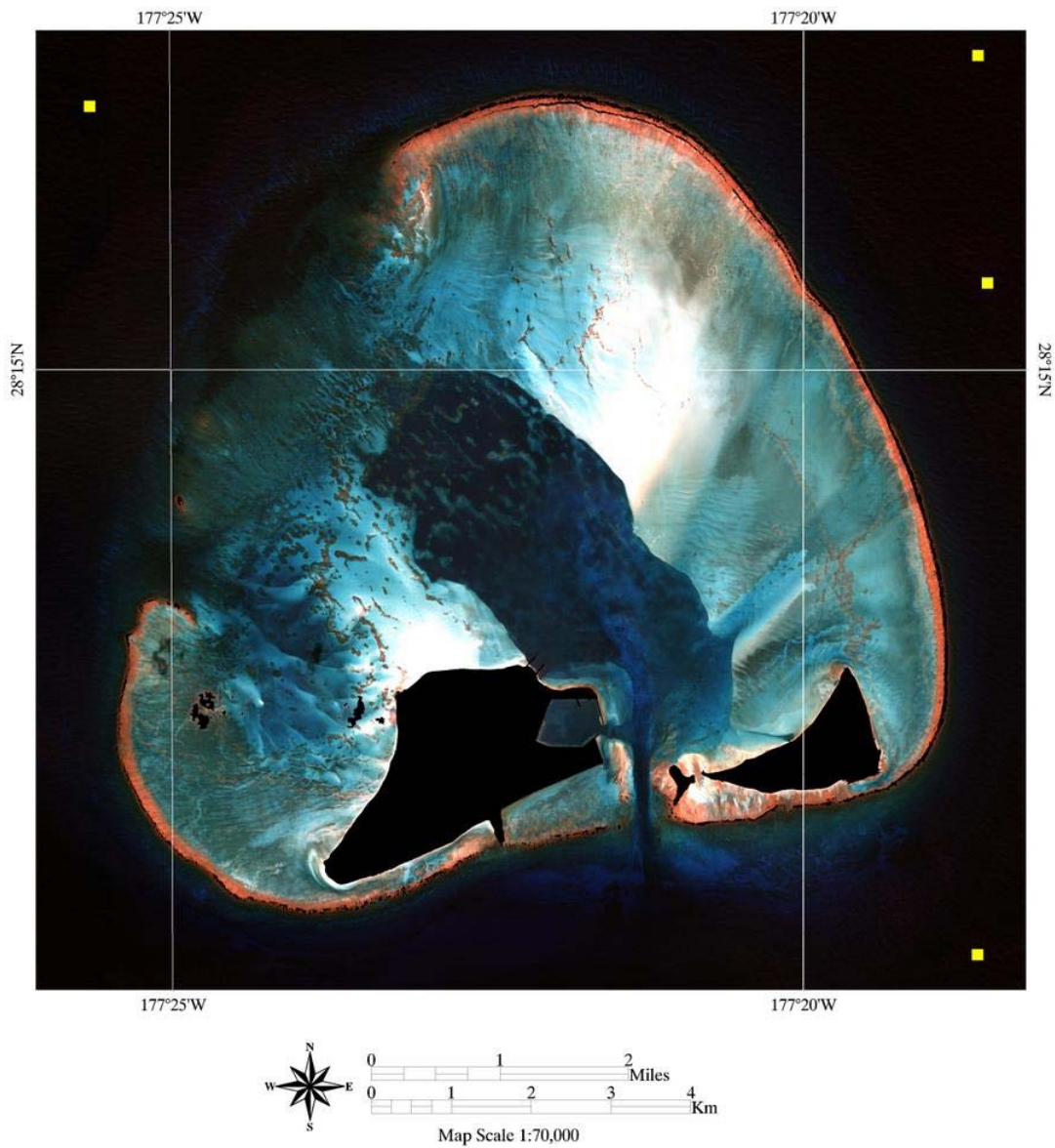
Figure 26.   QuickBird deglint correction sample sites (shown in yellow)

Three linear regressions were then performed on these sample pixels: Blue vs. NIR bands; Green vs. NIR bands; and Red vs. NIR bands. For illustration purposes, the Red vs. NIR bands regression is displayed in Figure 27. Coefficient of Determination (R^2) values from each regression are outlined in Table 5.

The band math function in ENVI 4.4 was then used to apply Equation (7) (without the *Min$_{NIR}$* term) to our data and produce a deglinted image. The results of the deglint technique are displayed in Figures 28 and 29.

Red vs. NIR

$y = 0.8183x + 25.064$

$R^2 = 0.6428$
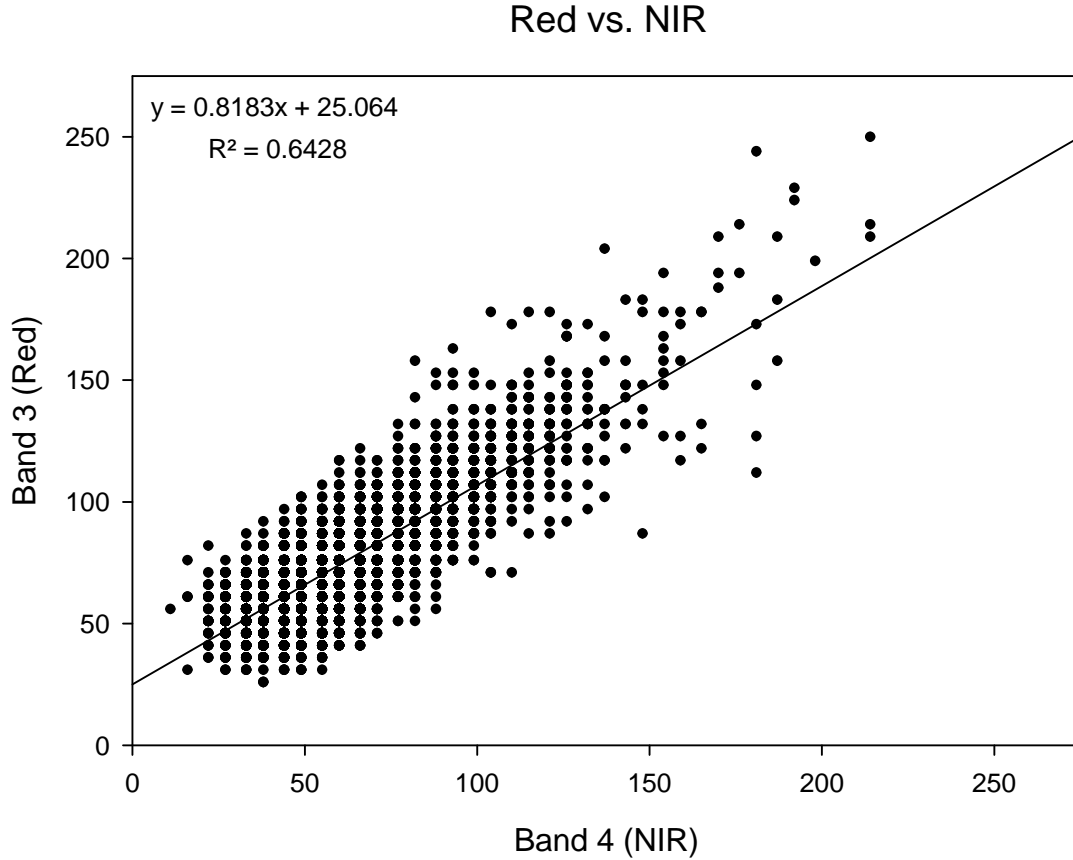
Figure 27.   Red vs. NIR bands linear regression of QuickBird image

Band Regression	R^2
Blue vs. NIR	0.461
Green vs. NIR	0.634
Red vs. NIR	0.642

Table 5.   QuickBird glint removal regression R^2 values
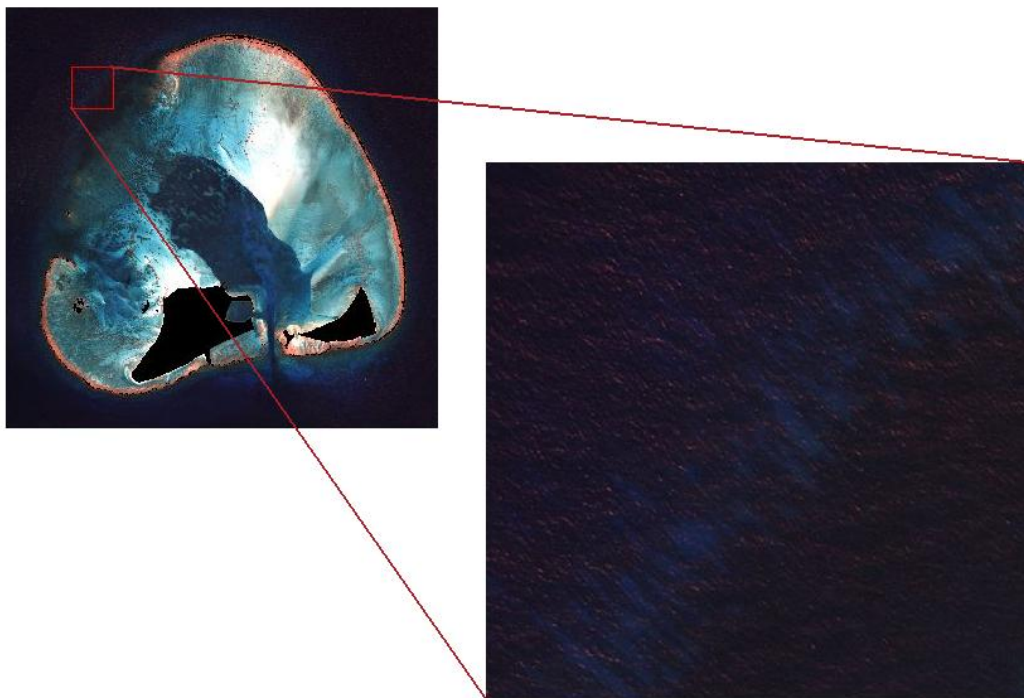
Figure 28.   QuickBird ACORN corrected image (before deglinting)
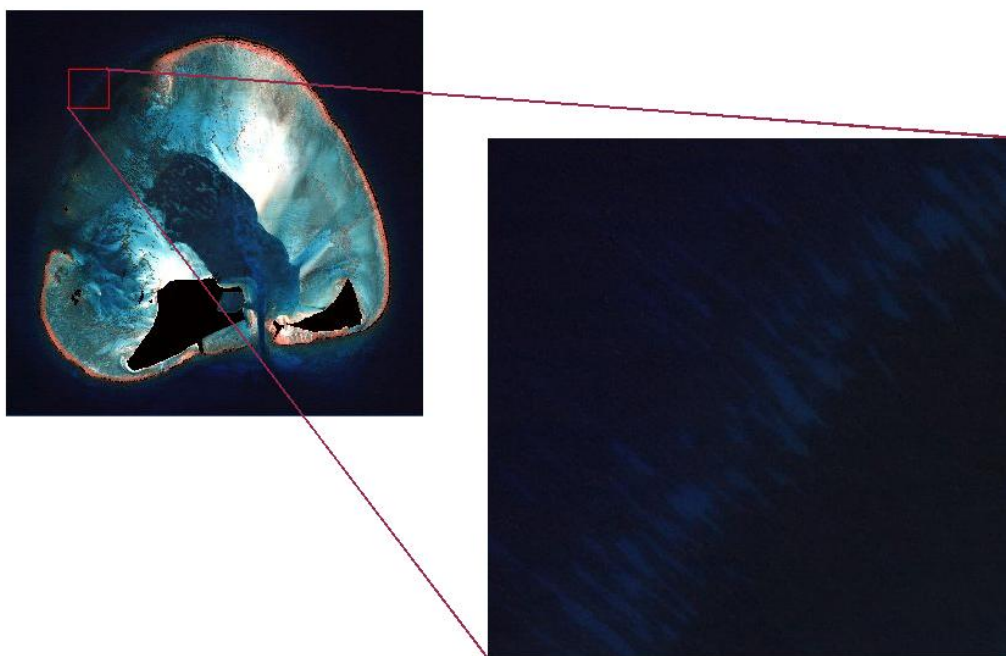
Figure 29.   QuickBird sun glint corrected image

e. *Water Column Correction (WCC)*

As outlined in Chapter II, Section D, the interactions between light and water significantly affect the ability to derive information from remotely sensed measurements of underwater habitats (Green et al., 2000). Variable water depth in these environments profoundly affects the amount of bottom reflectance that reaches an orbiting sensor (Mumby et al., 1998). Lyzenga (1978; 1981) devised an image-based process to compensate for the effects of varying water depth on benthic features. This method produces a depth-invariant bottom index from each pair of spectral bands. Mumby et al. (1998) built on this technique and provided an easily implemented method of producing depth-invariant bands (DIB). Their method is outlined in Equations (8) through (12).

$$DIB_{ij} = \ln(L_i) - \left[\left(\frac{k_i}{k_j} \right) \ln \left(L_j \right) \right] \tag{8}$$

Where i and j represent image bands, L is the pixel reflectance value and the ratio of attenuation coefficients (k_i/k_j) is defined by:

$$\frac{k_i}{k_j} = a + \sqrt{\left(a^2 + a \right)} \tag{9}$$

Where a is the difference in the variances of bands i and j divided by twice their covariance, as shown below:

$$a = \frac{\sigma_{ii} - \sigma_{jj}}{2\sigma_{ij}} \tag{10}$$

The covariance σ_{ij} is the mean of the products of X_i and X_j minus the product of the means of X_i and X_j:

$$\sigma_{ij} = \overline{X_i X_j} - \overline{X_i} \bullet \overline{X_j} \tag{11}$$

Where X is the natural log of pixel reflectance (L).

$$X_i = \ln(L_i) \tag{12}$$

This step was performed on the ACORN atmospherically corrected, masked image subset after the deglint correction had been applied. A sample of pixels across the image representing a single substrate at different water depths is needed to implement the water column correction. Sand pixels were chosen from multiple locations

at variable water depths because of the relative ease of recognizing this substrate in the image without *a priori* field knowledge. The sand pixels chosen are illustrated in Figure 30.
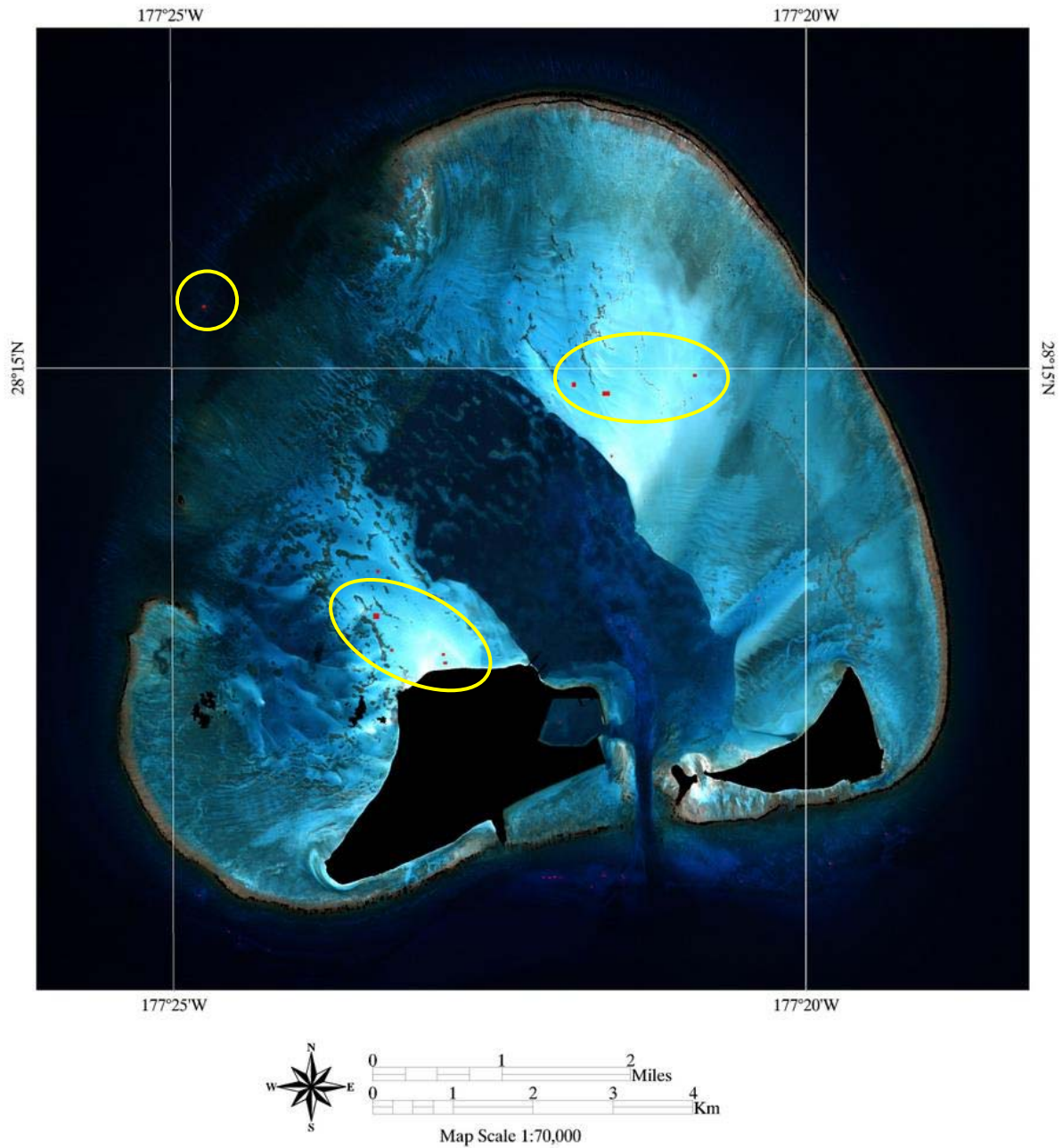
Figure 30.   QuickBird WCC sample (shown in red, some highlighted with circles)

This sample was then used to generate the k_i/k_j terms for the 3 band combinations: blue vs. green; blue vs. red; and green vs. red. Equation (8) was then applied to the image using the band math utility in ENVI 4.4 to create 3 depth-invariant bands. These bands were combined into the image displayed in Figure 31.
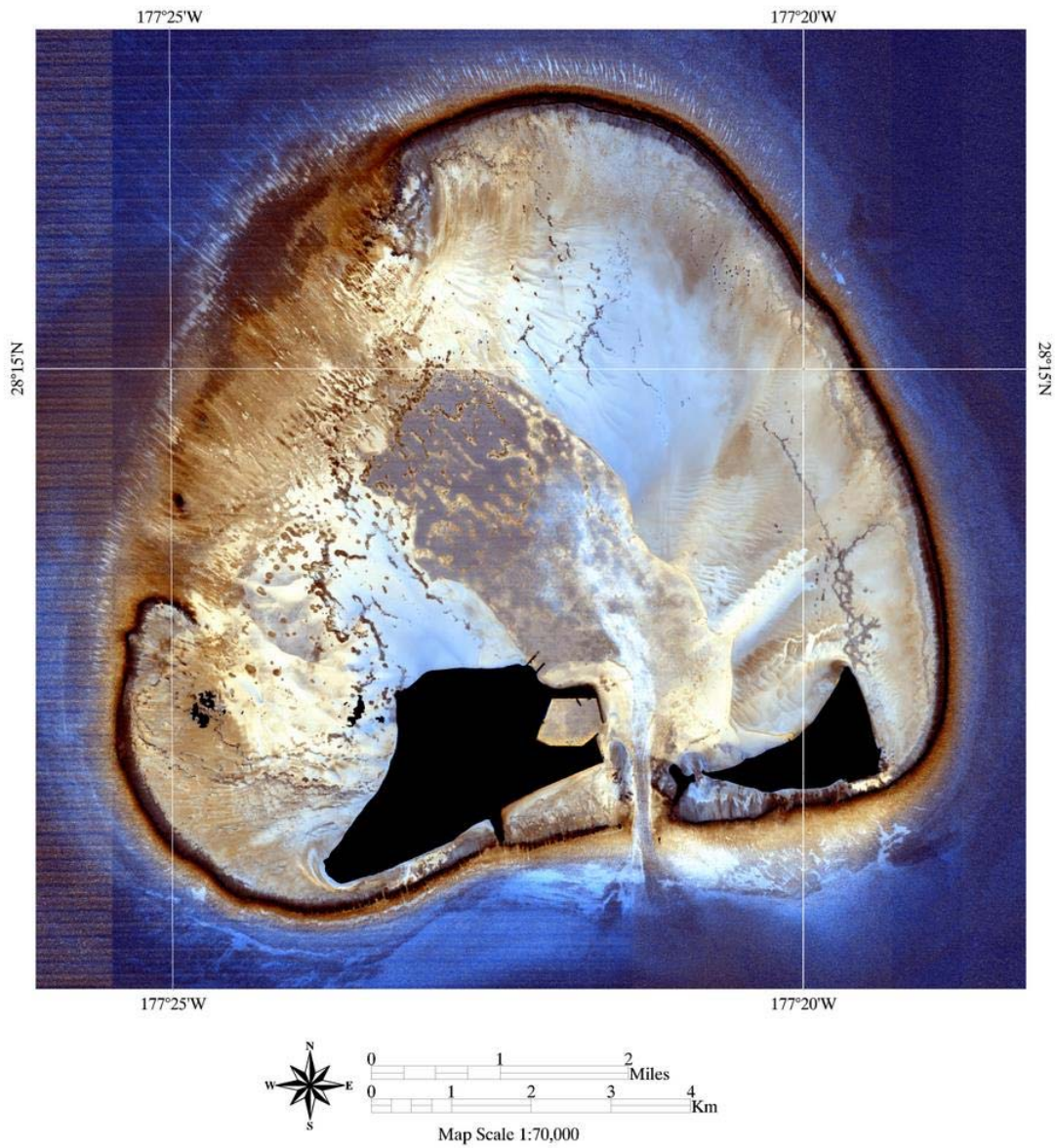
Figure 31. QuickBird water column corrected image

f.   ***Benthic Classification***

An unsupervised, Iterative Self-Organizing Data Technique of Analysis (ISODATA) classification method was used to classify the benthic substrates of the processed image of Midway Atoll. This technique is the most used method for unsupervised classification (Tso and Mather, 2001). Unsupervised ISODATA classification was used by Call et al. (2003) in their coral reef habitat discrimination using Landsat TM multispectral imagery and by Mishra et al. (2006) in their benthic habitat mapping of tropical marine environments using QuickBird multispectral imagery.

ISODATA classification uses a minimum spectral distance to iteratively assign each candidate pixel to a class. It then redefines the criteria for each class and classifies again so that spectral distance patterns emerge from the data. After each iteration a new mean is calculated for each class. These new means are used to define the classes for the next iteration. The process continues until there is little change between iterations or until a user specified threshold is met (Calvo et al., 2003).

Additional criteria can be used to refine the ISODATA procedure. Users can set tolerances for maximum class standard deviation and minimal distance between classes. If a class has a standard deviation greater than the set maximum in any dimension then the class is split into 2 classes along that dimension. Similarly, if the distance between 2 cluster means is less than the set minimal distance then those 2 classes are merged into a single class (Tso and Mather, 2001).

Unsupervised ISODATA classifications were performed on 2 subsets of the water column corrected QuickBird image. This was done in order to produce classifications that facilitate a cross scale comparison between the imagery of the 2 satellites. The first subset represents a large area with a small spatial scale and contains imagery present and not obstructed by clouds in both the QuickBird and IKONOS acquisitions. This subset will be referred to as the "Central Atoll" subset. The Central Atoll subset was also chosen to decrease the total area of the image, thus reducing the amount of time necessary to determine the accuracy of the classification during fieldwork, due to the limited amount of available time in the field (two weeks). This

subset contains all environments of interest present in the original subset: deep water, outer reef, back reef, shallow lagoon, deep lagoon, land and the South pass.

A second subset was chosen that represents a smaller area with a larger spatial scale than the Central Atoll subset. This subset will be referred to as the "Patch Reef" subset since it contains only one small-to-medium sized patch reef (approximately 1.75 acres). Both subsets are displayed in Figure 32.
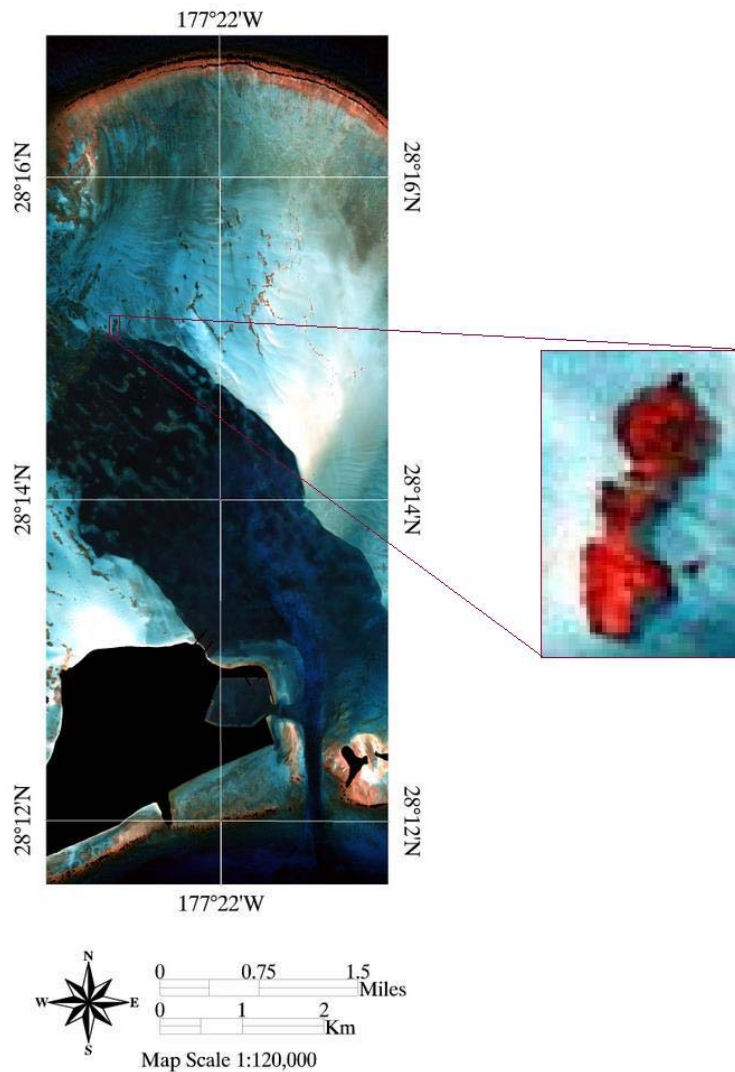
Figure 32. QuickBird (left) Central Atoll and (right) Patch Reef Subsets

ENVI 4.4 was used to perform an unsupervised ISODATA classification on both subsets. The parameters used for the Central Atoll classification are outlined in Table 6. The ISODATA classification process yielded 25 classes. Contextual editing was then used to merge these 25 classes down to 5 classes. The 5 classes represented algae/turf/coral, coral/coralline algae, rubble/turf, sand, and sand/rubble/turf. The final Central Atoll classification is shown in Figure 33.

Parameter	Value
Minimum Classes	45
Maximum Classes	60
Maximum Iterations	25
Minimum Pixels per Class	100
Maximum Standard Deviation	1
Minimum Class Distance	5

Table 6.　　QuickBird Central Atoll classification parameters
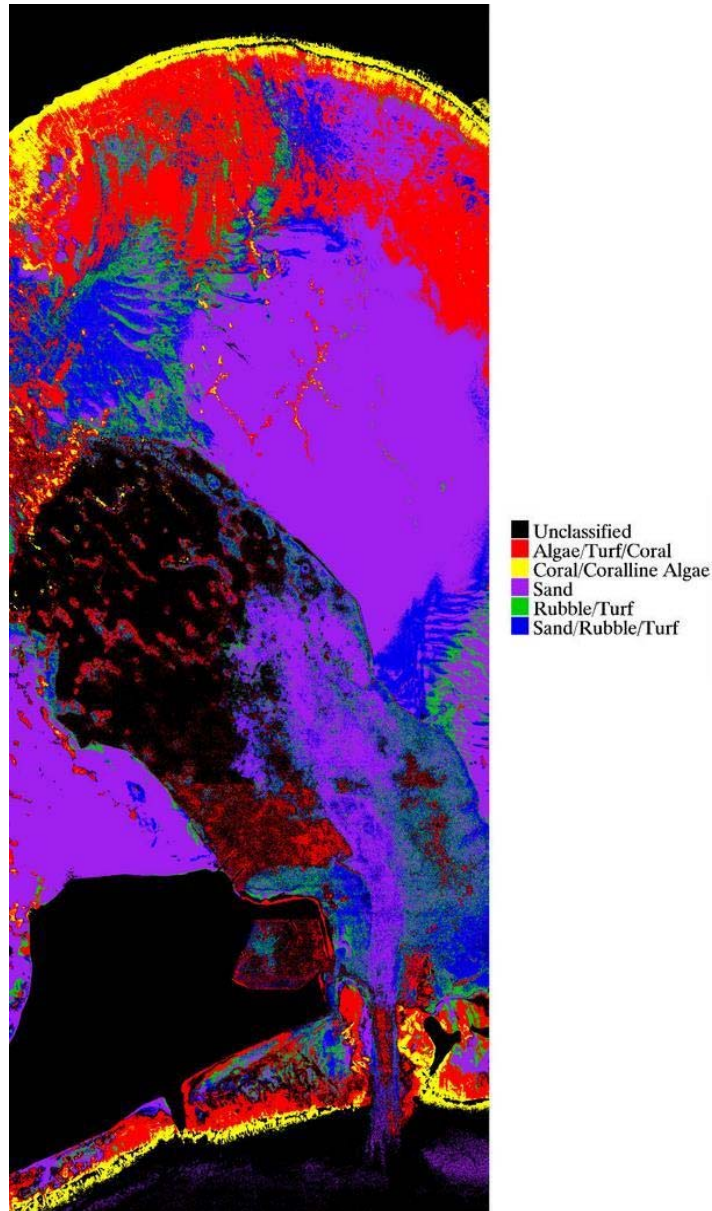
Figure 33.   QuickBird Central Atoll Classification

The parameters used for the Patch Reef classification are outlined in Table 7. The ISODATA classification process yielded 9 classes. These 9 classes were merged into 4 classes using contextual editing techniques. The final classification is shown in Figure 34.

Parameter	Value
Minimum Classes	45
Maximum Classes	60
Maximum Iterations	25
Minimum Pixels per Class	100
Maximum Standard Deviation	1
Minimum Class Distance	5

Table 7.   QuickBird Patch Reef classification parameters
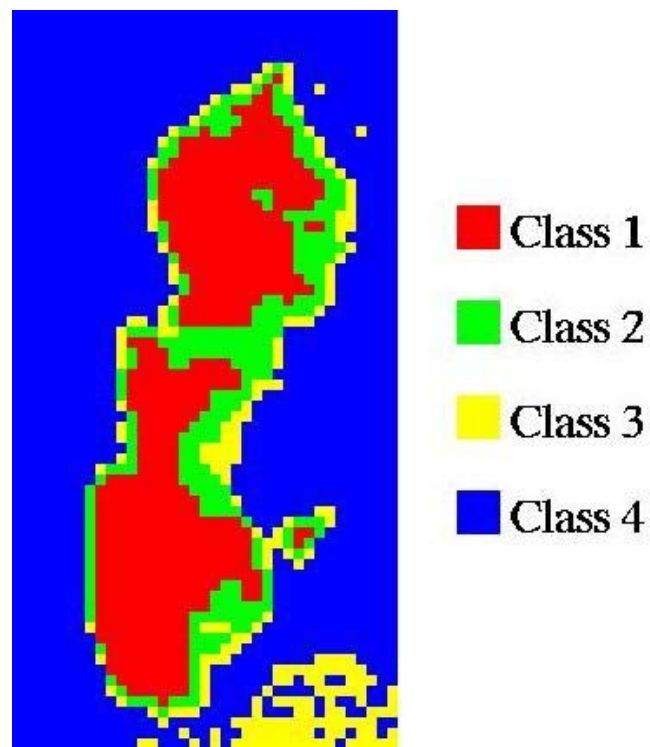
Figure 34.   QuickBird Patch Reef Classification

61

2. IKONOS

a.   *Spatial Subsetting*

The 16 May 2008 IKONOS image was subset for the same reasons outlined above in the QuickBird section (Chapter V Section B-1-*a*). A rectangular subset was chosen that includes all habitats, including the available portion of the lagoon in the acquired image, fore reef environments, and surrounding visible seaward benthic substrate. This masked subset is displayed in Figure 35.
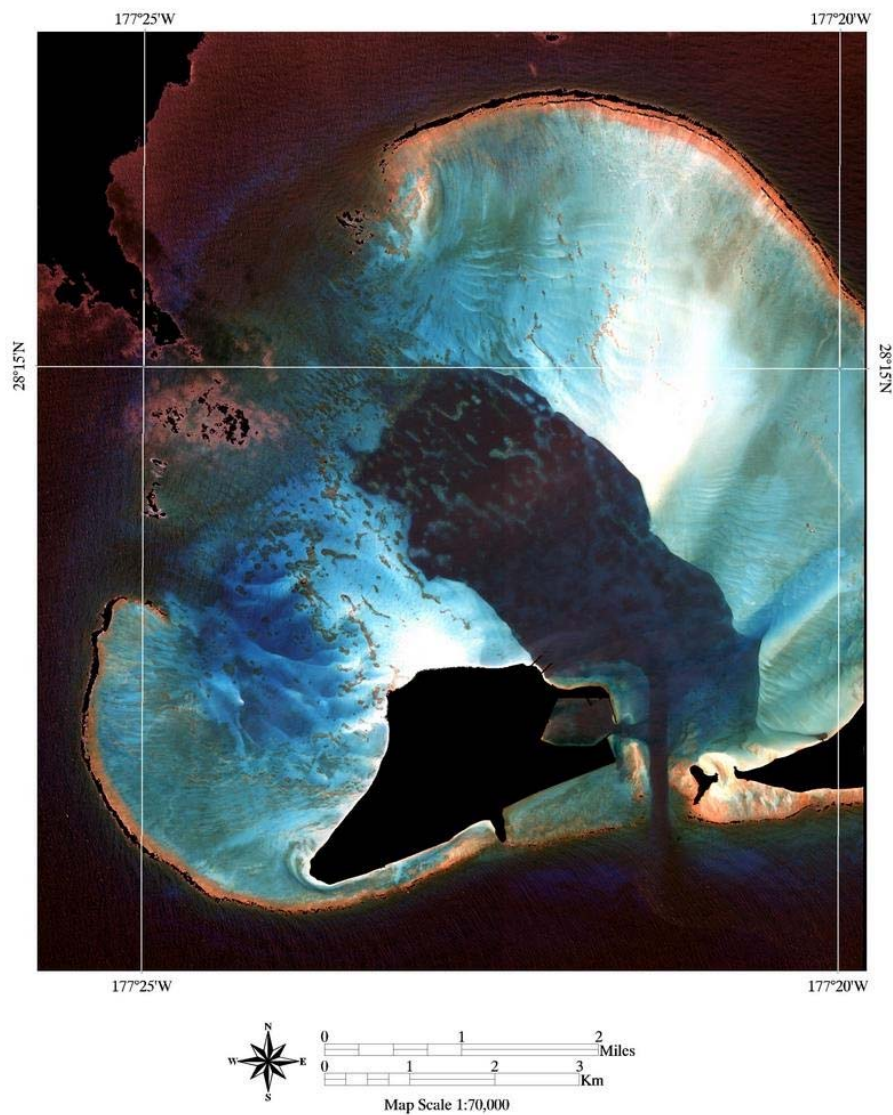
Figure 35.   Masked IKONOS image Subset

b. Radiance Conversion

IKONOS imagery products are delivered to customers as pixels represented by DNs. In order to further analyze this image a conversion to spectral radiance (L_λ) was performed by using Equation (13) (Fleming, 2001).

$$L_\lambda = \frac{DN}{CalCof_\lambda} \tag{13}$$

Where $CalCof_\lambda$ is a wavelength dependent calibration coefficient. These values were provided in Fleming (2001).

c. Atmospheric Correction

As with the QuickBird imagery, the ACORN and ATCOR atmospheric correction algorithms were applied to the IKONOS imagery along with a simple conversion to reflectance. Corrected vegetation spectra were compared in order to choose the best correction technique.

(1) Conversion to Top-of-Atmosphere Reflectance (TOAR): The equation used to convert the radiance subset image into top-of-atmosphere band-averaged reflectance (ρ_λ) is shown in Equation (14) (Fleming, 2001).

$$\rho_\lambda = \frac{\pi \bullet L_\lambda \bullet d^2}{ESUN_\lambda \bullet \cos(\theta_s)} \tag{14}$$

Where L_λ is spectral radiance, d is the Earth Sun distance in astronomical units, $ESUN_\lambda$ is the band dependent mean solar exoatmospheric irradiance, and θ_s is the solar zenith angle. Values for $ESUN_\lambda$ were provided in Fleming (2001). All other values were obtained or derived from the image metadata. Vegetation spectra from the 3 corrected images (TOAR shown in red) are displayed in Figure 36, next to the vegetation spectrum from the unprocessed image.
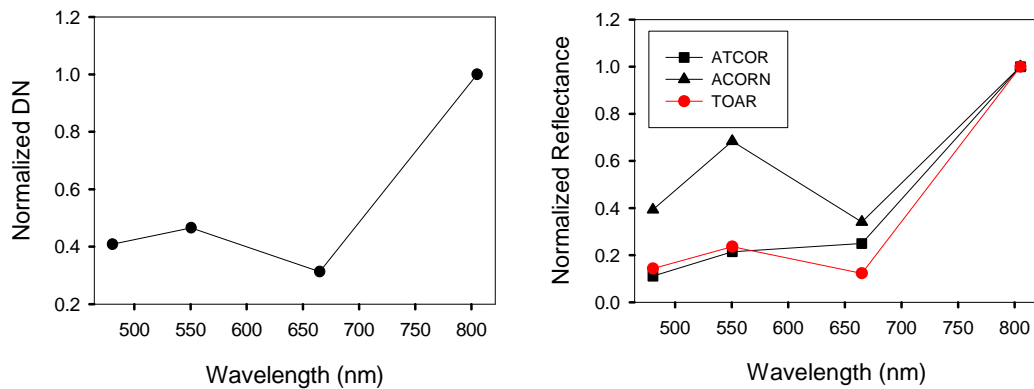
Figure 36.   IKONOS vegetation spectral profiles: (left) unprocessed, (right) top-of-atmosphere reflectance (shown in red)

(2) ACORN 5.0: The image was also processed using ACORN's atmospheric correction algorithm. This step was performed on the original DN image subset (.bil format of signed integers as required by ACORN) because ACORN incorporates a radiance conversion into its algorithm. The data for the multispectral response file was provided by GeoEye. The input gain and offset files were created using the method described in Fleming (2001). The correction was performed using the inputs outlined in Table 8, and image location and collection time were obtained from the image metadata. Vegetation spectral profiles from the ACORN output (shown in red) and the unprocessed image are shown in Figure 37.

Variable	Value	Source
Atmospheric Model	"Tropical"	Experimentation
Atmospheric Visibility	100 km	ACORN User's Manual
Atmospheric Water Vapor	25 mm	ACORN User's Manual

Table 8.   IKONOS ACORN input values
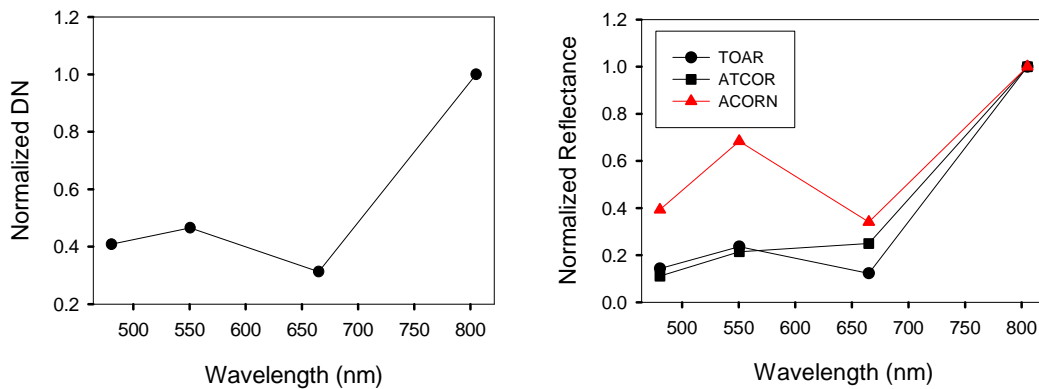
Figure 37.   IKONOS vegetation spectral profiles: (left) unprocessed, (right) ACORN atmospheric correction (shown in red)

(3) ATCOR: ATCOR2 for ERDAS IMAGINE 9.0 was used to perform the third atmospheric correction technique for comparison. This algorithm was applied to the original DN image subset. The ATCOR User manual was used to derive the values for solar zenith angle, tilt angle, azimuth angle, and the values in the calibration file. The atmospheric model used was "US Standard Maritime" with 120 km used for scene visibility. A vegetation spectrum taken from the ATCOR output (shown in red) is displayed in Figure 38, along with the corresponding spectral profile from the unprocessed image.
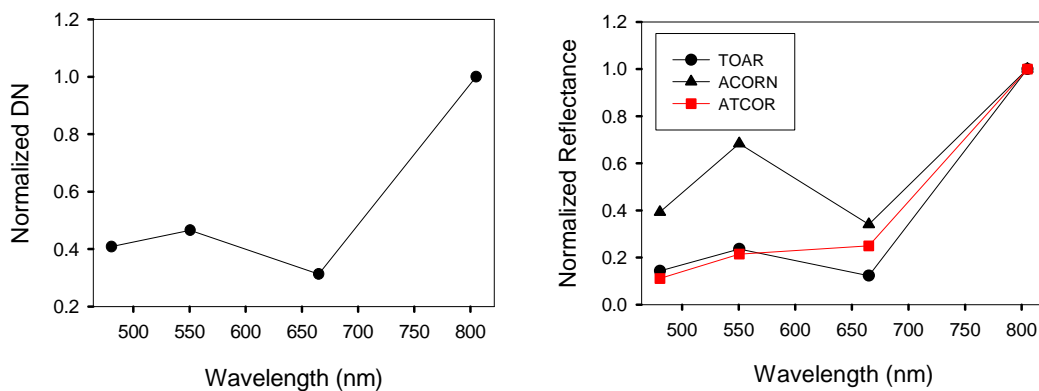
Figure 38.   IKONOS vegetation spectral profiles: (left) unprocessed, (right) ATCOR atmospheric correction (shown in red)

ACORN was again chosen as the best atmospheric correction algorithm after careful comparison of the vegetation spectra from each method. The ATCOR method produced large numbers of negative pixels in the red band of deep water pixels, mimicking the results for QuickBird and the results obtained by Camacho (2006).

d.   *Glint Removal*

The Hedley et al. (2005) sun glint removal technique was applied to the ACORN atmospherically corrected and masked subset. A sample of image pixels was selected from multiple sites of optically deep water featuring uniform sun glint. Figure 39 illustrates the sample sites.
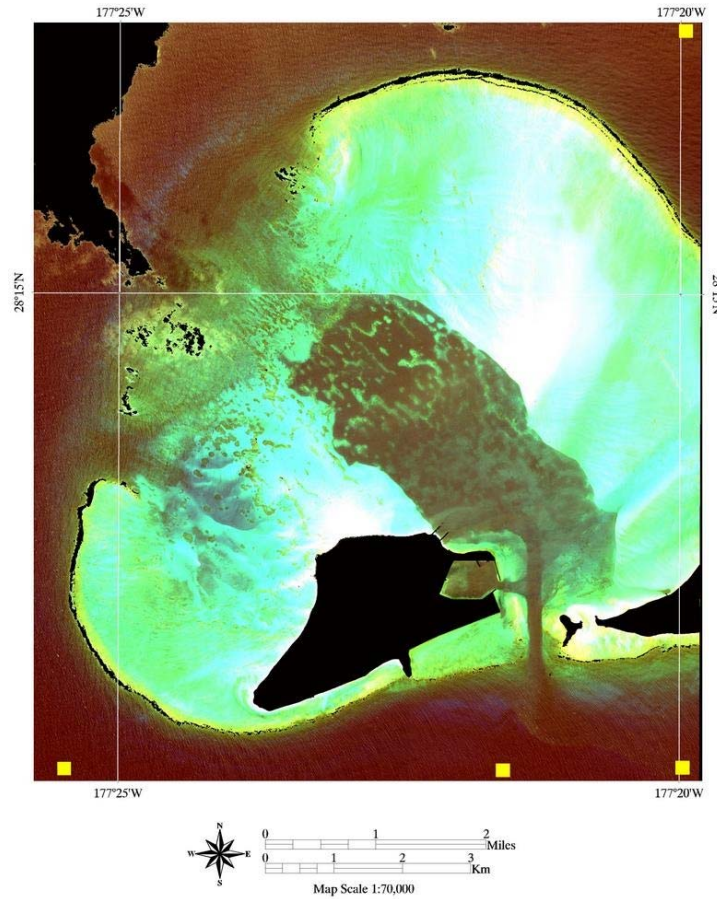
Figure 39.   IKONOS deglint correction sample sites (shown in yellow)

Linear regressions were performed on the sample pixels for the blue vs. NIR bands; the green vs. NIR bands; and the red vs. NIR bands. Figure 40 shows the red vs. NIR bands regression to illustrate this step. Values for the coefficient of determination (R^2) for each biplot are displayed in Table 9. The band math function in ENVI 4.4 was then used to apply Equation (7) (without the Min_{NIR} term). The results of the deglint technique are displayed in Figures 41 and 42.
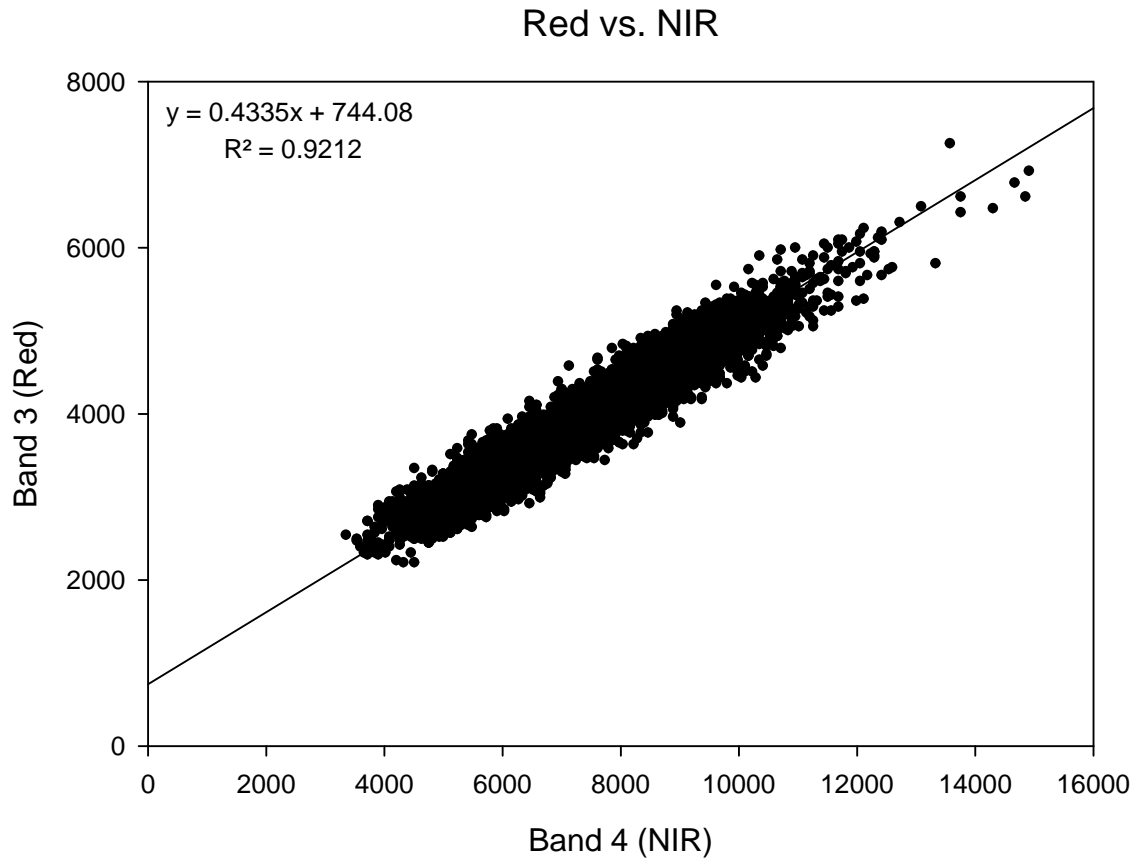
Figure 40.   Red vs. NIR bands linear regression of IKONOS image

Band Regression	R^2
Blue vs. NIR	0.811
Green vs. NIR	0.875
Red vs. NIR	0.921

Table 9.   IKONOS glint removal regression R^2 values
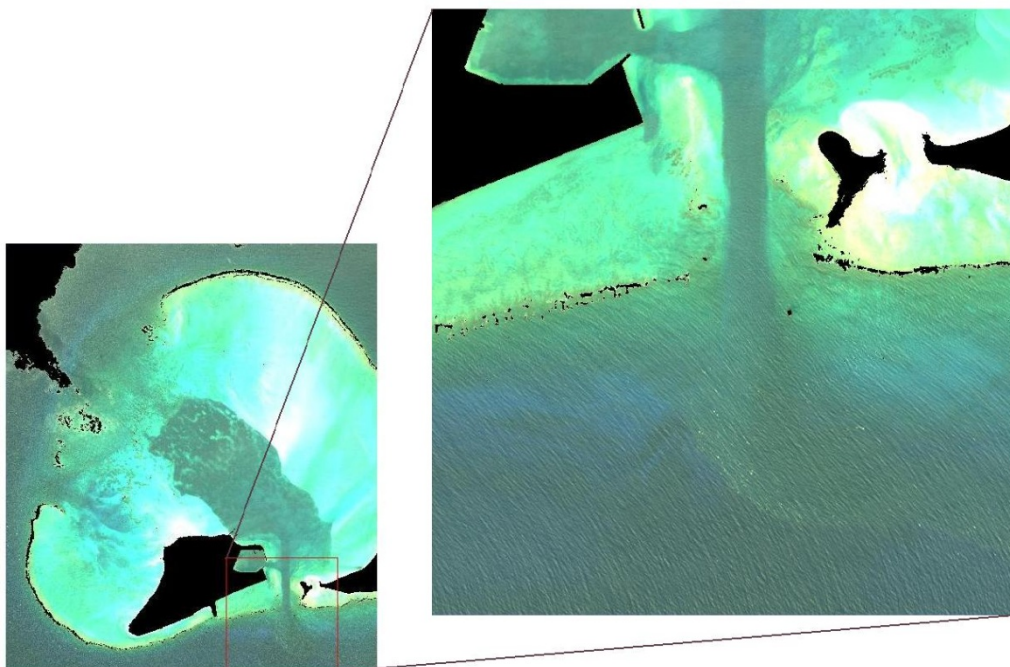
Figure 41.   IKONOS ACORN corrected image (before deglinting)
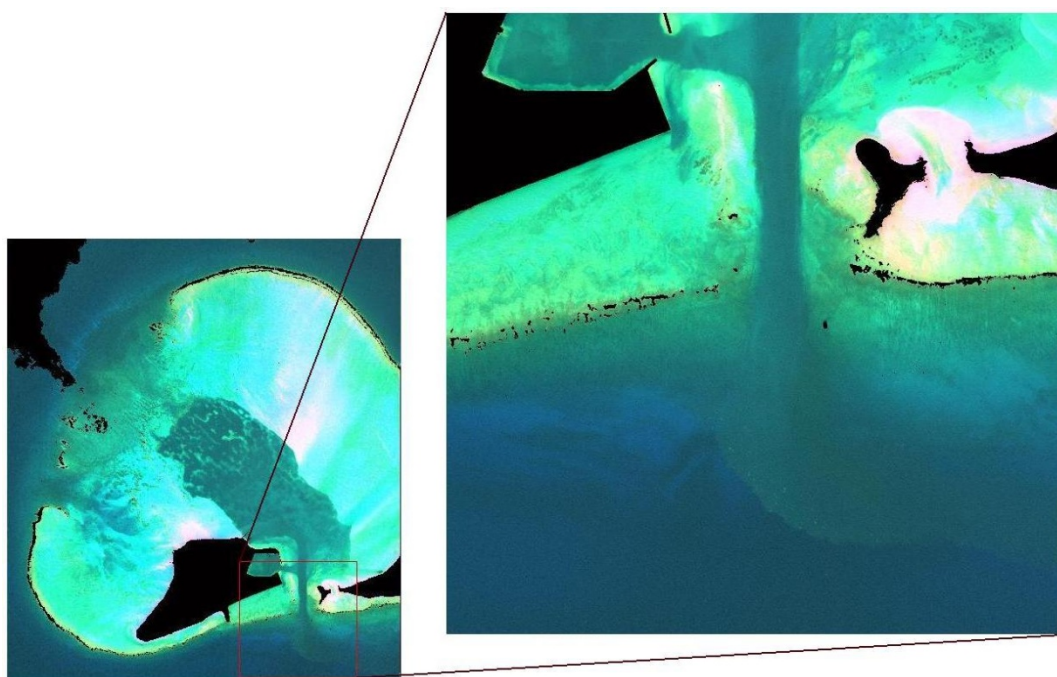
Figure 42.   IKONOS sun glint corrected image

e. Water Column Correction (WCC)

The Mumby et al. (1998) water column correction technique was performed on the ACORN atmospherically corrected IKONOS image subset after the sun glint correction. A sample of uniform sand pixels was chosen from multiple locations representing variable water depths, as shown in Figure 43.
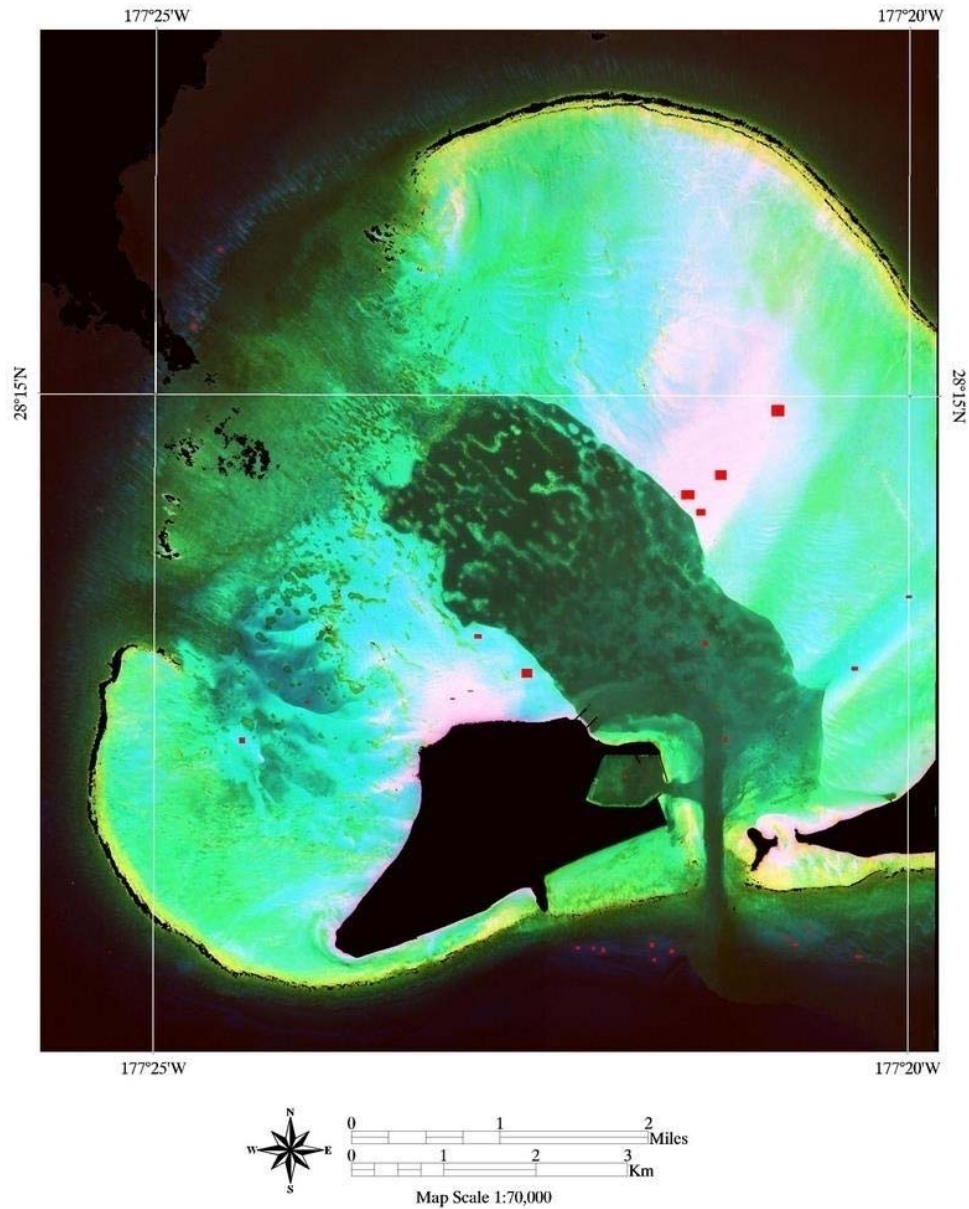
Figure 43.   IKONOS WCC sample (shown in red)

This sample was then used to calculate the ratio of attenuation coefficients (k_i/k_j), following Equations (9) through (12) outlined in Section B-1-*e*, for the 3 band combinations: blue vs. green; blue vs. red; and green vs. red. ENVI's band math utility was then used to apply Equation (8) to the image and create three depth-invariant bands. These 3 depth-invariant bands were then combined into a single image that is displayed in Figure 44.
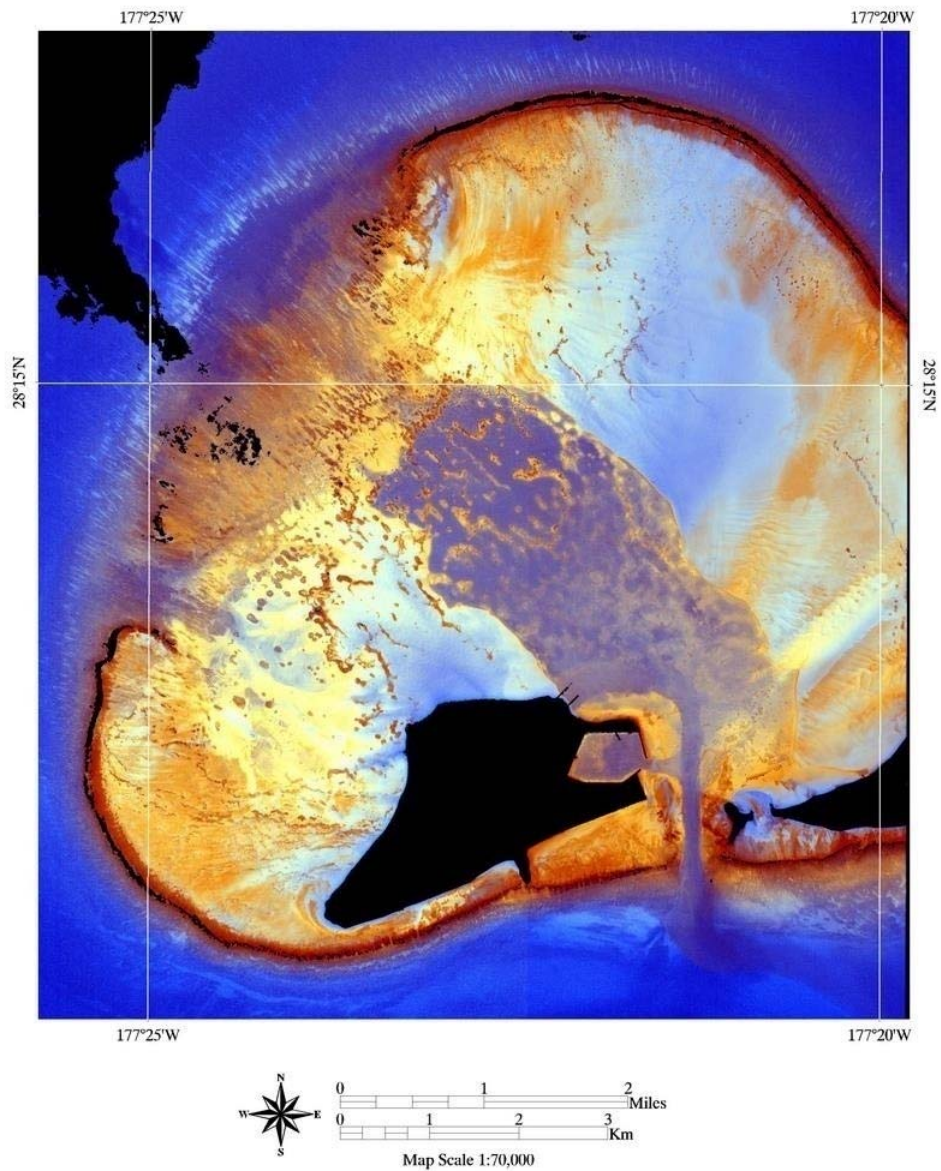
Figure 44.   IKONOS water column corrected image

f. Benthic Classification

The water column corrected image was subsetted before ISODATA classifications were performed. Two subsets were chosen to match the Central Atoll and Patch Reef subsets that were taken from the QuickBird imagery, using geographic landmarks to define the subset boundaries. The Central Atoll and Patch Reef subsets for the IKONOS image are displayed in Figure 45.
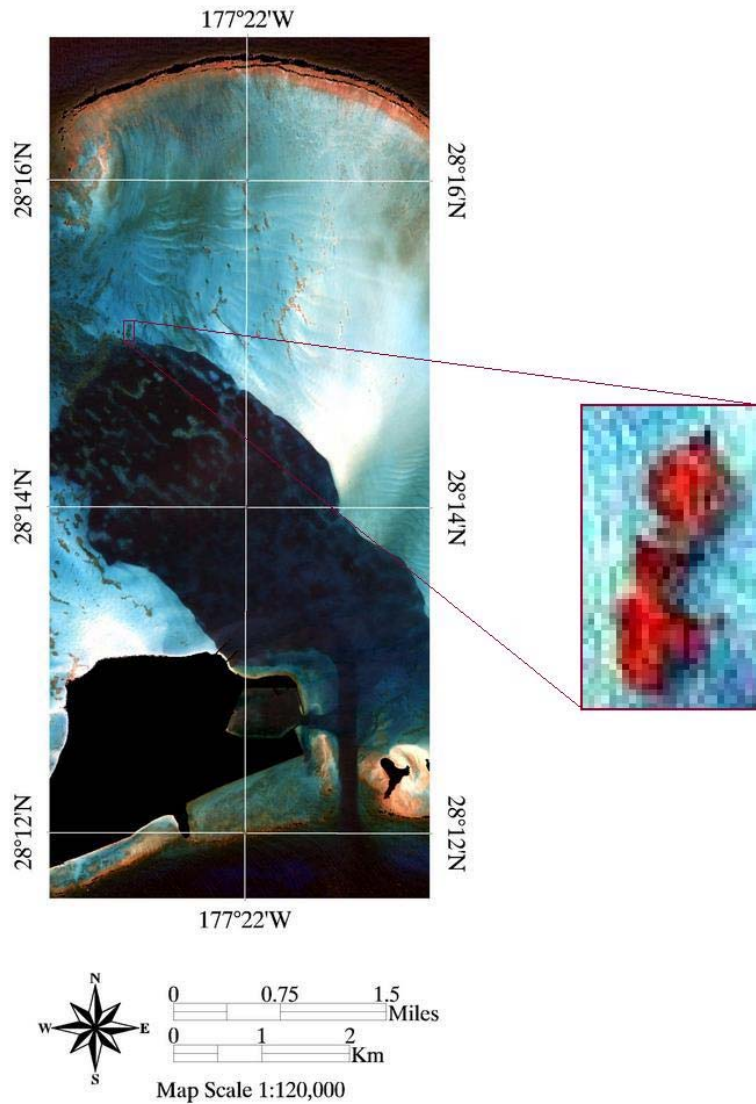
Figure 45. IKONOS Central Atoll and Patch Reef subsets

An unsupervised ISODATA classification was performed on each subset using ENVI 4.4. The parameters used in the Central Atoll subset are summarized in Table 10. The ISODATA classification process yielded 25 classes. Contextual editing was then used to merge these 25 classes down to the following 5: algae/turf/coral, coral/coralline algae, rubble/turf, sand, and sand/rubble/turf. The final classification is shown in Figure 46.

Parameter	Value
Minimum Classes	45
Maximum Classes	60
Maximum Iterations	25
Minimum Pixels per Class	100
Maximum Standard Deviation	1
Minimum Class Distance	5

Table 10.   IKONOS Central Atoll classification parameters
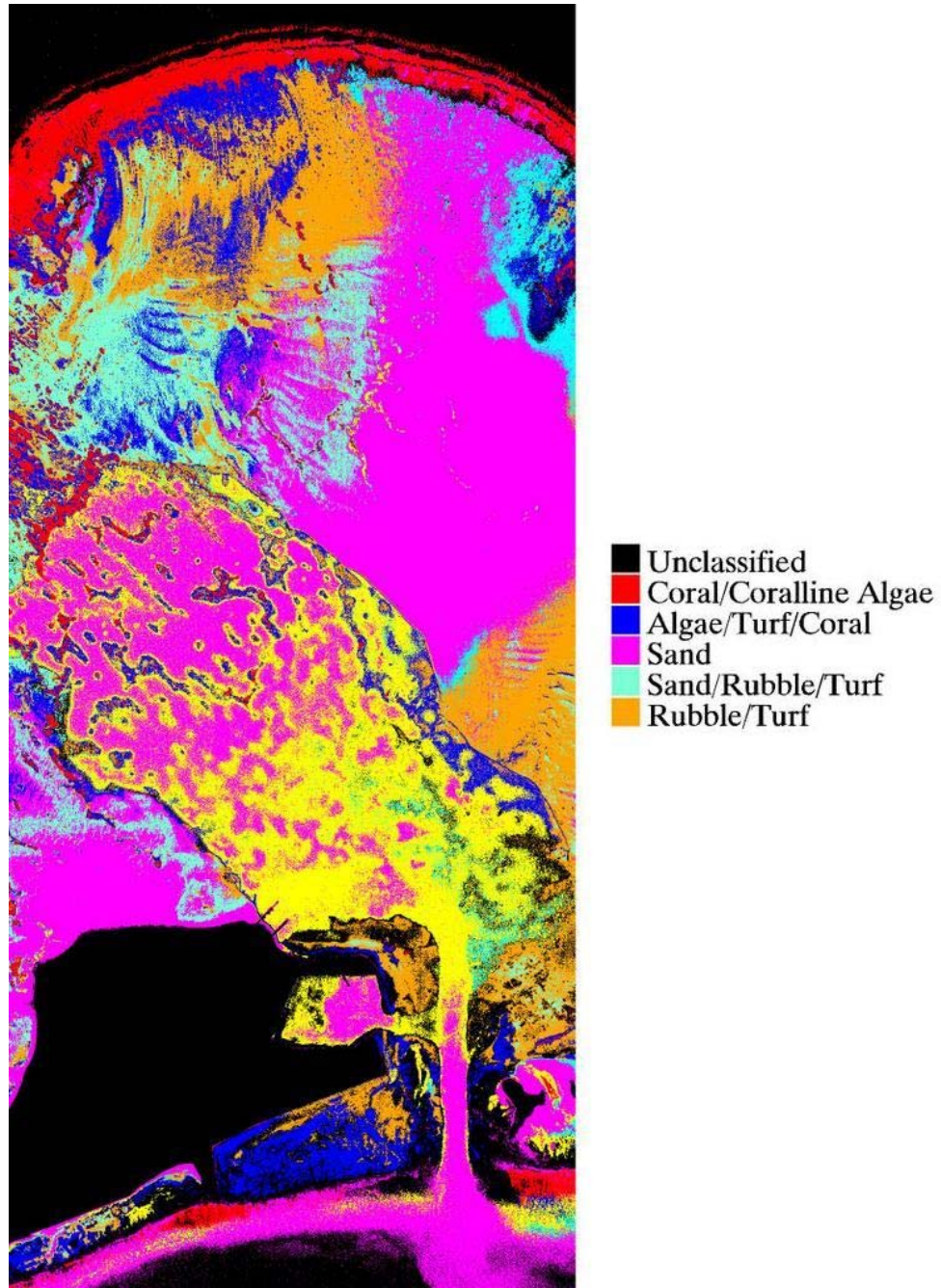
Figure 46.   IKONOS Central Atoll classification

The parameters used for Patch Reef subset are summarized in Table 11. The ISODATA classification process yielded 10 classes that were merged into 4 classes using contextual editing. The final Patch Reef classification is displayed in Figure 47.

Parameter	Value
Minimum Classes	45
Maximum Classes	60
Maximum Iterations	25
Minimum Pixels per Class	30
Maximum Standard Deviation	1
Minimum Class Distance	5

Table 11.　　IKONOS Patch Reef classification parameters
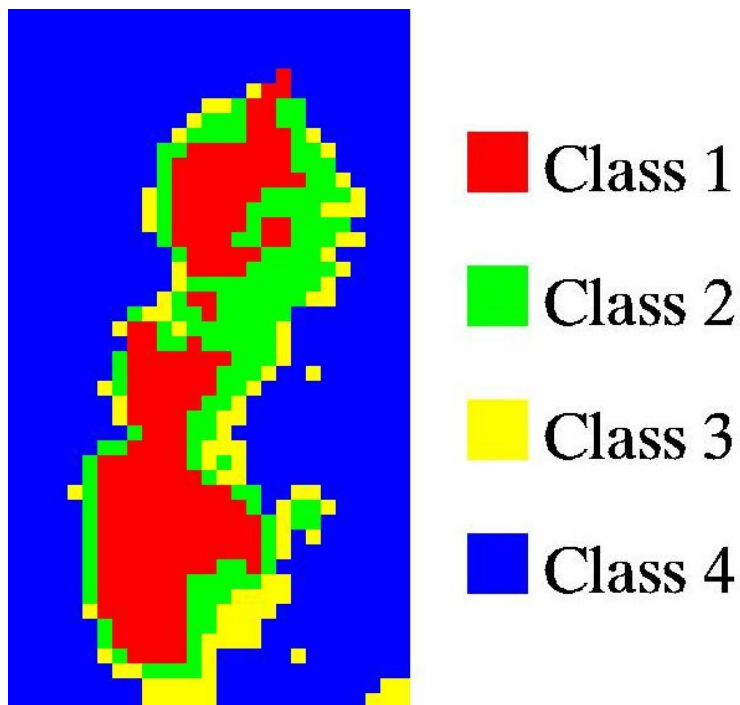
Figure 47.　IKONOS Patch Reef classification

C. FIELDWO　RK

1.　Choosing Groundtruth Locations

A random stratified sampling pattern was used to identify groundtruth points for the benthic ISODATA classifications of the Central Atoll. This method randomly selects sites from each class in proportion to the size (or significance) of the class (McCoy, 2005). A set of stratified random points was first generated from the IKONOS classification. Then a smaller set of stratified random points was chosen from the

74

QuickBird classification. These two sets were combined to create a set of 220 groundtruth points with the following distribution (total points [points from IKONOS, points from QuickBird]): algae/turf/coral 65[50,15], coral/coralline algae 72[60,12], rubble/turf 30[25,5], sand 28[20,8], and sand/rubble/turf 25[20,5].

2. Techniques Used in the Field

Fieldwork was conducted at Midway Atoll over a 2 week period in July 2008. A two person team surveyed a transect of the Patch Reef and as many sites as time permitted from the Central Atoll groundtruth sample points. In the field, the team utilized SCUBA or snorkeling to survey each site. The majority of sites were surveyed by snorkeling due to the shallow water depths at many locations.

a. Central Atoll Groundtruth

A total of 135 sites, from the randomly generated set of 220, were surveyed over a 10 day period of the fieldwork. The two person team used an 18 foot Boston Whaler to reach each groundtruth point with guidance from a hand held GPS unit (Garmin 60CSx). The portion of the atoll surveyed was chosen on a day by day basis. Each day the team would travel to a different section of the lagoon and survey as many points as possible based on proximity. Predicted class totals for completed survey sites were calculated daily. Near the completion of fieldwork, sites were chosen based on predicted class and lagoon location in order to maintain similar class and location distribution to the 220 point groundtruth set.

At each site the team would use the hand held GPS unit to pilot the boat to the pre-programmed waypoint of the site's coordinates. Once the location was reached the boat was anchored as close as possible to the waypoint. The GPS unit was then used to estimate a bearing and range to the dive site before the team entered the water. Once in the water the team would swim to the site and survey its benthic characteristics. Each site was defined as a circle centered on its GPS coordinates with a diameter of 10 meters. A hierarchical reef habitat classification scheme (Appendix C) was used to record the observations at each dive site. Atoll zone, geomorphic habitat, bottom cover, depth and

bottom cover abundance data were collected at each dive site. Several photographs were also taken at each site for future cross referencing.

b. *Patch Reef*

A transect approach was used to groundtruth the Patch Reef. The survey team located the Patch Reef using its image derived GPS coordinates. Once on site, the team used SCUBA to conduct the survey. A transect was laid down the center of the reef using an underwater tape measure starting at the Northern tip of the reef and following a magnetic compass bearing of 180º. Substrate data were recorded every 2 meters along the transect. The classification area was a 1 m^2 centered on the distance mark of the underwater tape measure. Pictures were also taken at the 2 m intervals along the transect for cross reference.

VI. RESULTS

A. CENTRAL   ATOLL

The Central Atoll classification accuracy for each satellite sensor was assessed using the error matrix technique described by Congalton and Green (1999). An error matrix is a useful way to represent classification accuracy because it represents the accuracy within each class and includes errors of inclusion and errors of exclusion (Congalton, 1991). The columns of the error matrices in the results displayed on the following pages represent groundtruth data; the rows represent remotely sensed data. Each error matrix is accompanied by Overall accuracy, a Producer's accuracy, and a User's accuracy for each class. The Overall accuracy is the number of correctly classified sites divided by the total number of sites classified. The Producer's accuracy is the number of correctly classified sites within a class divided by the number of groundtruth sites with that classification (column total). This accuracy shows the probability of a groundtruth site being correctly classified and is a measure of exclusion or "omission" error. The User's accuracy is the number of correctly classified sites within a class divided by the total number of sites classified in that class (row total). This accuracy shows the probability that a site classified on the image actually represents that class in the field and also represents inclusion or "commission" error (Congalton and Green, 1999; Congalton, 1991).

The first 2 error matrices show the results from the QuickBird and IKONOS Central Atoll benthic classifications with the original 5 classes, and are displayed in Tables 12 and 13.

Groundtruth Data

		ATC	CCA	RT	S	SRT	Row Total
QuickBird Data	ATC	22	7	20	0	13	62
	CCA	6	18	0	0	0	24
	RT	2	0	2	1	8	13
	S	0	0	1	9	13	23
	SRT	0	0	3	1	9	13
	Column Total	30	25	26	11	43	135

Producer's Accuracy		User's Accuracy		Benthic Classes
ATC	73.33%	ATC	35.48%	ATC = Algae/Turf/Coral
CCA	72.00%	CCA	75.00%	CCA = Coral/Coralline Algae
RT	7.69%	RT	15.38%	RT = Rubble/Turf
S	81.82%	S	39.13%	S = Sand
SRT	20.93%	SRT	69.23%	SRT = Sand/Rubble/Turf

Overall Accuracy
44.44%

Table 12. QuickBird 5 class error matrix

Groundtruth Data

		ATC	CCA	RT	S	SRT	Row Total
IKONOS Data	ATC	15	0	12	0	6	33
	CCA	12	25	2	0	2	41
	RT	2	0	12	1	14	29
	S	1	0	0	6	10	17
	SRT	0	0	0	4	11	15
	Column Total	30	25	26	11	43	135

Producer's Accuracy		User's Accuracy	
ATC	50.00%	ATC	45.45%
CCA	100.00%	CCA	60.98%
RT	46.15%	RT	41.38%
S	54.55%	S	35.29%
SRT	25.58%	SRT	73.33%

Overall Accuracy
51.11%

Table 13. IKONOS 5 class error matrix

Tables 14 and 15 show the error matrices for QuickBird and IKONOS Central Atoll benthic classifications with 4 classes rather than 5 (2 classes were collapsed together). The inclusion of these additional accuracy assessments is explained in the discussion section.

Groundtruth Data

QuickBird Data		ATC	CCA	S	SRT	Row Total
	ATC	22	7	0	33	62
	CCA	6	18	0	0	24
	S	0	0	9	14	23
	SRT	2	0	2	22	26
	Column Total	30	25	11	69	135

Producer's Accuracy		User's Accuracy	
ATC	73.33%	ATC	35.48%
CCA	72.00%	CCA	75.00%
S	81.82%	S	39.13%
SRT	31.88%	SRT	84.62%

Overall Accuracy
52.59%

Table 14.   QuickBird 4 class error matrix

Groundtruth Data

IKONOS Data		ATC	CCA	S	SRT	Row Total
	ATC	15	0	0	18	33
	CCA	12	25	0	4	41
	S	1	0	6	10	17
	SRT	2	0	5	37	44
	Column Total	30	25	11	69	135

Producer's Accuracy		User's Accuracy	
ATC	50.00%	ATC	45.45%
CCA	100.00%	CCA	60.98%
S	54.55%	S	35.29%
SRT	53.62%	SRT	84.09%

Overall Accuracy
61.48%

Table 15.   IKONOS 4 class error matrix

B. PATCH   REEF

The data recorded in the field during the Patch Reef transect survey is displayed in Figure 48 along with the QuickBird and IKONOS classifications for the pixels along the same transect. The figure consists of 3 graphs, 1 for each set of data. The horizontal axis of each graph represents the distance in meters along the transect from the starting point at the edge of the patch reef, while the vertical axis represents different classes. These graphs are stacked vertically to facilitate cross referencing between the 3 sets of data. Class transitions are identified by letters, and some transitions to the same class within a small distance are grouped together (i.e., transition A in QuickBird and transition C in the groundtruth data) in an effort to make discussion of these results easier.
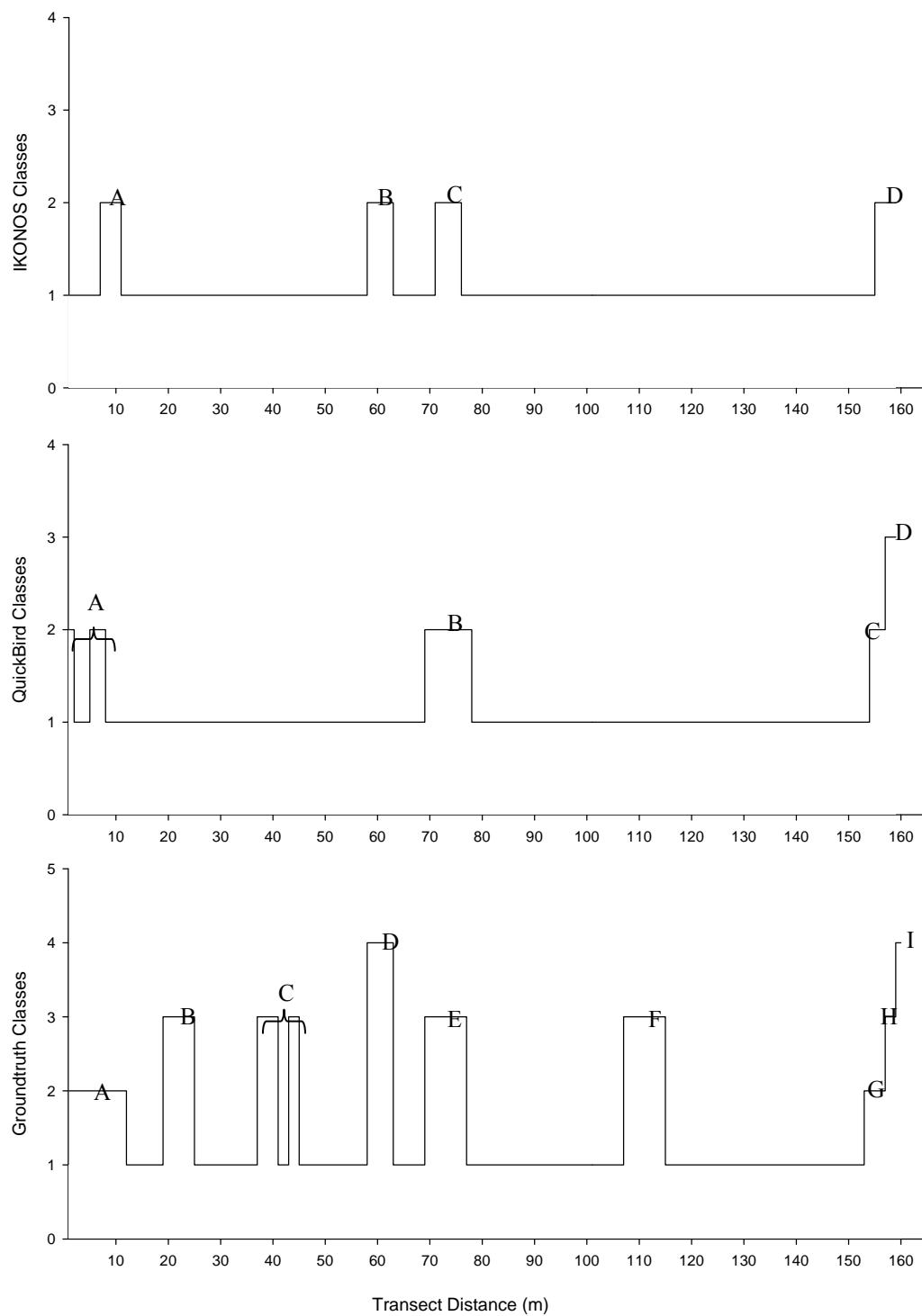
Figure 48.   Patch Reef Transect: (Bottom) Groundtruth classification; (Middle)
QuickBird classification; (Top) IKONOS classification

THIS PAGE INTENTIONALLY LEFT BLANK

VII. DISCUSS ION

Remote sensing provides an important, complementary approach to *in situ* fieldwork for monitoring benthic habitats in shallow water environments. This research builds on the work of Mumby and Edwards (2002); Capolsini et al. (2003); and Benefield et al. (2007), mapping coral reef environments, and Wang et al. (2004), classifying coastal mangrove habitats. The overarching goal is to determine the effects of higher spatial resolution on classification accuracy. These studies have shown that the increase in resolution from Landsat (30 m pixels) to IKONOS (4 m pixels) and (QuickBird 2.8 m pixels) produced improvements in classification accuracy. The research presented here examines the effects on classification accuracy achieved by the smaller increase in resolution from QuickBird to IKONOS in a coral reef environment, where, due to its high spatial heterogeneity, even a small increase in spatial resolution is hypothesized to result in higher classification accuracy.

A. CENTRAL   ATOLL

Overall accuracies for the benthic classifications derived from QuickBird and IKONOS imagery for Midway Atoll are lower than those for similar classifications carried out by other researchers elsewhere using these same satellites with similar processing techniques (Andréfouët et al., 2003; Wang et al., 2004; Benfield et al., 2007). Overall accuracy for QuickBird was 44.44% and for IKONOS was 51.11% based on the 5 class error matrix (Tables 12 and 13). Producer's accuracies saw mixed results between the two satellite sensors. QuickBird had greater than 70% Producer's accuracy in 3 of the 5 classes (algae/turf/coral, coral/coralline algae, and sand) with the remaining two classes' Producer's accuracies less than 25%. Only 1 of IKONOS's Producer's accuracies was greater than 70%: the coral/coralline algae class with 100%. Producer's accuracies in the other 4 classes were less than 55%. On average the User's accuracies were lower than Producer's accuracies for both satellite sensor classifications. Both QuickBird and IKONOS had only one class with User's accuracy higher than 70% (coral/coralline algae and sand/rubble/turf respectively).

These results showed unusually low classification accuracies for the rubble/turf and sand/rubble/turf classes for both satellite sensors. For QuickBird, the rubble/turf class had the lowest Producer's and User's accuracies; while the sand/rubble/turf class had the lowest Producer's accuracy for IKONOS. These 2 classes are difficult to differentiate in the field, even to trained eyes. The low accuracies for rubble/turf and sand/rubble/turf were the first indicator of a significant source of error in this research: the quality of the groundtruth data collection. The two authors of this thesis conducted the *in situ* survey and produced the Central Atoll groundtruth data without being trained as marine scientists. This was also our first attempt at this type of fieldwork. Fieldwork of this nature is ideally conducted by individuals with extensive knowledge of coral reef environments and previous experience in performing underwater surveys. Our fieldwork team received familiarization training on the plants, animals, and habitats that characterize the benthic environment of Midway Atoll before entering the field. Training utilized taxonomic field guides, satellite imagery, maps, and underwater photographs. We were trained on photographic examples of all 5 classes used in the classification, and were required to identify substrates from underwater photographs taken at Midway Atoll as part of this training. However, no amount of offsite training can ever substitute for the knowledge and experience gained from actually conducting fieldwork *in situ*.

Therefore, misclassification errors likely resulted from the quality of the groundtruth data. In an effort to minimize errors caused by the difficulty in distinguishing the rubble/turf class from the sand/rubble/turf class in the field, these 2 classes were merged into a single class which maintained the name sand/rubble/turf. The accuracy results based on these 4 classes are displayed in Tables 14 and 15. The Overall 4 class error matrix accuracy achieved by QuickBird and IKONOS were 52.59% and 61.48% respectively (Tables 14 and 15). The consolidation of the rubble/turf and the sand/rubble/turf class did not affect the satellite sensors ranking based on Overall classification performance: both satellites saw an increase in Overall accuracy of about 10%. QuickBird retained 3 classes with Producer's accuracies greater than 70% and saw an increase in those classes with User's accuracy greater than 70% (coral/coralline algae and sand/rubble/turf). IKONOS saw no increase in the number of classes with

Producer's or User's accuracies higher than 70%, and retained one class above 70% in each type of accuracy (coral/coralline algae and sand/rubble/turf respectively). On average the sand/rubble/turf class experienced an increase of 16.28% across Producer's and User's accuracies between the two satellites after the merger of the rubble/turf and sand/rubble/turf classes.

The Overall accuracies suggest that IKONOS performed better than QuickBird in classifying benthic substrates at Midway Atoll, although the results are likely not statistically significant. This finding agrees with the results reported by Wang et al. (2004) on mapping mangrove populations using these two satellite sensors.

Geoposition accuracy was another potential source of error for the Central Atoll groundtruth. There were several possible sources for geoposition error in this research: the imagery geopositional accuracy (23 meters CE90% for QuickBird and 15 meters CE90% for IKONOS, based on the images used in this research); the extrapolation of locations from one image to the other; and the variable geopositional accuracy of the handheld GPS units (<10 meters, 95% typical) used during fieldwork. The accuracy for handheld units varies spatially and temporally depending on the number of GPS satellites in view from the unit. This also resulted in a couple of occasions where benthic substrates observed in the field did not agree with QuickBird or IKONOS classifications, but the predicted class from one or both satellite sensors was located adjacent to the survey site (within 25 meters).

B. PATCH   REEF

A transect was used to record the *in situ* benthic substrate data of the Patch Reef in the lagoon of Midway Atoll. Transects are commonly used to groundtruth data in benthic environments. Joyce et al. (2004) and Hodgson et al. (2004) are 2 examples of the use of benthic transects in coral reef habitats. Additionally Roelfsema et al. (2004) suggest that a transect is an appropriate validation method for high spatial resolution multispectral data such as QuickBird imagery.

In assessing the performance of the Patch Reef classifications, error matrices were not used due to the elongated (directional) shape of the reef, and the uneven distribution

of classes found along the transect (disproportionately representing 1 class over the others). A graphical display was chosen instead to highlight class transitions along the benthic transect. When comparing the satellite classifications to the groundtruth data in the Patch Reef results (Figure 48), the most noticeable difference is the greater number of transitions in the groundtruth data: the groundtruth contains 9 substrate transitions while the QuickBird and IKONOS classification each contain only 4 class transitions.

Algae was the most abundant class along the transect and is represented in each graph by Class 1. The groundtruth data indicates that the beginning of the transect is characterized by 12 meters of Class 2 (groundtruth transition A). The classifications for QuickBird and IKONOS both contain a class transition within the first 12 meters, but they do not agree entirely with the groundtruth. Near the center of the transect the groundtruth data contains transitions D and E to classes 4 and 3 respectively. The IKONOS classification contains transitions B and C, both to class 2, and the QuickBird classification only identified the second transition (QuickBird transition B). At the end of the transect the groundtruth data contains 3 substrate transitions: G, H, and I. The QuickBird classification only identified 2 transitions (QuickBird transitions C and D) while the IKONOS classification only has 1 class transition (IKONOS transition D). Finally, the groundtruth data contains 3 additional transitions that were omitted by both QuickBird and IKONOS (groundtruth transitions B, C, and F).

A count of omissions and misclassifications will be used to summarize the discussion of these data sets. The QuickBird classification contains 5 omission errors when compared to the groundtruth data. These correspond to groundtruth transitions B, C, D, F, and I. The IKONOS classification also contains 5 omission errors. The omissions correspond to transitions B, C, F, H, and I in the groundtruth. IKONOS also misclassified groundtruth transition D.

Based on these findings, QuickBird may seem to perform better than IKONOS at identifying class transitions along a transect, but these results are likely not statistically significant: the small improvement is based on one less misclassification than IKONOS. Both satellite sensors contained 5 omission errors out of 9 class transitions so neither performed very well in identifying class transitions at this scale. Perhaps the feature

86

variability within the Patch reef was not well suited to determine the effects of higher spatial resolution on classification accuracy at this scale. The average feature (class) size along the transect was > 5 m. A feature size of 3 - 4 m, between the resolutions of the 2 sensors, might be better suited for this experiment.

The Patch Reef transect was placed in the field starting at a known point (most northern tip of the reef) and followed a magnetic bearing of 180º in the presence of ocean currents. In order to compare the groundtruth data to the QuickBird and IKONOS classifications the transect had to be plotted in the image analysis software ENVI. There was no precise way to translate a magnetic bearing in ENVI and reproduce the field transect exactly. Instead the known point was used in conjunction with the measured length of the transect. The known start point was easily located on the images in ENVI and the Measurement Tool was used to find a bearing to the Southern edge of the patch reef, producing a transect with equal length to the transect length measured in the field. This process likely introduced geopositional error with contingent misclassifications at the Patch Reef scale.

C. CROSS   SCALE COMPARISON

Ju et al. (2005) highlight the increasing need for applications involving land classifications at multiple spatial scales. Some classification techniques require classifications to be performed at a fine scale (such as the Path Reef) so that information obtained from the fine scale can be applied to a coarser scale (such as the Central Atoll) to classify the coarse scale with higher accuracy (Laliberte, et al., 2005). Additionally, Raptis et al. (2003) show that a single scale cannot accurately represent all classes in a complex scene. These studies demonstrate a need to understand the accuracy of remotely sensed data at various spatial scales.

On a coarse scale level (Central Atoll subset), IKONOS achieved higher overall classification accuracies, while QuickBird was better at identifying class transitions on a fine scale level (Patch Reef subset). However these results are not statistically significant, and only marginal improvements in accuracy were suggested by their

performances in each scale. The minor difference in accuracies for each sensor suggests that their performance is consistent and comparable across scales.

D. OVERALL FINDINGS

This research does not show any significant improvement in classification accuracy of the QuickBird sensor over the IKONOS sensor for the highly heterogeneous coral reef environment of Midway Atoll. Further research is necessary to demonstrate this finding with any level of statistical significance. Perhaps the increase in spatial resolution between these 2 satellite sensors (4 m to 2.8 m) is too small to produce a substantial increase in classification accuracy as shown in previous comparisons. The difference in accuracy between these 2 classifications could be within the range of the environmental variations occurring at image acquisition.

VIII. COST BENEFIT ANALYSIS

A cost benefit analysis was conducted to consider the benthic classification accuracy results obtained from QuickBird and IKONOS in a different light. The goal here was to examine the impact of various factors on the decision regarding which imagery products to use for benthic classification research. The framework for this analysis was derived from the Department of Defense's Enterprise Integration Toolkit (Version 2.0): Business Case Development Guide (2003). It should be noted that the process in that document was designed to turn a problem statement into a business decision and to provide financial justification for that decision. Research applications for satellite imagery do not typically fall into that scenario, but the underlying principles behind the business case development can be directly applied to this area of research in order to facilitate matching imagery investments to research needs.

This analysis will be divided into the following steps:

- Confirm understanding of the problem / opportunity

- Identify potential solutions

- State key assumptions

- Analyze each solution to detail costs and benefits

- Assess risks

- Present results

- Perform sensitivity analysis

- Determine whether further analysis is warranted

A.   PROBLEM / OPPORTUNITY

The commercial sector is not flooded with opportunities to exploit the classification of benthic environments. Unlike the commercial industry, the studies of oceanography and marine biology have several uses for such techniques. Two important

questions posed by researchers today involve assessing the current state of the world's coral reefs and determining the impact that mankind's footprint has on coral reefs (Lubin et al., 2001). In order to answer these questions researchers need to assess the extent, biodiversity, and health of large areas of coral reefs, many of which occur in remote areas of the planet. A cost effective solution to this problem would provide tremendous benefit to this field of research.

B. POTENTI   AL SOLUTIONS

There are 2 broad categories for solutions to the problem on assessing the extent, biodiversity, and health of coral reef habitats. The first is to send personnel and equipment into the field to survey reefs habitats. The second is to assess these properties of a reef using some form of remote sensing.

Fieldwork of this nature will often involve some type of underwater surveying, usually SCUBA or snorkeling. This can be accomplished by people, robotic submersibles, or some combination of the two. The major drawback to fieldwork is that it is expensive, arduous, and time consuming (Mumby et al., 1999).

Remote sensing offers many potential solutions to this problem. There are multiple ways to obtain remotely sensed data. Two possibilities are airborne sensors and satellite sensors. Airborne sensors are not always an option due to physical and political limitations imposed on the airspace in certain parts of the world. There are no such limitations on satellite sensors. This does not imply that there are no limitations on the acquisition of satellite data, rather it means that every spot on the planet is accessible by satellite, and that to date there are no legal restrictions to prevent satellite over flight. After a remote sensing platform is chosen, there are several options for sensor type such as panchromatic, multispectral, and hyperspectral.

For the purposes of this cost benefit analysis, and to remain within the scope of this research, benthic classifications derived from QuickBird and IKONOS multispectral data will be examined. These 2 satellite sensors are routinely used to determine the extent and size of coral reef habitats, and by proxy, to assess the biodiversity and health of coral reefs.

90

C. ASSUMP   TIONS

Three key assumptions were made in order to conduct this cost benefit analysis. These assumptions were chosen to duplicate the data used in the methods section of this research. The effects of varying these assumptions will be examined in the sensitivity analysis.

The first assumption is that the same processing techniques will be applied to both sets of imagery. This is a necessary assumption since unprocessed multispectral imagery is of little use in assessing the extent, biodiversity, or health of coral reef habitats. The imagery must be processed and classified in order to retrieve this type of information. The image processing does not have to be the same as outlined in the Methods section of this thesis, but the same process has to be applied to both the QuickBird and the IKONOS multispectral imagery.

The next assumption is that the area encompassing the coral reefs of interest is 40 km^2. This area was chosen since it is the approximate size of the Central Atoll subset used in this thesis. The important factor here is that the classification areas from both QuickBird and IKONOS are the same size.

The final assumption pertains to the timeliness of the satellite imagery. It is assumed that imagery will be usable for up to one year before it is considered superseded or obsolete. The period was chosen based on the dates of the imagery used in this research (October 2007 and May 2008). One year might be considered too long of an interval by some coral reef researchers, but shorter time periods will be considered in the sensitivity analysis.

D. COSTS

The cost for this analysis will be divided into two categories, price and size. The price of imagery is a direct cost for this type of research. The size of that imagery also contributes to the overall cost for this type research. As imagery size increases so does the cost associated with storing and transmitting it. One might point out that there are labor costs associated with processing the imagery in order to obtain useful information.

This is true, but labor costs have been omitted from this analysis based on the assumption that the same type of processing is being applied to both types of imagery.

Neither Digital Globe nor GeoEye publish printed commercial pricing lists for their imagery. Pricing information was obtained over the phone directly from customer service representatives from each company. Pricing data for QuickBird is displayed in Table 16 and IKONOS data is displayed in Table 17. The information in these tables reflects imagery pricing as of 15 August 2008.

Image Source	Minimum Order Area (km^2)	Price (per km^2)	Minimum Order Cost
Archive	25	$ 24	$ 600
New Tasking	64	$ 28	$ 1792

Table 16.   QuickBird imagery pricing (DigitalGlobe, pers. comm.)

Image Source (Age)	Minimum Order Area (km^2)	Price (per km^2)	Minimum Order Cost
Archive (older than 6 months)	49	$ 7	$ 343
Archive (within 6 months)	49	$ 18	$ 864
New Tasking	100	$ 18	$ 1800

Table 17.   IKONOS imagery pricing (GeoEye, pers. comm.)

Based on the information in Tables 16 and 17 the cost for the imagery used for the Central Atoll classification for QuickBird was $960 (40 km^2 x $24) and for IKONOS was $864 (minimum order cost for archived imagery taken within the last 6 months).

Data size is a little bit trickier to calculate than price. The QuickBird image was delivered as a single National Imagery Transmission (.NTF) file with a size of 89.849 megabytes (MB). The IKONOS image was delivered as 4 .NTF files with a total size of 86.040 MB. The QuickBird .NTF file contains "JPEG2000" compression while the IKONOS .NTF file is not compressed. The sizes of the original imagery files should not be compared directly since they cover different amounts of area and one format utilizes

compression. Instead comparisons will be made using a common file format covering the same size area. The ENVI file format was chosen for this comparison since that is the format used for the image processing in this research. The Central Atoll Subset was used as the classification area for the purpose of this comparison. The QuickBird data for the Central Atoll was 42.285 MB while the IKONOS data was 20.514 MB: the QuickBird data is roughly twice the size of the IKONOS data for a given area.

E. BENEFITS

Given the problem / opportunity of assessing the extent, biodiversity, and health of coral reef habitats the most important benefit for this analysis is classification accuracy, both Overall accuracy and accuracy in classifying coral reefs. Based on the results outlined in Chapter VI, QuickBird achieved an overall classification accuracy of 52.59% with coral/coralline algae Producer's accuracy of 72.00% and User's accuracy of 75.00%. IKONOS achieved an Overall accuracy of 61.48% with a coral/coralline algae Producer's accuracy of 100.00% and User's accuracy of 60.98%. The goal is to determine which set of accuracies provides greater benefit for the problem / opportunity.

Taking the accuracies at face value and leaving statistical significance aside, IKONOS's Overall accuracy is better than the Overall accuracy achieved by QuickBird, but Overall accuracy is not actually the best metric for the problem / opportunity of assessing the extent, biodiversity, and health of coral reefs. IKONOS also has a higher Producer's accuracy, and 100% would seem like a convincing statistic. QuickBird, on the other hand, achieved a higher User's accuracy in the coral/coralline algae class. In order to see which of these accuracies poses more of a benefit, one must consider what each type of accuracy really means. IKONOS's Producer accuracy says that if coral/coralline algae exist in the classification area that IKONOS identifies it correctly 100% of the time. QuickBird's User accuracy says that 75% of the area that it classifies as coral/coralline algae is actually coral/coralline algae. For the purpose of assessing the extent, biodiversity, and health of coral reefs the User's accuracy provides a greater benefit than the Producer's accuracy since coral reef researchers need to know that the results of their classifications accurately represent the actual reef habitats.

With IKONOS having a higher Overall accuracy and QuickBird having a higher User's accuracy how does one decide which is more beneficial? The answer to that question depends on the specific research application. Considering the problem / opportunity posed in this analysis a very slight edge would be given to QuickBird, based on its higher coral/coralline algae User's accuracy.

F. RISKS

The risk associated with using either set of satellite imagery to assess the extent, biodiversity, and health of coral reefs is misclassification of the imagery. Based on the User's accuracies there is a 25% chance that bottom types classified as coral/coralline algae by QuickBird will actually be a different substrate. There is a 40% chance that bottom types classified as coral/coralline algae by IKONOS will be misclassified. QuickBird clearly has a lower risk, but whether 25% is an acceptable risk depends on the research application, and will be determined by individual researchers.

G. RESULTS

Given the costs associated with these 2 solutions and the small benefit obtained by using QuickBird imagery, it is difficult to determine with certainty which solution coral reef researchers should use. Considering that QuickBird imagery costs 10% more than IKONOS and takes up twice as much space with only a small increase in benefit, one could not fault a researcher for choosing to use IKONOS imagery instead. Based on the assumptions of this analysis, it is too close to declare either solution as the preferred choice based on the costs and benefits uncovered in this analysis.

H. SENSITI   VITY ANALYSIS

The first variable to be examined in this sensitivity analysis is observation area. We will consider the effects of both reducing and increasing the area of observation on the imagery price. Table 18 shows the effects to image price based on various observation areas.

Size (km²)	QuickBird Price	IKONOS Price
20	$ 600	$ 343
80	$ 1920	$ 1440
100	$ 2400	$ 1800
200	$ 4800	$ 3600
500	$ 12000	$ 9000
1000	$ 24000	$ 18000

Table 18.   Affect of observation area on image price

With the original area of 40 km² the IKONOS imagery was 10% cheaper than QuickBird. Table 18 shows that reducing that area to 20 km² makes IKONOS imagery approximately 40% less expensive. Increasing the area to 80 km² makes IKONOS imagery 25% less expensive. IKONOS imagery maintains this ratio to QuickBird imagery for all areas greater than 80 km² due to a linear relationship between price and area after the minimum order size has been reached for both types of imagery. Across the spectrum of observation area, IKONOS imagery is less expensive than QuickBird imagery with small areas seeing the greatest price differential. This could justify a researcher's decision to use IKONOS imagery to reduce research cost while accepting a reduction in accuracy.

Next the timeliness of the satellite imagery will be examined. One of the original assumptions was that imagery could be up to 1 year old. Now the effect on price of requiring that imagery is acquired within the past six months and as recently as possible by placing a new tasking order will be considered. Acquisition time's affect on imagery price is displayed in Table 19.

Acquisition Time	QuickBird Price	IKONOS Price
Within 6 months	$ 960	$ 864
New Tasking	$ 1792	$ 1800

Table 19.   Affect of acquisition time on imagery price

Requiring that imagery be acquired within the last six months had no affect on the price based on the pricing tiers of Digital Globe and GeoEye. IKONOS imagery is still approximately 10% cheaper for this timeframe. If new tasking is required the price of IKONOS imagery becomes slightly more expensive, $8 more to be exact. In research that requires new tasking the cost of the imagery becomes essentially equal so one could be justified in choosing QuickBird imagery for its slight improvement at accurately identifying coral/coralline algae.

I. FURTHE   R ANALYSIS

The first consideration to be given to future analysis is a larger sample. The assessment accuracy achieved from this relatively small sample (135 sites) could be improved by using a larger sampling of sites. A better accuracy assessment would produce a more accurate benefit assessment for the two products and give researchers more useful guidance on when and where each type of imagery could be used for different research applications. Considering the relatively simple tiered pricing system for each type of imagery, there is no need for further analysis of imagery cost from either imaging satellite.

One area that lies well outside the scope of a cost benefit analyses but could prove beneficial to future benthic classifications is research on the processing techniques used on growing data sets. There is roughly twice as much data in the QuickBird imagery as in the IKONOS imagery covering the same area, yet the same processing techniques are used on both images. It is not surprising that roughly the same amount of accurate information can be extracted from the two different data sets based on the same processing techniques. Perhaps research should be devoted into new and different ways to process imagery in order to extract more useful information from data sets with higher data densities per unit area.

IX. CONCLUSIONS   AND RECOMMENDATIONS

This research does not identify any improvements in thematic mapping accuracy at Midway Atoll based on the use of QuickBird's higher spatial resolution satellite imagery. The higher resolution imagery did not demonstrate a significant improvement in classification accuracy over the classification results achieved by IKONOS. This finding is in agreement with the results of Wang et al. (2004), but contrasts the conclusions of Mumby and Edwards (2002), Capolsini et al. (2003), and Benefield et al. (2007). The cross scale accuracy comparison showed that the overall classification accuracy of both satellite sensors was consistent across spatial scales.

When assessing the extent, biodiversity, and health of coral reefs from a cost and benefit perspective, these results showed that IKONOS imagery comes with a lower overall cost and only a minor degradation in coral reef User's classification accuracy. However, this conclusion considers only one problem / opportunity for benthic classification research. Other problems / opportunities could drastically alter the cost benefit ratio. The decision of which imagery to use for a given application is ultimately left up to individual applications and researcher's needs.

Several opportunities exist to improve on the research findings presented here. Most notably would be the collection of new groundtruth data by a more experienced survey team. To further improve the results, future studies should incorporate an *in situ* collection of a training dataset which requires longer field time or multiple trips to the field site. The training dataset would then be used to perform supervised classifications before the team returned to the field to collect the final evaluation dataset. This process should produce better accuracies across the board for both satellite sensors. Finally, as hypothesized in the cost benefit analysis, perhaps more research should be devoted to developing new techniques to process the larger amounts of data that higher spatial resolution imagery possesses.

THIS PAGE INTENTIONALLY LEFT BLANK

APPENDIX A.   METADATA FILE FOR QUICKBIRD IMAGE

```
version = "AA";
generationTime = 2008-04-22T17:57:45.000000Z;
productOrderId = "005759233010_01_P002";
productCatalogId = "90100100237BB400";
childCatalogId = "20200100237BB300";
imageDescriptor = "Basic1B";
bandId = "Multi";
panSharpenAlgorithm = "None";
numRows = 7168;
numColumns = 7168;
productLevel = "LV1B";
productType = "Basic";
numberOfLooks = 1;
radiometricLevel = "Corrected";
bitsPerPixel = 16;
compressionType = "JPEG2000";
jpegProfileName = "nga_npje_pan_nl";
BEGIN_GROUP = BAND_B
        ULLon = -177.45685139;
        ULLat =   28.34181712;
        ULHAE =    -1.00;
        URLon = -177.25308095;
        URLat =   28.34091560;
        URHAE =    -1.00;
        LRLon = -177.25229003;
        LRLat =   28.17550307;
        LRHAE =    -1.00;
        LLLon = -177.45798927;
        LLLat =   28.17459241;
        LLHAE =    -1.00;
        absCalFactor = 1.604120e-02;
        effectiveBandwidth = 6.800000e-02;
END_GROUP = BAND_B
BEGIN_GROUP = BAND_G
        ULLon = -177.45685139;
        ULLat =   28.34181712;
        ULHAE =    -1.00;
        URLon = -177.25308095;
        URLat =   28.34091560;
        URHAE =    -1.00;
        LRLon = -177.25229003;
        LRLat =   28.17550307;
        LRHAE =    -1.00;
        LLLon = -177.45798927;
        LLLat =   28.17459241;
        LLHAE =    -1.00;
```

```
        absCalFactor = 1.438470e-02;
        effectiveBandwidth = 9.900000e-02;
END_GROUP = BAND_G
BEGIN_GROUP = BAND_R
        ULLon = -177.45685139;
        ULLat =   28.34181712;
        ULHAE =    -1.00;
        URLon = -177.25308095;
        URLat =   28.34091560;
        URHAE =    -1.00;
        LRLon = -177.25229003;
        LRLat =   28.17550307;
        LRHAE =    -1.00;
        LLLon = -177.45798927;
        LLLat =   28.17459241;
        LLHAE =    -1.00;
        absCalFactor = 1.267350e-02;
        effectiveBandwidth = 7.100000e-02;
END_GROUP = BAND_R
BEGIN_GROUP = BAND_N
        ULLon = -177.45685139;
        ULLat =   28.34181712;
        ULHAE =    -1.00;
        URLon = -177.25308095;
        URLat =   28.34091560;
        URHAE =    -1.00;
        LRLon = -177.25229003;
        LRLat =   28.17550307;
        LRHAE =    -1.00;
        LLLon = -177.45798927;
        LLLat =   28.17459241;
        LLHAE =    -1.00;
        absCalFactor = 1.542420e-02;
        effectiveBandwidth = 1.140000e-01;
END_GROUP = BAND_N
outputFormat = "NITF21NCDRD";
BEGIN_GROUP = IMAGE_1
        satId = "QB02";
        mode = "FullSwath";
        scanDirection = "Forward";
        CatId = "101001000746DD00";
        TLCTime = 2007-10-18T23:02:34.928985Z;
        numTLC = 2;
        TLCList = (
        (0,  0.000000),
        (6930,  4.017391)           );
        firstLineTime = 2007-10-18T23:02:34.928986Z;
        avgLineRate = 1725.00;
        exposureDuration = 0.00057971;
        minCollectedRowGSD =   2.657;
```

```
        maxCollectedRowGSD =   2.667;
        meanCollectedRowGSD =   2.661;
        minCollectedColGSD =   2.906;
        maxCollectedColGSD =   2.938;
        meanCollectedColGSD =   2.923;
        meanCollectedGSD =   2.789;
        rowUncertainty =   38.29;
        colUncertainty =   55.93;
        minSunAz = 167.3;
        maxSunAz = 167.3;
        meanSunAz = 167.3;
        minSunEl =  51.3;
        maxSunEl =  51.5;
        meanSunEl =  51.4;
        minSatAz = 265.6;
        maxSatAz = 273.9;
        meanSatAz = 269.5;
        minSatEl =  64.7;
        maxSatEl =  65.5;
        meanSatEl =  65.1;
        minInTrackViewAngle =  -4.2;
        maxInTrackViewAngle =  -2.9;
        meanInTrackViewAngle =  -3.6;
        minCrossTrackViewAngle = -23.1;
        maxCrossTrackViewAngle = -22.6;
        meanCrossTrackViewAngle = -22.9;
        minOffNadirViewAngle =  23.1;
        maxOffNadirViewAngle =  23.1;
        meanOffNadirViewAngle =  23.1;
        PNIIRS = 2.8;
        cloudCover = 0.000;
        resamplingKernel = "CC";
        TDILevel = 13;
        positionKnowledgeSrc = "R";
        attitudeKnowledgeSrc = "R";
        revNumber = 33718;
END_GROUP = IMAGE_1
END;
```

THIS PAGE INTENTIONALLY LEFT BLANK

APPENDIX B.   METADATA FILE FOR IKONOS IMAGE

```
=============================================================
Version Number: 2.0
=============================================================
Company Information
    Address
        GeoEye
        12076 Grant Street
        Thornton, Colorado 80241
        U.S.A.
    Contact Information
        On the Web: http://www.geoeye.com
        Customer Service Phone (U.S.A.): 1.800.232.9037
        Customer Service Phone (World Wide): 1.703.480.5670
        Customer Service Fax (World Wide): 1.703.450.9570
        Customer Service Email: info@geoeye.com
        Customer Service Center hours of operation:
            Monday - Friday, 8:00 - 18:00 Eastern Standard Time
=============================================================
Product Order Metadata

Creation Date: 05/19/08
Product Work Order Number: -00148344
Product Order Number: 283179
Customer Project Name: 0071009201-00001 /US/ Image Date 05/08/08-05/16/08
Ground Station ID: PGS
License Type: Nextview
Product Order Area (Geographic Coordinates)
  Number of Coordinates: 4
    Coordinate: 1
    Latitude: 28.1666667000 degrees
    Longitude: -177.4500000000 degrees
    Coordinate: 2
    Latitude: 28.2916667000 degrees
    Longitude: -177.4500000000 degrees
    Coordinate: 3
    Latitude: 28.2916667000 degrees
    Longitude: -177.2833333000 degrees
    Coordinate: 4
    Latitude: 28.1666667000 degrees
    Longitude: -177.2833333000 degrees
Product Order Area (Map Coordinates in Map Units)
    Coordinate: 1
    Map X (Easting): 472184.87 meters
    Map Y (Northing): 3115697.58 meters
    Coordinate: 2
    Map X (Easting): 455822.87 meters
    Map Y (Northing): 3115747.01 meters
    Coordinate: 3
    Map X (Easting): 455874.32 meters
    Map Y (Northing): 3129594.60 meters
    Coordinate: 4
```

Map X (Easting): 472217.26 meters
Map Y (Northing): 3129545.03 meters
Sensor Type: Satellite
Sensor Name: IKONOS-2
Processing Level: Standard Geometrically Corrected
Image Type: PAN/MSI
Interpolation Method: Cubic Convolution
Multispectral Algorithm: None
Stereo: Mono
Mosaic: No
Map Projection: Universal Transverse Mercator
  UTM Specific Parameters
    Hemisphere: N
    Zone Number: 1
Datum: WGS84
Product Order Pixel Size: 1.0000000000 meters
Product Order Map Units: meters
MTFC Applied: Yes
DRA Applied: No
Media: DVD
Product Media Format: DVD
File Format: NITF
  Compressed: No
  Bits per Pixel per Band: 11 bits per pixel
  UTM_MGRS_Geocoding: Yes
Multispectral Files: Four Files

===

Source Image Metadata

Number of Source Images: 2

Source Image ID: 2008050822480160000011621644
Product Image ID: 000
Sensor: IKONOS-2
Acquired Nominal GSD
  Pan Cross Scan: 0.92 meters
  Pan Along Scan: 0.86 meters
  MS Cross Scan: 3.66 meters
  MS Along Scan: 3.46 meters
Scan Azimuth: 180.03 degrees
Scan Direction: Reverse
Panchromatic TDI Mode: 13
Nominal Collection Azimuth: 261.0797 degrees
Nominal Collection Elevation: 70.35747 degrees
Sun Angle Azimuth: 125.3546 degrees
Sun Angle Elevation: 72.87940 degrees
Acquisition Date/Time: 2008-05-08 22:48 GMT
Percent Cloud Cover: 8

Source Image ID: 2008051622383980000011629646
Product Image ID: 001
Sensor: IKONOS-2
Acquired Nominal GSD
  Pan Cross Scan: 0.93 meters

Pan Along Scan: 1.05 meters
MS Cross Scan: 3.72 meters
MS Along Scan: 4.20 meters
Scan Azimuth: 179.98 degrees
Scan Direction: Reverse
Panchromatic TDI Mode: 13
Nominal Collection Azimuth: 14.2335 degrees
Nominal Collection Elevation: 60.79291 degrees
Sun Angle Azimuth: 115.4977 degrees
Sun Angle Elevation: 72.18840 degrees
Acquisition Date/Time: 2008-05-16 22:38 GMT
Percent Cloud Cover: 12
==
Product Space Metadata

Number of Image Components: 2
  X Components: 1
  Y Components: 1
Product MBR Geographic Coordinates
  Number of Coordinates: 4
    Coordinate: 1
    Latitude: 28.2916649704 degrees
    Longitude: -177.4505246186 degrees
    Coordinate: 2
    Latitude: 28.2921141802 degrees
    Longitude: -177.2833282465 degrees
    Coordinate: 3
    Latitude: 28.1666495089 degrees
    Longitude: -177.2829970925 degrees
    Coordinate: 4
    Latitude: 28.1662026422 degrees
    Longitude: -177.4499980586 degrees
Product Map Coordinates (in Map Units)
  UL Map X (Easting): 455822.87 meters
  UL Map Y (Northing): 3129594.60 meters
Pixel Size X: 1.0000000000 meters
Pixel Size Y: 1.0000000000 meters
Product Order Map Units: meters
Columns: 16396 pixels
Rows: 13900 pixels
Reference Height: 0.0000000000 meters
==
Product Component Metadata

Number of Components: 2

Component ID: 0000000
Product Image ID: 000
Component   File   Name: po_283179_pan_0000000.ntf   po_283179_red_0000000.ntf
po_283179_grn_0000000.ntf po_283179_blu_0000000.ntf po_283179_nir_0000000.ntf
  Thumbnail File Name: po_283179_rgb_0000000_ovr.jpg
Country Code:
Component Geographic Corner Coordinates
  Number of Coordinates: 4
    Coordinate: 1
105

Latitude: 28.2916844956 degrees
Longitude: -177.3445871982 degrees
Coordinate: 2
Latitude: 28.2918253226 degrees
Longitude: -177.2833274816 degrees
Coordinate: 3
Latitude: 28.1666495089 degrees
Longitude: -177.2829970925 degrees
Coordinate: 4
Latitude: 28.1665094148 degrees
Longitude: -177.3441853771 degrees
Component Map Coordinates (in Map Units)
  UL Map X (Easting): 466210.87 meters
  UL Map Y (Northing): 3129562.60 meters
Pixel Size X: 1.0000000000 meters
Pixel Size Y: 1.0000000000 meters
Product Order Map Units: meters
Columns: 6008 pixels
Rows: 13868 pixels
Percent Component Cloud Cover: 36

Component ID: 0010000
Product Image ID: 001
Component   File   Name: po_283179_pan_0010000.ntf   po_283179_red_0010000.ntf
po_283179_grn_0010000.ntf po_283179_blu_0010000.ntf po_283179_nir_0010000.ntf
Thumbnail File Name: po_283179_rgb_0010000_ovr.jpg
Country Code:
Component Geographic Corner Coordinates
  Number of Coordinates: 4
    Coordinate: 1
    Latitude: 28.2916649704 degrees
    Longitude: -177.4505246186 degrees
    Coordinate: 2
    Latitude: 28.2920089003 degrees
    Longitude: -177.3301986743 degrees
    Coordinate: 3
    Latitude: 28.1666531013 degrees
    Longitude: -177.3298130725 degrees
    Coordinate: 4
    Latitude: 28.1663109638 degrees
    Longitude: -177.4499985118 degrees
Component Map Coordinates (in Map Units)
  UL Map X (Easting): 455822.87 meters
  UL Map Y (Northing): 3129594.60 meters
Pixel Size X: 1.0000000000 meters
Pixel Size Y: 1.0000000000 meters
Product Order Map Units: meters
Columns: 11800 pixels
Rows: 13888 pixels
Percent Component Cloud Cover: 10

==

APPENDIX C.   REEF HABITAT CLASSIFICATION SCHEME

DATE:	TIME:	DIVE/SNORKEL #:	GPS coords:
Dive dist. and bearing from boat:		**Photos #:**	**Depth:**

REEF HABITAT CLASSIFICATION SCHEME FOR MIDWAY ATOLL, NWHI

ATOLL ZONES (select all that apply)	REEF HABITATS (select all that apply)	
A. LAND <u>modifiers</u> 　　tree (type:)　　　　shrub 　　grass 　　artificial (seawall, paving, 　　　　　bldgs., docks, etc.) *B. SHORELINE -INTERTIDAL* <u>modifiers</u> 　　sand/unconsolidated, artificial 　　consolidated, tidepools *C. REEF CREST* *D. FORE REEF* *E. SHELF- TERRACE* *F. DEEP ESCARPMENT* *G. LAGOON* *H. BACK REEF* North　　South　　West　　East	*GEOMORPHIC:* <u>modifiers</u> 1. calcareous pavement- 2. simple patch reef- 3. complex patch reefs- 4. linear reef- 5. pinnacle reef- 6. hole or pool- 7. vertical wall- 8. spurs and grooves- 9. pass or channel-	*BOTTOM COVER:* <u>ecological modifiers</u> a. unconsolidated sediments- *mud, sand,* 　　　*rubble, cobbles, boulders, etc.)* b. hard bottom (other than live coral) c. submerged vegetation- 　　turf algae 　　macro (fleshy) algae- 　　calcareous or coralline algae- d. live coral-　　　*percent cover:* _____ 　　*encrusting　semi-dome　monospecific* 　　*massive　　branching　　mixed* e. other invertebrates- sea urchins, sponges f. artificial- 　　concrete　　marine debris 　　metal　　　wood

Shelf-terrace quadrant diagram: 2 | 1 (top), 3 | 4 (bottom)

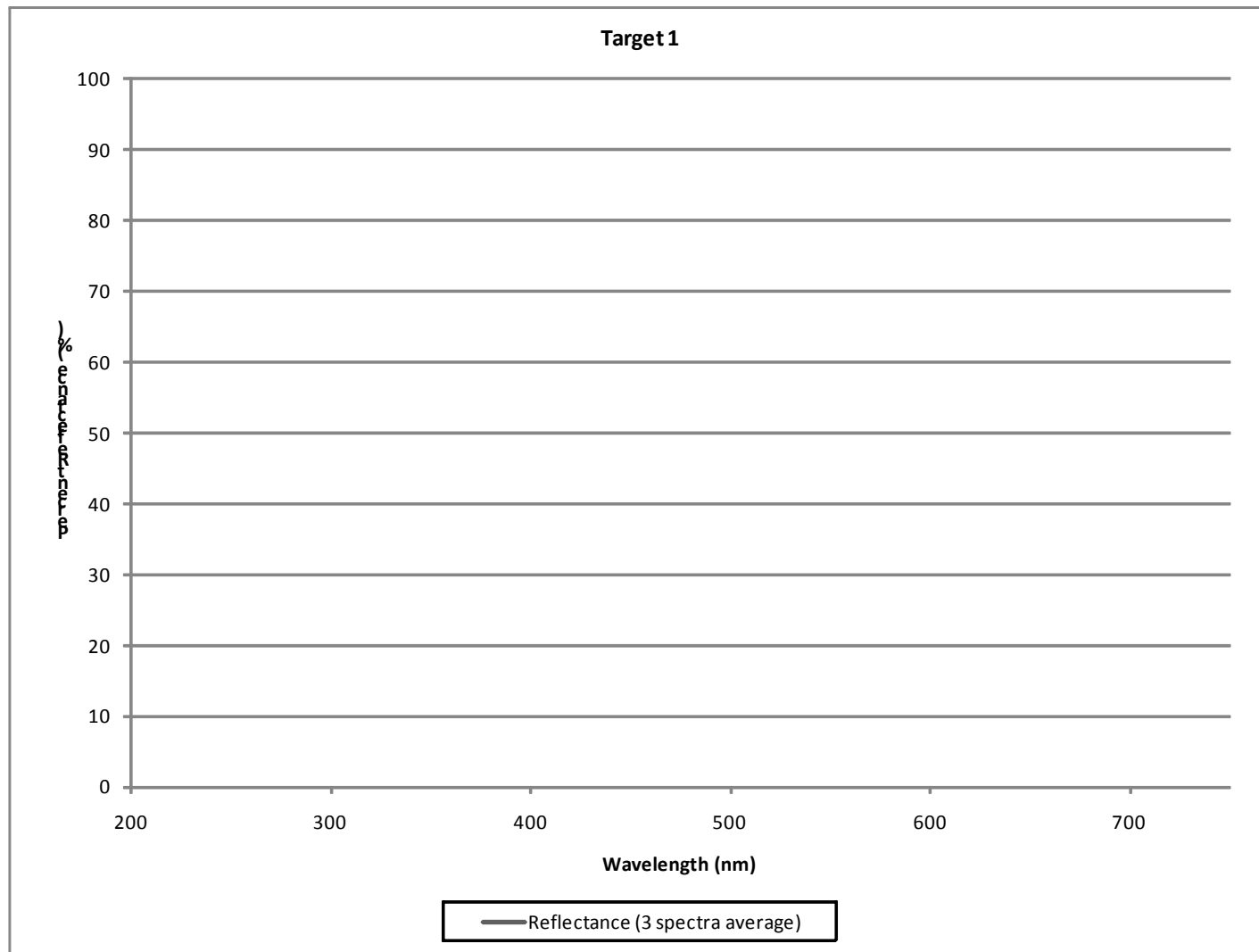| *Bottom cover abundance rating:*	D = Dominant	A = Abundant	C = Common	O = Occasional	R = Rare

NOTES:

THIS PAGE INTENTIONALLY LEFT BLANK
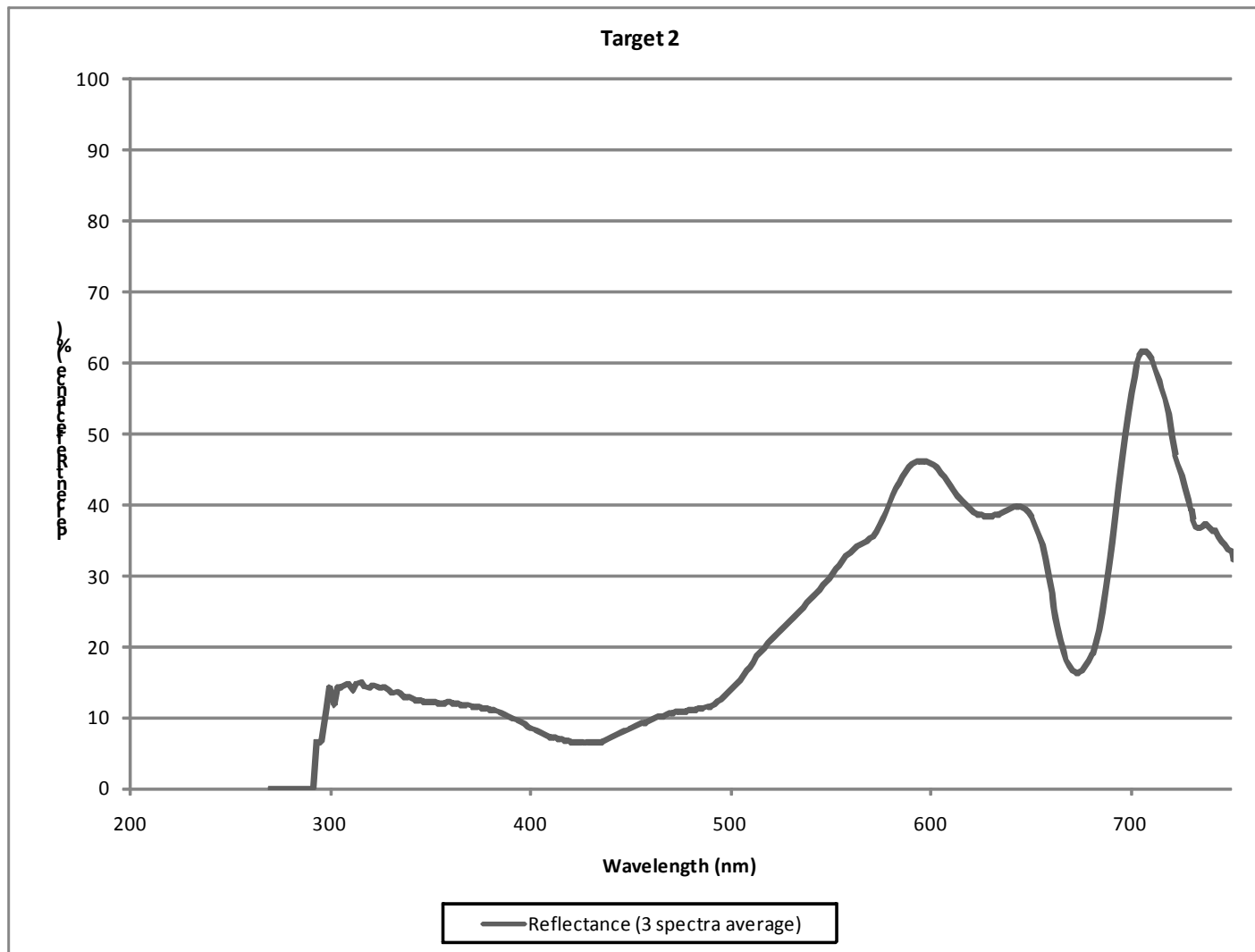
APPENDIX D.   LYNGBYA SPECTRA

While at Midway Atoll, several target spectra were recorded to add data to the Naval Postgraduate School's Remote Sensing Lab's cyanobacteria *Lyngbya* spp. spectral library. This appendix includes the procedure used to record the target spectra and the graphs of the 9 target spectra recorded. Each spectral graph is an average of 3 spectra for each target.

The following procedure was used to record spectra of the cyanobacteria *Lyngbya* spp. at Midway Atoll in July 2008 using a GER 1500 spectrometer:

1. Record a reference spectrum at the same depth as the sample. Hold the reference approximately 15 cm from the lens of the housing and at a 45 degree angle while recording. Be careful not to cast a shadow on the reference while taking the spectrum.

2. Record the target spectrum by holding the GER approximately 15 cm from the sample at a 45 degree angle to the target on the opposite side of the sun. Record 3 spectra of the *Lyngbya* spp. target.

3. Record spectra of surrounding substrates such as coral, sand, algae or turf covered rubble using the technique described in step 2.

4. Remember to record a new reference spectrum for each new sample site or after the sunlight conditions change conspicuously.

5. Download the spectra into the computer using the GER 1500 software.
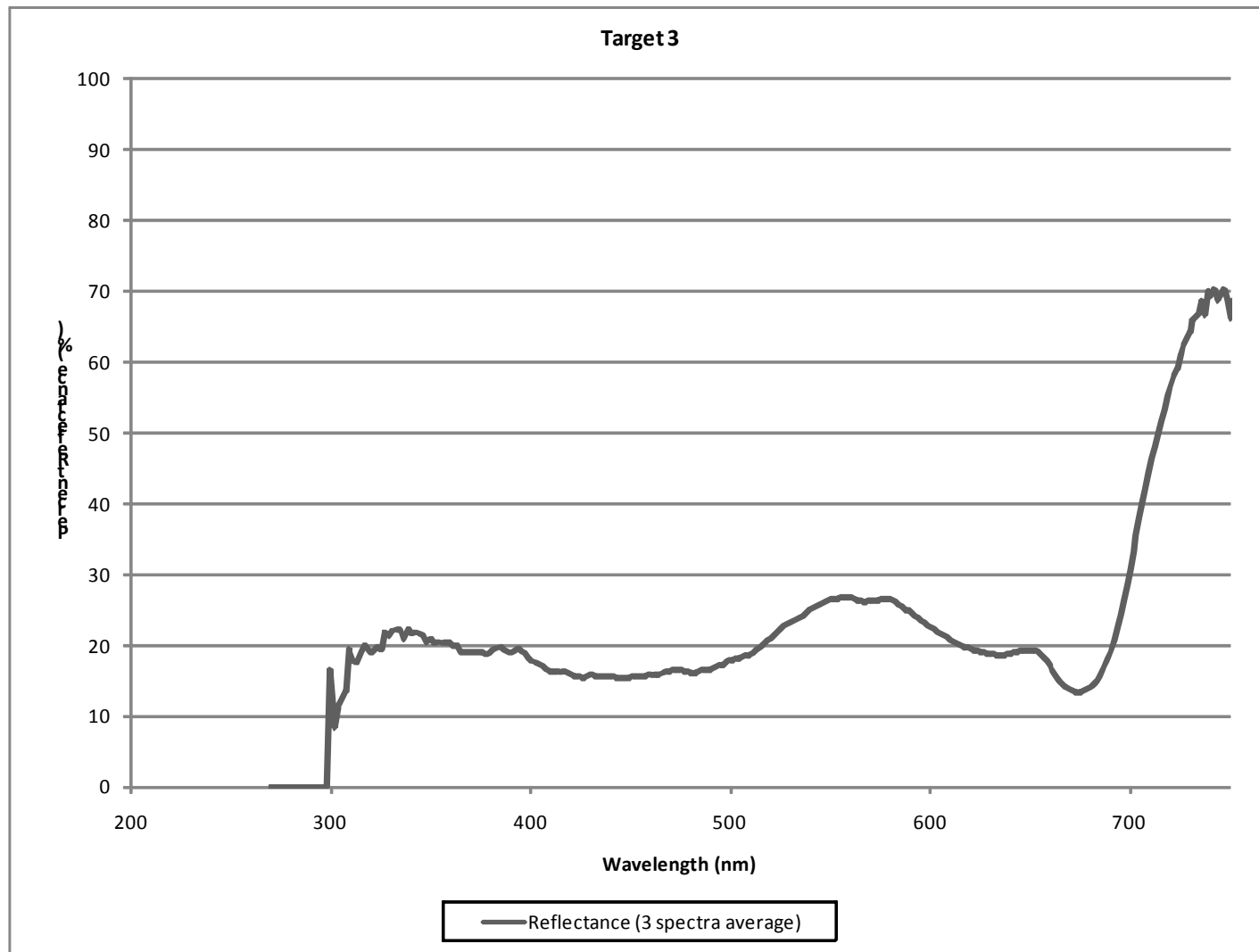
Target 1

Y-axis label: Reflectance (%)

X-axis label: Wavelength (nm)

Legend: Reflectance (3 spectra average)

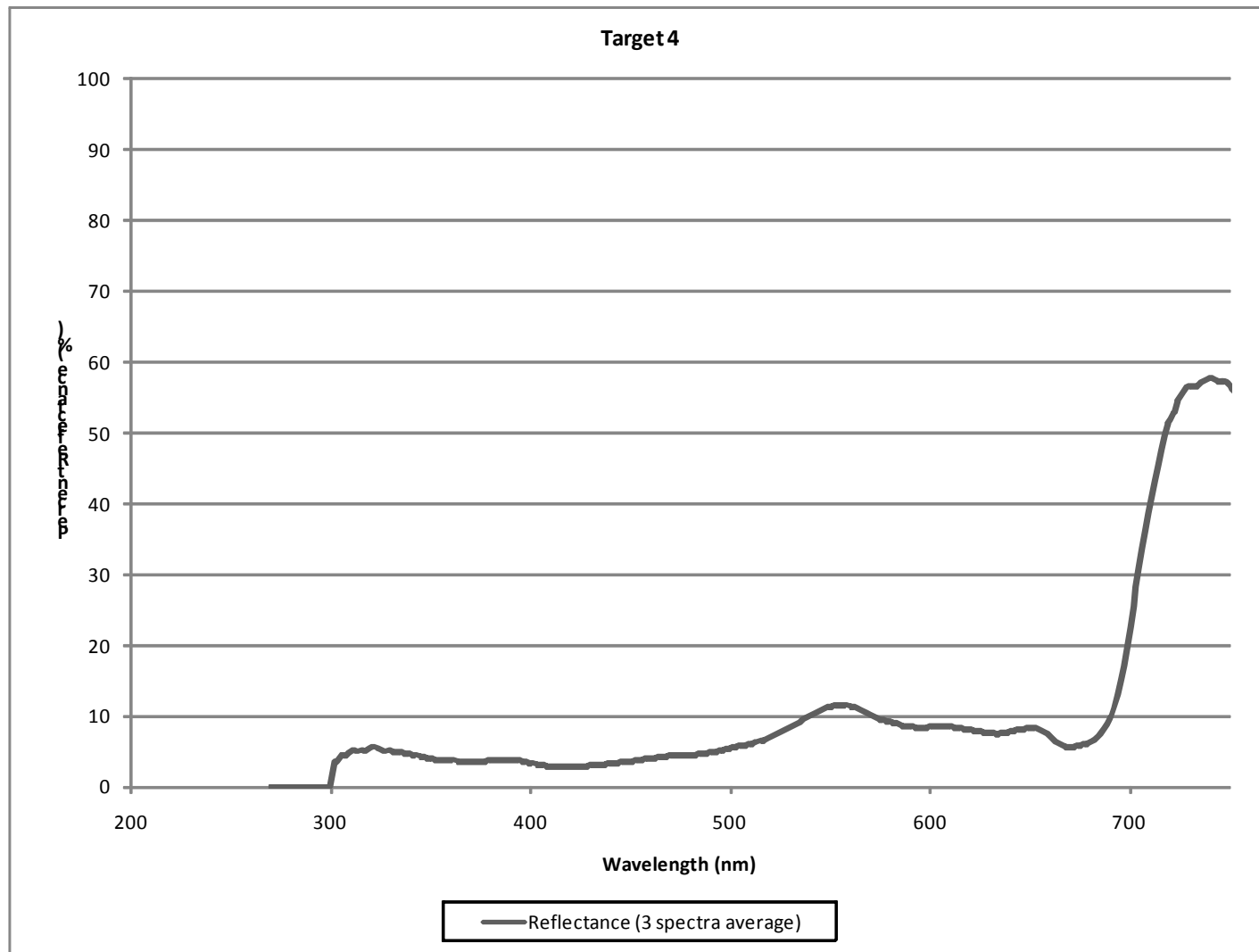Target 1 Spectra: Corresponds to picturesP7230003 and P7230004

110

Target 2 Spectra: Corresponds to pictures P7230011, P7230012, P7230016, P7230018, and P720019
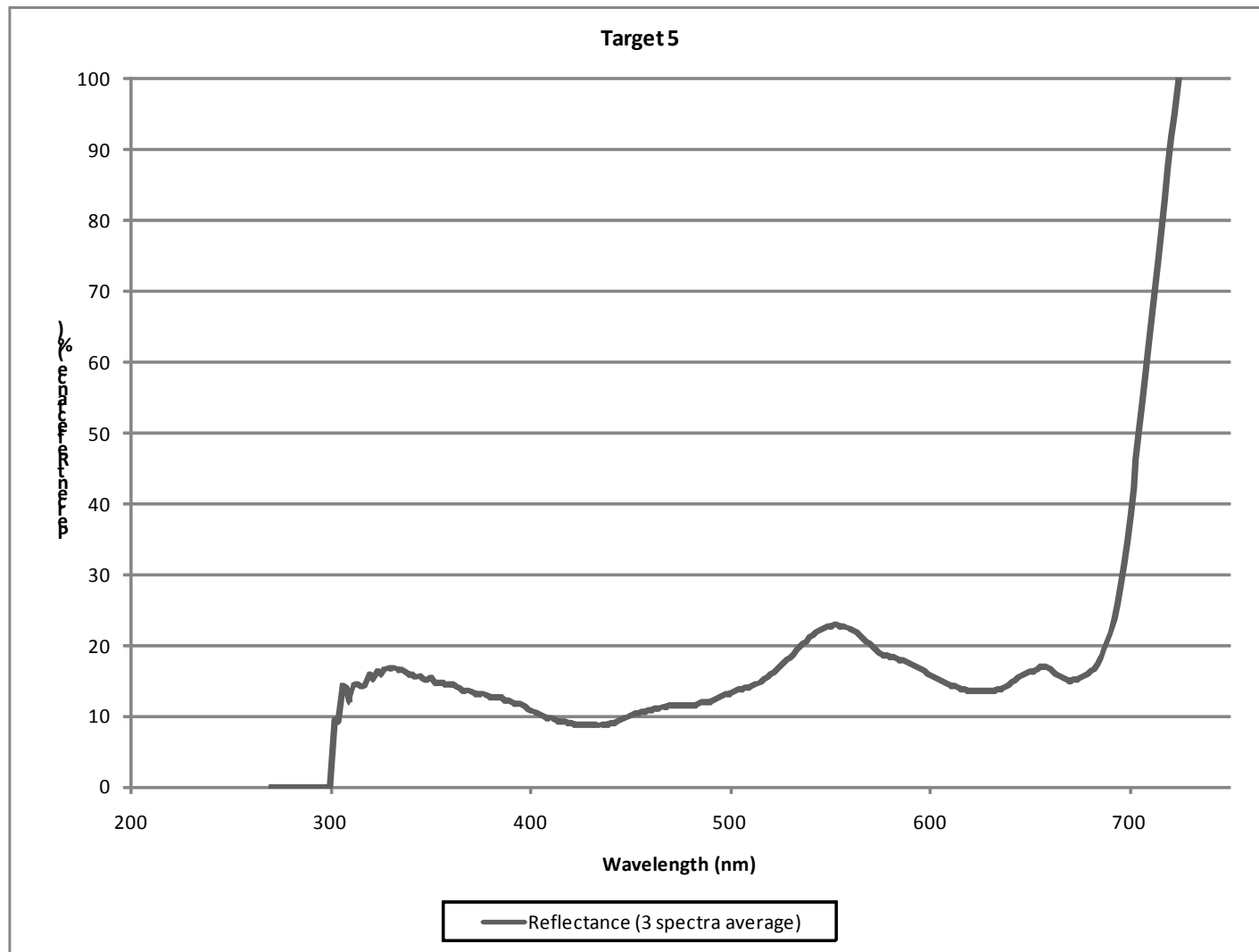
111

Target 3 Spectra: Corresponds to pictures P7230024 and P7230025

Target 4 Spectra: Corresponds to pictures P7230323 and P7230033
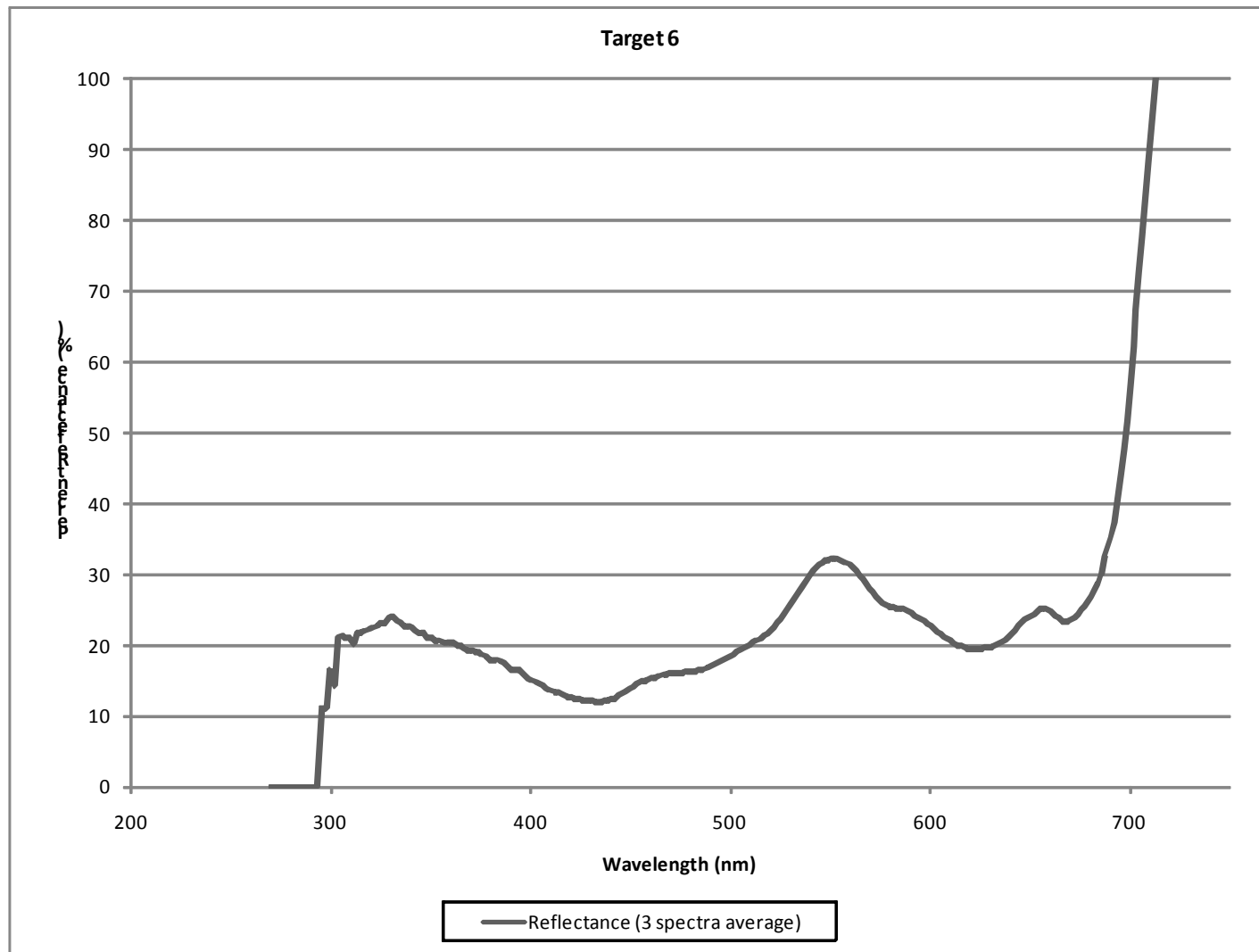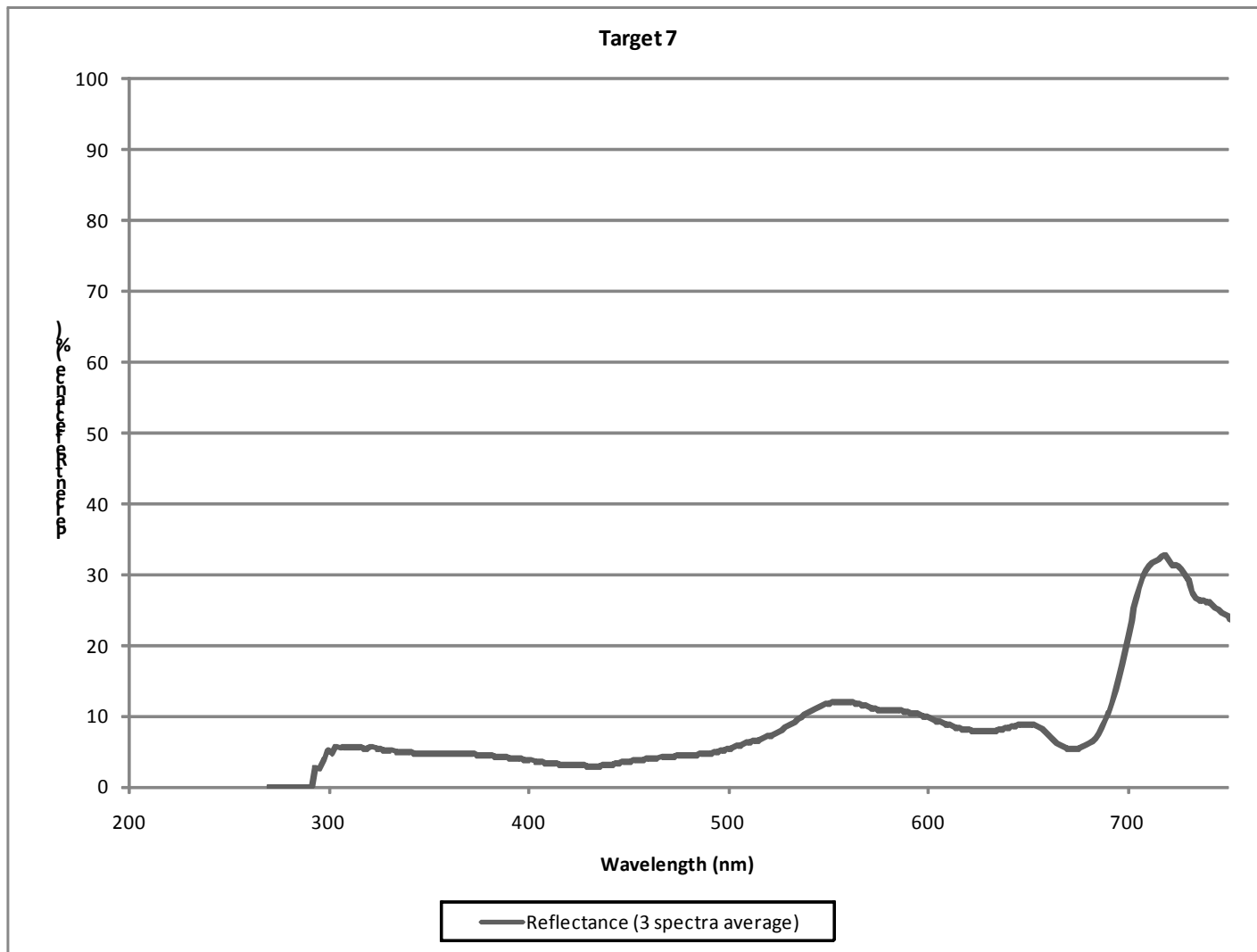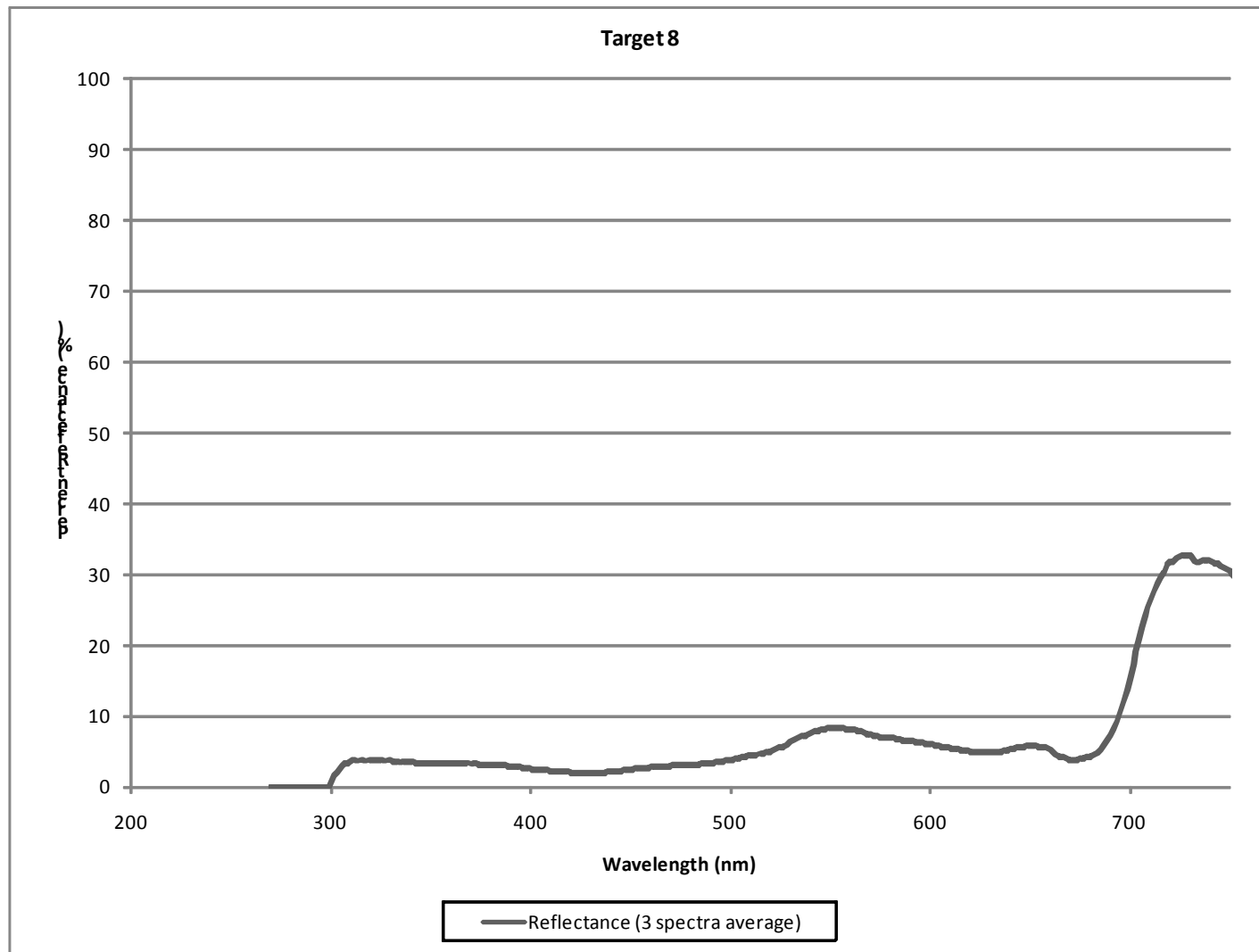
113

Target 5 Spectra: Corresponds to pictures P7240072 and P7240073
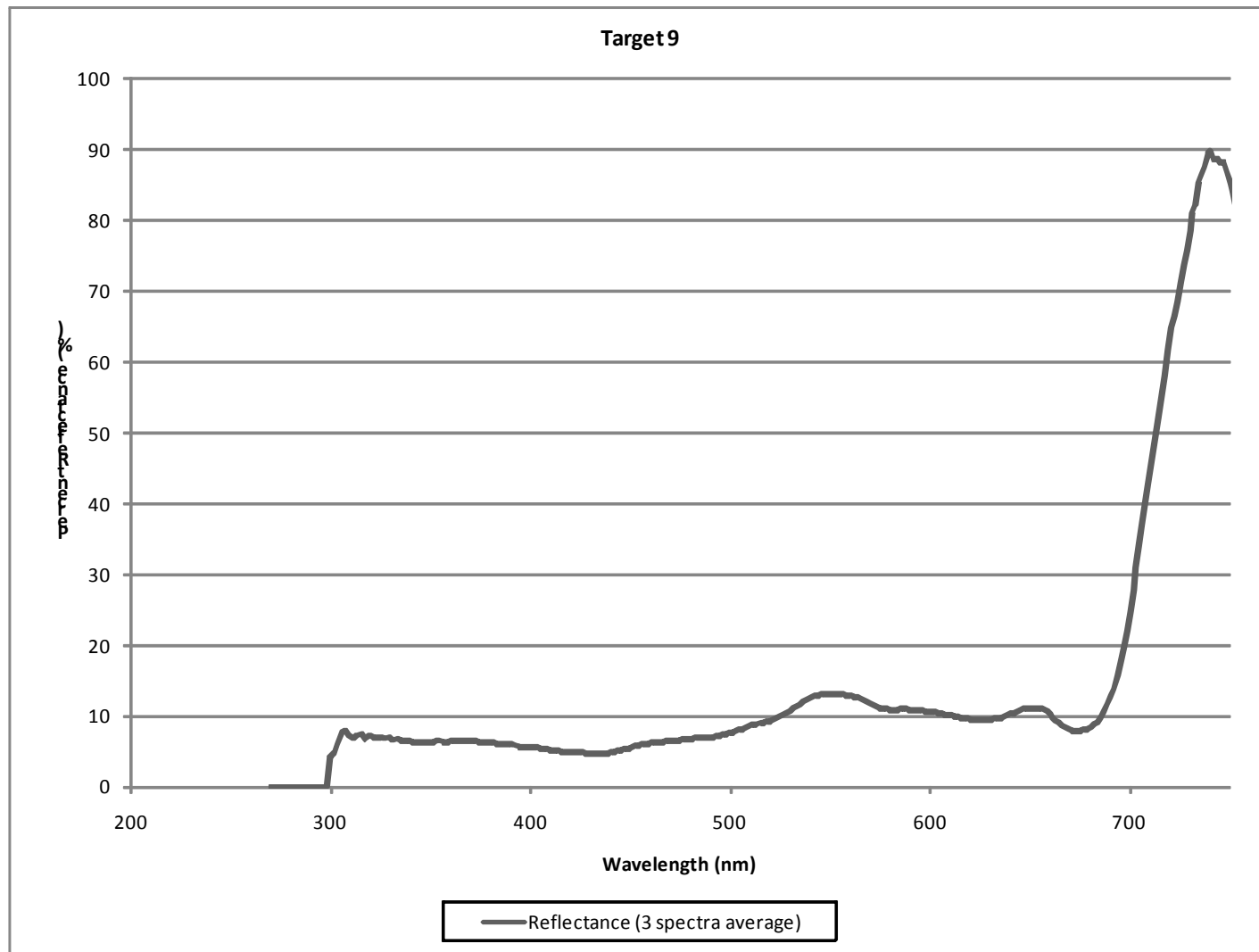
114

Target 6 Spectra: Corresponds to pictures P7240075 and P7240076

115

Target 7 Spectra: Corresponds to pictures P7240077 and P7240078

116

Target 8

Target 8 Spectra: Corresponds to pictures P7240082, P7240083, P7240084, and P7240085

117

Target 9 Spectra: Corresponds to pictures P7240086 and P7240087

LIST OF REFERENCES

Air Force Research Laboratory (AFRL). (2008). *U.S. Air Force fact sheet: TACTICAL SATELLITE-3.* New Mexico: Air Force Research Laboratory.

Andréfouët, S., Kramer, P., Torres-Pulliza, D., Joyce, K. E., Hochberg, E. J., Garza-Pérez, R., et al. (2003). Multi-site evaluation of IKONOS data for classification of tropical coral reef environments. *Remote Sensing of Environment, 88*(1-2), 128-143.

Beisl, U., & Woodhouse, N. (2004). Correction of atmospheric and bidirectional effects in multispectral ADS40 images for mapping purposes geo-imagery bridging continents. *International Society for Photogrammetry and Remote Sensing.* Istanbul, Turkey.

Bellwood, D. R., Hughes, T. P., Folke, C., & Nystroem, M. (2004). Confronting the coral reef crisis. *Nature, 429*(6994), 827-833.

Benfield, S. L., Guzman, H. M., Mair, J. M., & Young, J. (2007). Mapping the distribution of coral reefs and associated sublittoral habitats in Pacific Panama: A comparison of optical satellite sensors and classification methodologies. *International Journal of Remote Sensing, 28*(22), 5047-5070.

Berg, H., Ohman, M. C., Troeng, S., & Linden, O. (1998). Environmental economics of coral reef destruction in Sri Lanka. *Ambio, 27*(8), 627-634.

Berk, A., Anderson, G. P., Bernstein, L. S., Acharya, P. K., Dothe, H., Matthew, M. W., et al. (1999). MODTRAN 4 radiative transfer modeling for atmospheric correction. *Proceedings of SPIE- The International Society for Optical Engineering, 3756*, 348-353.

Brander, L. M., Van Beukering, P., & Cesar, H. S. J. (2007). The recreational value of coral reefs: A meta-analysis. *Ecological Economics, 63*(1), 209-218.

Burger, J., & Gochfeld, M. (2000). Metal levels in feathers of 12 species of seabirds from Midway Atoll in the northern Pacific Ocean. *The Science of the Total Environment, 257*(1), 37-52.

Presidential Proclamation 8031, (2006).

Call, K. A., Hardy, J. T., & Wallin, D. O. (2003). Coral reef habitat discrimination using multivariate spectral analysis and satellite remote sensing. *International Journal of Remote Sensing, 24*(13), 2627-2639.

Calvo, S., Ciraolo, G., & La Loggia, G. (2003). Monitoring posidonia oceanica meadows in a Mediterranean coastal lagoon (Stagnone, Italy) by means of neural network and ISODATA classification methods. *International Journal of Remote Sensing, 24*(13), 2703-2716.

Camacho, M. A. (2006). *Depth analysis of Midway Atoll using QuickBird multi-spectral imaging over variable substrates.* Master of Science in Space Systems Operations, Naval Postgraduate School.

Capolsini, P., Andrefouet, S., Rion, C., & Payri, C. (2003). A comparison of Landsat ETM, SPOT HRV, IKONOS, ASTER, and airborne MASTER data for coral reef habitat mapping in South Pacific islands. *Canadian Journal of Remote Sensing, 29*(2), 187-200.

Carpenter, K. E., Abrar, M., Aeby, G., Aronson, R. B., Banks, S., Bruckner, A., et al. (2008). One-third of reef-building corals face elevated extinction risk from climate change and local impacts. *Science, 321*, 560-563.

Congalton, R. (1991). A review of assessing the accuracy of classifications of remotely sensed data. *Remote Sensing of Environment, 37*, 35-46.

Congalton, R. G., & Green, K. (1999). *Assessing the accuracy of remotely sensed data: Principles and practices*. London: CRC Press.

Cooley, T. (2008). *ARTEMIS tactical satellite 3 21 may 2008*. New Mexico: Air Force Research Laboratory.

DigitalGlobe. (2007). *QuickBird imagery products, product guide*. Longmont: Digital Globe, Inc.

DigitalGlobe. (2008). *Phone conversation with customer service.* 15 August 2008.

DigitalGlobe. (2008). *Worldview-2 satellite.* Retrieved 9/7/2008, 2008, from http://www.digitalglobe.com/index.php/88/WorldView-2

Fleming D. (2001). *IKONOS DN value conversion to planetary reflectance values*. Maryland: University of Maryland.

Friedlander, A. M., Aeby, G., Balwani, S., Bowen, B., Brainard, R., Clark, A., et al. (2008). The state of coral reef ecosystems of the northwestern Hawaiian Islands. *The state of coral reef ecosystems of the United States and Pacific freely associated states: 2008* (Waddell, J.E.;Clarke, A.M. ed., pp. 263-306). Silver Spring, MD: NOAA.

GeoEye. (2006). *IKONOS imagery products guide*. Dulles: GeoEye.

GeoEye. (2008). *Phone conversation with customer service.* 15 August 2008.

Green, E. P., Mumby, P. J., & Clark, C. D. (2000). In Edwards A. J. (Ed.), *Remote sensing handbook for tropical coastal management*

Grigg, R. W., Polovina, J., Friedlander, A. M., & Rohmann, S. O. (2008). Biology of coral reefs in the northwest Hawaiian islands. In: B. M. Riegl, & R. E. Dodge (Eds.) *Coral reefs of the USA*. (pp. 573-594). New York: Springer.

Harborne, A. R., Mumby, P. J., Micheli, F., Perry, C. T., Dahlgren, C. P., Holmes, K. E., et al. (2006). The functional value of caribbean coral reef, seagrass and mangrove habitats to ecosystem processes. *Advances in Marine Biology, 50*(50), 57-189.

Hedley, J. D., Harborne, A. R., & Mumby, P. J. (2005). Simple and robust removal of sun glint for mapping shallow-water benthos. *International Journal of Remote Sensing, 26*(10), 2107-2112.

Hochberg, E. J., Andrefouet, S., & Tyler, M. R. (2003). Sea surface correction of high spatial resolution ikonos images to improve bottom mapping in near-shore environments. *Geoscience and Remote Sensing, IEEE Transactions on, 41*(7), 1724-1729.

Hodgson, G., Kiene, W., Mihaly, J., Liebeler, J., Shuman, C., & Maun, L. (2004). Reef check instruction manual: A guide to reef check coral reef monitoring. *Reef Check, Institute of the Environment, University of California at Los Angeles, Los Angeles (92),*

Holden, H., & Ledrew, E. (1999). Hyperspectral identification of coral reef features. *International Journal of Remote Sensing, 20*(13), 2545-2563.

ImSpec LLC. (2004). *ACORN 5.0 User's Manual.* ImSpec LLC.

ITT Industries Corporation. (2007). *ENVI, get the information you need from imagery*. Boulder: ITT Industries Corporation.

Jensen, J. R. (2000). *Remote sensing of the environment: An earth resource perspectives*. Upper Saddle River, NJ: Prentice Hall.

Jerlov, N. G. (1976). *Marine Optics.* Elsevier Science Ltd.

Joyce, K. E., Phinn, S. R., Roelfsema, C. M., Neil, D. T., & Dennison, W. C. (2004). Combining Landsat ETM and reef check classifications for mapping coral reefs: A critical assessment from the southern Great Barrier Reef, Australia. *Coral Reefs, 23*(1), 21-25.

Ju, J., Gopal, S., & Kolaczyk, E. D. (2005). On the choice of spatial and categorical scale in remote sensing land cover classification. *Remote Sensing of Environment, 96*(1), 62-77.

Krause, K. (2003). *Radiance conversion of QuickBird data*. Longmont: Digital Globe, Inc.

Krause, K. (2005). *Radiometric use of QuickBird imagery*. Longmont: Digital Globe, Inc.

Laliberte, A., Rango, A., Frederickson, E., & Fredrickson, E. (2005). Multi-scale, object-oriented analysis of QuickBird imagery for determining percent cover in arid land vegetation. *American Society for Photogrammetry and Remote Sensing Proceedings,* Baltimore, MD.

Leica Geosystems. (2006). *ATCOR for imagine 9.0*. Norcross: Leica Geosystems.

Lillesand, T. M., Kiefer, R. W., & Chipman, J. W. (2004). *Remote sensing and image interpretation.*John Wiley & Sons Ltd Chichester, UK.

Louchard, E. M., Reid, R. P., Stephens, F. C., Davis, C. O., Leathers, R. A., & Downes, T. V. (2003). Optical remote sensing of benthic habitats and bathymetry in coastal environments at Lee Stocking Island, Bahamas: A comparative spectral classification approach. *Limnology and Oceanography, 48*(1), 511-521.

Lubin, D., Li, W., Dustan, P., Mazel, C., & Stamnes, K. (2001). Spectral signatures of coral reefs-features from space. *Remote Sensing of Environment, 75*(1), 127-137.

Lyzenga, D. R. (1978). Passive remote sensing techniques for mapping water depth and bottom features. *Applied Optics, 17*(3), 379-383.

Lyzenga, D. R. (1981). Remote sensing of bottom reflectance and water attenuation parameters in shallow water using aircraft and landsat data. *International Journal of Remote Sensing, 2*(1), 71-82.

Martin, S. (2004). *An Introduction to Ocean Remote Sensing*. Cambridge, UK: Cambridge University Press.

McCoy, R. M. (2005). *Field Methods in Remote Sensing*. New York: Guilford Press.

Mishra, D., Narumalani, S., Rundquist, D., & Lawson, M. (2006). Benthic habitat mapping in tropical marine environments using QuickBird multispectral data. *Photogrammetric Engineering and Remote Sensing, 72*(9), 1037-1048.

Mishra, D. R., Narumalani, S., Rundquist, D., & Lawson, M. (2005). Characterizing the vertical diffuse attenuation coefficient for downwelling irradiance in coastal waters: Implications for water penetration by high resolution satellite data. *ISPRS Journal of Photogrammetry and Remote Sensing, 60*(1), 48-64.

Mobley, C. D. (1994). *Light and Water.* Academic Press San Diego.

Morel, A., & Prieur, L. (1977). Analysis of variations in ocean color. *Limnol.Oceanogr., 22*(4), 709-722.

Mumby, P. J., Clark, C. D., Green, E. P., & Edwards, A. J. (1998). Benefits of water column correction and contextual editing for mapping coral reefs. *International Journal of Remote Sensing, 19*(1), 203-210.

Mumby, P. J., & Edwards, A. J. (2002). Mapping marine environments with IKONOS imagery: Enhanced spatial resolution can deliver greater thematic accuracy. *Remote Sensing of Environment, 82*(2), 248-257.

Mumby, P. J., Green, E. P., Edwards, A. J., & Clark, C. D. (1999). The cost-effectiveness of remote sensing for tropical coastal resources assessment and management. *Journal of Environmental Management, 55*(3), 157-166.

Olsen, R. C. (2007). *Remote Sensing from Air and Space*. Bellingham, WA USA: SPIE.

Pandolfi, J. M., Bradbury, R. H., Sala, E., Hughes, T. P., Bjorndal, K. A., Cooke, R. G., et al. (2003). Global trajectories of the long-term decline of coral reef ecosystems. *Science, 301*(5635), 955-958.

Raptis, V. S., Vaughan, R. A., & Wright, G. G. (2003). The effect of scaling on land cover classification from satellite data. *Computers and Geosciences, 29*(6), 705-714.

Rauzon, M. J. (2001). *Isles of refuge: Wildlife and History of the Northwestern Hawaiian Islands.* University of Hawaii Press.

Robinson, I. S. (2004). *Measuring the Oceans from Space: The Principles and Methods of Satellite Oceanography.* Springer.

Roelfsema, C. M., Phinn, S. R., & Joyce, K. E. (2004). Evaluating benthic survey techniques for validating maps of coral reefs derived from remotely sensed images. *International Coral Reef Symposium Proceedings,* Okinawa, Japan.

Rooney, J. J., Wessel, P., Hoeke, R., Weiss, J., Baker, J., Parrish, F., et al. (2008). Geology and geomorphology of coral reefs in the northwestern Hawaiian islands. In: B. M. Riegl, & R. E. Dodge (Eds.) *Coral reefs of the USA.* (pp. 519-571). New York: Springer.

Smith, R. C., & Baker, K. S. (1981). Optical properties of the clearest natural waters(200-800 nm). *Applied Optics, 20*(2), 177-184.

Thomas, G. E., & Stamnes, K. (1999). *Radiative Transfer in the Atmosphere and Ocean.* Cambridge University Press.

Tso, B., & Mather, P. M. (2001). *Classification Methods for Remotely Sensed Data*. New York: CRC Press.

US Department of Defense. (2003). *Enterprise Integration Toolkit (version 2.0): Business Case Development Guide.*

Wang, L., Sousa, W. P., Gong, P., & Biging, G. S. (2004). Comparison of IKONOS and QuickBird images for mapping mangrove species on the Caribbean coast of Panama. *Remote Sensing of Environment, 91*(3-4), 432-440.

INITIAL DISTRIBUTION LIST

1. Defense Technical Information Center
    Ft. Belvoir, Virginia

2. Dudley Knox Library
    Naval Postgraduate School
    Monterey, California

3. Dr. Daria Siciliano
    Naval Postgraduate School
    Monterey, California

4. Dr. Richard C. Olsen. Code PH OS
    Naval Postgraduate School
    Monterey, California

5. Glenn Cook
    Nava Postgraduate School
    Monterey, California

6. Matt Brown
    U.S. Fish & Wildlife Service
    Midway Atoll National Wildlife Refuge